Spring 2003

Free solution electrophoresis measurements and their theoretical relationships to net protein valence

Jennifer A. Durant
University of New Hampshire, Durham

INFORMATION TO USERS

This manuscript has been reproduced from the microfilm master. UMI films the text directly from the original or copy submitted. Thus, some thesis and dissertation copies are in typewriter face, while others may be from any type of computer printer.

The quality of this reproduction is dependent upon the quality of the copy submitted. Broken or indistinct print, colored or poor quality illustrations and photographs, print bleedthrough, substandard margins, and improper alignment can adversely affect reproduction.

In the unlikely event that the author did not send UMI a complete manuscript and there are missing pages, these will be noted. Also, if unauthorized copyright material had to be removed, a note will indicate the deletion.

Oversize materials (e.g., maps, drawings, charts) are reproduced by sectioning the original, beginning at the upper left-hand corner and continuing from left to right in equal sections with small overlaps.

ProQuest Information and Learning
300 North Zeeb Road, Ann Arbor, MI 48106-1346 USA
800-521-0600

FREE SOLUTION ELECTROROPHORESIS MEASUREMENTS AND THEIR THEORETICAL RELATIONSHIPS TO NET PROTEIN VALENCE

BY

Jennifer A. Durant
B.S., University of New Hampshire, 1996

DISSERTATION

Submitted to the University of New Hampshire
in Partial Fulfillment of
the Requirements for the Degree of

Doctor of Philosophy
in
Biochemistry

May 2003

UMI Number: 3083727

ProQuest Information and Learning Company
300 North Zeeb Road
P.O. Box 1346
Ann Arbor, MI 48106-1346

This dissertation has been examined and approved.

Dissertation Director, Thomas. L. Laue
Professor of Biochemistry

John F. Collins
Professor of Biochemistry

James Stewart
Professor Emeritus of Biochemistry

Thomas P. Moody
Research Assistant Professor of Biochemistry

N. Dennis Chasteen
Professor of Chemistry

2/7/03
Date

DEDICATION

To Megan, Maddison and baby boy

ACKNOWLEDGEMENTS

Professional: T4 lysozyme wild type and mutant clones were donated by Brian Matthews. Walter Baase was kind enough to offer advice on the purification process of T4 lysozyme. The boundary element modeling discussed herein is the work of Stuart Allison and his graduate student Chuanying Chen. Nick Pace supplied the Ribonuclease Sa proteins.

Personal: The Laue Lab. In the beginning, there were the dueling sound bites of John C and Ian M. I owe them, Kari H., Jon K. and Daryl L. many thanks for helping me with my first analytical centrifuge and MCE runs. Sue L. can never retire ...besides being a great resource for us all, where would we have our coffee? But since Sue C. and Michelle G. and Maribeth J. have joined, we really need to knock that wall down. Think anyone will notice? Rachel, thanks for getting us all out once in awhile. Glad your back. I would like to thank Tim W. and Terry R., for sharing their insights on the MCE and for their witticisms that kept dealing with a prototype bearable. I owe a great deal of thanks to Tom Moody for his help on many fronts. He has always been very generous with his time and brings a lot to the Laue Lab. Upon divulging once that I worked for Tom Laue, I was told that I was working for a "real biochemist". How true. Tom is indisputably talented and dedicated. But in addition to being adept in a vast number of areas, he possesses a contagious enthusiasm that makes the Laue Lab a fantastic place to work and learn. I should also acknowledge my husband, Yvon, who, himself a scientist, has always encouraged me in this endeavor. He knows more about T4 lysozyme and the MCE than he ever wanted to know. Remember to take care of the rocks first.

TABLE OF CONTENTS

LIST OF TABLES

LIST OF FIGURES

LIST OF ABBREVIATIONS

2K	Ribonuclease Sa Mutant (D17E/E41K)
5K	Ribonuclease Sa Mutant (D17E/E41K/D1K/D25K/E74K)
aa	Amino Acid
AUC	Analytical Ultracentrifugation
BE	Boundary Element
BTP	Bis-Tris Propane
CE	Capillary Electrophoresis
CIEF	Capillary Isoelectric Focusing
CIEF	Capillary Isoelectric Focusing
CZE	Capillary Zone Electrophoresis
DHH	Debye-Hückel-Henry
DLS	Dynamic Light Scattering
DLVO	Derjaguin-Landau-Verwey-Overbeek
DM	Double Mutant
EA	Ethanolamine
EDC	1-Ethyl-3-(3-dimethylaminopropyl) Carbodiimide
EOF	Endoosmotic Flow
HEL	Hen Egg-White Lysozyme
IPTG	Isopropyl-1-thio-β-D-galactopyranoside
M	Macroion
MCE	Membrane Confined Electrophoresis
MES	N-[2-Morpholino]ethanesulfonic acid
PAGE	Polyacrylamide Gel Electrophoresis
PB	Poisson Boltzmann
QM	Quadruple Mutant
SM	Single Mutant
SPR	Surface Plasmon Resonance
SSE	Steady State Electrophoresis
TM	Triple Mutant
WT	Wild Type

LIST OF SYMBOLS

symbol	units	description
D	cm^2/s (equiv. $x10^7$ Fick)	diffusion coefficient
ε	dimensionless	dielectric constant
ε_0	8.854×10^{-12} $C^2/J \cdot m$	Permittivity of vacuum
E	V/cm	electric field
e	1.6029×10^{-19} Coulomb	charge on electron
κ	cm^{-1}	inverse Debye length
k	S/m	conductivity
c	g/mL or M as specified	concentration
μ	$cm^2/V \cdot s$	mobility
ρ	g/cm^3	solution density
ρ_c	C/cm^3	charge density
σ	cm^{-1}	reduced molar mass
σ_c	cm^{-1}	reduced molecular charge
$\bar{\nu}$	mL/g	partial specific volume
v	cm/s	velocity
v_{EOF}	cm/s	endosomotic flow velocity
A	cm^2	area
i	ampere	current
R_s	cm	Stokes radius
a	cm	collision diameter
r	cm	molecular radius
f	g/s	frictional coefficient
N_A	6.0221×10^{23} /mol	Avogadro's number
k_B	1.3807×10^{-23} J/K	Boltzmann constant
R	8.314 J/K·mol	gas constant
ζ	V	zeta or electrokinetic potential
z_{eff}	dimensionless	effective valence
z	dimensionless	valence
G_{el}	J/mol	electrostatic free energy
ψ	V	potential
η	g/cm·s	solution viscosity
F	96484 C/mol	the Faraday
I	mol/L	ionic strength

ABSTRACT

FREE SOLUTION ELECTROROPHORESIS MEASUREMENTS AND THEIR THEORETICAL RELATIONSHIPS TO NET PROTEIN VALENCE

by

Jennifer A. Durant

University of New Hampshire, May, 2003

Biochemical solutions are composed to a large degree of charged molecules (proteins, DNA, dissolved salts, etc) which can *interact* and therefore exert a *force* on each other. Analytical determination of the valence of biological macro-ions contributes to our understanding of the forces involved in both intra- and inter-molecular interactions. This dissertation uses two free solution techniques, membrane confined electrophoresis (MCE) and capillary electrophoresis (CE), to study valence in the context of a series of charge mutants of T4 lysozyme and RNase Sa. The use of these mutants allows attribution of the changes in electrophoretic behavior entirely to changes in charge. Sedimentation velocity and dynamic light scattering were used to verify that the hydrodynamic radius was constant for a given series of charge mutants. Furthermore, this work compares the model predictions of Debye-Hückel-Henry (DHH), Booth, and the more recent boundary element (BE) modeling by Allison with experimental results.

The electrophoretic behavior of a macroion is affected in a complex manner by a variety of forces which arise from the applied field. Coupling of the macro-ion and small ion flows gives rise to non-conserved forces that are greater than those expected from ordinary hydrodynamic considerations. It is difficult to separate the hydrodynamic and

electrodynamic contributions to the macroion mobility. Membrane confined electrophoresis provides an experimental means by which to gain insight into these contributions. These experiments isolate the effects of charge on electrophoretic mobility and permit a unique test of theories.

Through MCE steady-state measurements, the effective valence (z_{eff}) of both sets of mutants was determined under an ionic strength of 0.11 M at pH 7.5. Further experimentation with T4 lysozyme at low and high ionic strengths was done to investigate how well the models reflected the observed electrodynamic changes. Parallel experiments with capillary electrophoresis were conducted. Diffusion coefficients determined by sedimentation velocity studies were used to convert between capillary electrophoresis and membrane confined electrophoresis results. Although Debye-Hückel-Henry and Booth provide reasonable first approximations, boundary element modeling by Allison and co-workers, using continuum hydrodynamics based on detailed structural information, provides the most accurate predictions of experimentally observed values.

CHAPTER I

INTRODUCTION

Biochemical solutions, to a large degree, are composed of charged molecules (proteins, DNA, dissolved salts, etc) which can *interact* and therefore exert a *force* on each other. One component of the total force, the electrostatic force, is a function of not only the magnitude of the charge but also their separation distance (r) and the nature of the intervening medium. It is this quantity with which this work will be concerned.

The work of Charles Coulomb in the 1780's led to the expression describing this force

$$F = \frac{z_A z_B e^2}{4\pi\varepsilon_0 \varepsilon r^2} \quad (1)$$

where ε_0 is the permittivity of a vacuum, ε the dimensionless dielectric constant, z is the valence on ion A or B, and e is the charge on an electron. The electrostatic free energy of interaction is then given by

$$G_{el} = -\int_{\infty}^{r} F dr = -\int_{\infty}^{r} \frac{z_A z_B e^2}{4\pi\varepsilon_0 \varepsilon r^2} dr = \frac{z_A z_B e^2}{4\pi\varepsilon_0 \varepsilon r} = ze\psi \qquad (2)$$

where ψ is the electrostatic potential. This expression, however, gives the electrostatic free energy only if there are no other ions present. In a living cell, a pharmaceutical formulation, or a typical laboratory experiment, this is an unlikely situation. The electrostatic free energy contribution is thus complicated in this manner; an unavoidable complication if we are to fully describe any of these systems.

Furthermore, charges exert forces both inter- and intramolecularly that may either increase or decrease the interaction energy. For example, a glycine to aspartate mutation at a binding site may cause intermolecular destabilization by unfavorably altering the last term in equation (3) (Elcock & McCammon, 2001):

$$\Delta G_{inter} = \Delta G_{steric} + \Delta G_{nonpolar} + \Delta G_{electrostatic} \qquad (3).$$

On the other hand, the formation of a salt bridge between a histidine and an aspartate, or the relocalization of a solvent-exposed lysine to the protein interior, are examples of intramolecular modulation of electrical free energy as given in the first term of equation (4) (Matthew & Gurd, 1986).

$$\Delta G_{stability} = \sum_{i=1}^{\#residues} (\Delta G_{i,electrostatic} + \Delta G_{i,hydrophobic} + \Delta G_{i,vanderWaals}) + \Delta G_{buried} + \Delta G_{s-s} \qquad (4)$$

While quantitation of intermolecular interactions is the ultimate goal, and much work has already been done to this end (Tanford & Kirkwood, 1957; Havranek & Harbury, 1999; Ladokhin & White, 2001; Friend et al., 1981), there is still experimental and theoretical work to be done on the latter case. In other words, our understanding of how charge contributes to protein properties such as stability and solubility is still incomplete. For example, although Linderstrom-Lang theory predicts the stability of a protein to be greatest at its pI, recent mutational studies have shown this can be off by more than 2 pH units (Linderstrom-Lang, 1924; Shaw et al., 2001). Only recently, as Yang and Honig have pointed out, have the deficiencies of this theory begun to be sorted out (Yang & Honig, 1993).

The electrostatic component is what gives rise to the pH (and ionic strength) dependence of protein properties such as stability. The classical expression for this dependency, as originally derived by Tanford and Kirkwood,

$$\frac{\partial \Delta G_{stability}}{\partial pH} = 2.303RT(z_{unfolded} - z_{folded}) \qquad (5)$$

requires knowledge of the net valence in the folded as well as unfolded states (Tanford, 1970; Tanford & Kirkwood, 1957; Stigter & Dill, 1990). Equation 5 was solved initially by applying sufficient restrictions on the system such that the Poisson-Boltzman equation could be solved as a sum of spherical harmonics (Tanford & Kirkwood, 1957). It can now be done using the finite difference Poisson-Boltzmann equation to calculate the pK_a's of each charge at every pH, as was first done by Bashford and Karplus (Bashford & Karplus, 1990). A major fault of this approach, however, resides with the assumption that the intrinsic pK_a of a residue is the same as that of the isolated amino acid (Yang & Honig, 1993). Furthermore, the self energy of charges is ignored and the protein/solvent interface is taken as a spherical boundary (Harvey, 1989).

Experimentally, estimation of the net valence is made using pK_a measurements obtained by titration. Frequently, these pK_a's are determined by NMR, albeit at protein concentrations high enough to warrant some skepticism as to the relevance to dilute solutions (Kohda et al., 1991). Furthermore, the titrations conditions are often significantly different from those of interest. For example, the available T4 lysozyme pK_a values, collected at an ionic strength of 0.12 M(25 °C), may be inaccurate at 0.02 M (20 °C).

Gurd and coworkers were the first to modify Tanford-Kirkwood theory to include information on both position and solvent accessibility of the charge (the latter improvement actually first suggested by Schellman) (Matthew et al., 1985; Shire et al., 1974; Matthew & Gurd, 1986; Schellman, 1953). Even so, by retaining the use of

isolated pK_a values for the folded protein, the results wrongly attribute *all* shifts in pK_a upon folding to electrostatic interactions between the charged groups.

More recent work has shown desolvation of the charged groups and interaction with neutral, polar groups also contribute to the pK_a's in the folded protein (Yang & Honig, 1993). Furthermore, Urry has described hydrophobically-induced pK_a shifts (Urry, 1997). To resolve these difficulties, Yang and Honig re-approached the problem using intrinsic pK_a's. However, they assumed no electrostatic interaction between the charged groups in the unfolded protein. This was justifiable in that, until very recently, our description of an unfolded protein was based on Tanford's random coil arrangement in which case the increased distance and dielectric would attenuate electrostatic interactions. Pace et al. have shown that because the denatured state of ribonuclease Sa, and many other proteins, is considerably more compact than predicted, there are favorable charge-charge interactions, especially near physiological pH (Pace et al., 2000). Elcock has found this to be true as well for barnase, chymotrypsin inhibitor 2 and ovomucoid third domain (Elcock, 1999).

The development of site-directed mutagenesis methods has opened new possibilities by which to study electrostatics and test existing theories. Additionally, as Urry points out, virtually every interaction and modification of a protein may be characterized in terms of its effect on its melting temperature (t_m) (Urry, 1997). This fact is now commonly exploited using the relation

$$\Delta\Delta G = \Delta t_m \Delta S \qquad (6)$$

where ΔS is the entropy of melting. Naturally, mutation induced changes in other interactions, such as hydrophobic and van der Waals, can contribute to the perturbation in

free energy. However, the *pH dependence* of this measurement reflects *only* the electrostatic contribution. Studies which have addressed the electrostatic contribution to stability by this method have produced conflicting results. Perry et al., for example, find that electrostatic interactions do influence stability, while Dao-pin et al. find that they contribute little (Dao-pin et al., 1991; Perry et al., 1989). As Negin and Carbeck have pointed out, one problem with these studies may be that they simply lack a sufficient number of mutants to accurately measure the average effects of charge on protein stability (Negin & Carbeck, 2001). For example, Dao-pin and Matthews mutated only 5 out of 28 of the positively charged residues of T4 lysozyme. All of these residues were highly solvent exposed and mobile. It is possible therefore, that other cationic residues which are not solvent exposed or mobile would have a greater effect. It should not be assumed that buried charges contribute little to the overall stability. Indeed, the importance of buried charges and their ionization states is a topic of current investigation by Gunner (NSF grant #0212696, July 2002).

Thanks to recent instrumentation developments, there are alternative experimental methods to assessing the electrostatics of proteins. Specifically, both capillary electrophoresis (CE) and membrane confined electrophoresis (MCE) offer analytical measurements of mobility (μ) and effective charge (z_{eff}), respectively, neither requiring the use of standards. Negin and Carbeck have recently made use of CE and protein charge ladders to differentiate between the $\Delta pK_{a\ unfolded\text{-}folded}$ and long range electrostatic influences on stability. The electrostatic component is often assumed to be predominately dependent on $\Delta pK_{a\ unfolded\text{-}folded}$ (Whitten & Garcia-Moreno, 2000; Dao-pin et al., 1991)

(Shaw et al., 2001; Negin & Carbeck, 2001) and the two influences on stability are difficult to measure independently. Negin and Carbeck give the expressions

$$\left(\frac{\partial \Delta G_{stability}}{\partial pH}\right)_{\Delta pKa} = 2.303RT(p_{folded} - p_{unfolded}) \qquad (7)$$

and

$$\left(\frac{\partial \Delta G_{stability}}{\partial pH}\right)_{\substack{long-range \\ electrostatics}} = \frac{\partial \Delta G}{\partial z}\frac{\partial z}{\partial pH} \qquad (8)$$

where p is the number of bound protons and z is the net valence. Using charge ladders (generated by partial acetylation of lysine groups of α-lactalbumin) instead of point mutations, they find that while proton binding dominates the electrostatic component at lower pHs, the long-range electrostatic contribution grows to the same order of magnitude as pH increases. In solving Equation 8, Negin and Carbeck used Debye-Hückel-Henry theory to determine z from CE mobility measurements (see Section 4.5). Alternatively, one can determine z from z_{eff} using the same theories (see Equation 31). This avoids the need for knowledge of accurate pK_a values.

The Debye-Hückel-Henry theory Negin and Carbeck used includes, unlike the work of Coulomb, effects from the presence of other ions. According to Debye and Hückel, (if r, *a*, and 1/κ are in m) the potential of an ion is calculated as

$$\psi = \frac{ze}{4\pi\varepsilon_0\varepsilon r}\left(\frac{1}{1+\kappa a}\right)e^{-\kappa(r-a)} = \frac{ze}{4\pi\varepsilon_0\varepsilon a}\left(\frac{1}{1+\kappa a}\right) \qquad \text{for } r = a \qquad (9)$$

and if Henry's modification is now included for the case of electrophoresis, z_{eff} is then

$$z_{eff}e = \Psi 4\pi\varepsilon_0\varepsilon a = ze\left(\frac{f(\kappa a)_{1\text{-}1.5}}{1+\kappa a}\right) = \mu f \qquad (10)$$

where a is the effective radius of the central ion, κ is the Debye length, f is the frictional coefficient, and $f(\kappa a)$ is Henry's function (see Section 4.5). This result uses the linear approximation to the Poisson-Boltzmann (PB) equation, which is analytically tractable. The approximation, however, limits its applicability to ionic strengths of about < 0.001 M and molecules of spherical geometry (although experimental work has shown that the approximation appears valid over a much wider range of conditions) (Kalman et al., 1995). *Clearly more comprehensive alternatives to this solution are desirable.* More recently, programs such as Delphi have been developed which numerically solve the full PB for macroions of arbitrary shape (Honig & Nicholls, 1995). Additionally, Allison and co-workers have developed a boundary element (BE) model which uses continuum hydrodynamics based on detailed structural information to provide mobility (and thus z_{eff}) predictions (Allison et al., 1997).

The computationally intensive electrostatic modeling of recent years has produced a number of results which have yet to be fully tested. It is the aim of this work to not only compare the results of BE modeling to experimental findings, but to calculate the magnitude of improvement provided over the older, classical methods which rely heavily on a number of assumptions. It is hypothesized that the MCE gives direct, accurate measures of effective valence and that the hydrodynamic and electrodynamic contributions to the macroion mobility are correctly accounted for by BE modeling. In this context, traditional test macromolecules include ribonuclease A (Elcock, 1999; Antosiewicz et al., 1996a; Antosiewicz et al., 1996b; Hermans & Scheraga, 1961), hen egg white lysozyme (Yang & Honig, 1993; Elcock, 1999; Elcock & McCammon, 2001; Antosiewicz et al., 1996a), and T4 bacteriophage lysozyme (Xu et al., 2001; Dao-pin et

al., 1991; Allison, 2002), the latter of which has been chosen as the focus for this work. Additionally some initial findings for ribonuclease Sa and α-chymotrypsin are included. The availability of a number of charge mutants of the T4 lysozyme and ribonuclease Sa, along with extensive existing crystallographic data, make them ideal choices for exploring *intra*molecular electrostatics. The work with α-chymotrypsin and its homodimer is the beginning of what should eventually be a complex investigation of the role of *inter*molecular electrostatics. As Urry nicely summarizes, "to the physical chemist, the basic problem of biology becomes how changes in intensive variables of the free energy give rise to changes in folding and assembly to perform useful work. ... the performance of a particular kind of work is simply that kind of energy on display" (Urry, 1997).

CHAPTER 2

BACKGROUND

Though the theory of electrophoresis dates back to the days of Helmholtz (1821-1894), our use of electrophoresis as an *absolute*, *quantitative* means has been limited. This is especially true with respect to its use in characterizing a fundamental property of many biomolecules: charge. Though ubiquitous to the field of biochemistry, electrophoresis has until recently been primarily limited to that performed in gels, a method that is dependent on the use of standards. Free solution techniques initially relied on microscopes to monitor migration. Even the Tiselius apparatus of the 1930s, the first to introduce Schlieren optics to such a device, was limited by its complexity and the large quantity of macroion needed. With such experimental limitations, there has thus been only moderate interest in advancing the theory.

The introduction of capillary electrophoresis (CE) in the 1980s, however, has stimulated new interest in free solution methods. However, CE is used more commonly for the separation of complex mixtures than it is for making absolute measurements. Thus, much of the recent work with CE has been developed empirically to optimize various separation conditions (Matsubara & Terabe, 1992; Oda & Landers, 1996; Pietta et al., 1999). Nonetheless, there are a growing number of workers interested in developing a more fundamental and comprehensive theory (Allison et al., 1997; Mazur et al., 2001; Carbeck & Negin, 2001). This is already broadening the scope of

electrophoretic applications (as mentioned in the introduction). Furthermore, a relatively new and complementary technique to CE, membrane confined electrophoresis (MCE), is providing yet another testing ground for electrophoretic theories (Durant et al., 2002). Requiring little in the way of sample quantity, as with capillary electrophoresis, MCE has two distinct advantages over existing techniques: 1) the exact same sample can be analyzed in a variety of buffers due to the in-line dialysis setup and 2) there is no electroendoosmotic flow, a complication of CE. By this method, direct measurements of both mobility and effective valence can be made.

The net valence on a macroion includes the sum of 1) the fixed amino acid side chain charge, as dictated by microenvironment and salt effects on these pK_a's, as well as 2) specific, site bound and 3) nonspecific, diffusely bound ions. The major obstacle in obtaining this charge is, as is often the case, perturbation of the system by the process of measurement. Indeed, this is why electrophoresis provides a measure of effective valence (z_{eff}) rather than the valence itself, and why z_{eff} is a system, rather than molecular, parameter. Nonetheless, it is still the most direct means of obtaining net valence information. Because the measurement is the time-average (assumed to be same as the ensemble average) effective valence of the 2^N possible ionization states of a macroion (with N residues) and its site/diffuse bound ions, the result is a non-integral effective valence.

If a macroion (M) is stationary, and no forces act on it for a moment, the charge on M results in an excess of counterion in the vicinity of the macroion. This excess of counterion over coion will be found, as defined by the linear PB, to be distributed around M according to

$$\frac{dq}{dr} = 4\pi r^2 \rho_c = -ze\kappa^2 \left(\frac{e^{\kappa a}}{1+\kappa a} \right) re^{-\kappa r} \quad r \geq a \quad (11)$$

where ρ_c is the charge density, a is the collision diameter, dq/dr is the total charge per unit thickness of a shell around M (Edsall & Wyman, 1958). The ionic strength (I) dependence arises from the parameter 1/κ which is known as the Debye-length (Debye, 1927) and is, in SI units, given by

$$\kappa^2 = \left(\frac{2 N_A e^2}{\varepsilon_0 \varepsilon k_B T} \right) \left(\frac{1000 \text{ L}}{1 \text{ m}^3} \right) (I) \quad (12)$$

This counterion cloud affects the potential (Ψ) at any distance from M such that macroion-ion electrostatic forces fall off at a rate greater than the inverse square law. Note the inverse relationship of the Debye length (1/κ), with the square root of the ionic strength. As will be discussed further in Chapter 5, the physical meaning of the parameter 1/ κ is lost for high ionic strengths. For the moment, it is sufficient to note that for large values of κ (i.e. high *salt* concentrations), Debye pointed out "the characteristic length, 1/κ, loses its effect in favor of the new length a, which measures the size of the ions" (Debye & Huckel, 1923a). This is already apparent in Figure 2.1, where at an ionic strength of only 0.01 M, the peak of the function approaches the value a. Debye and Hückel were primarily concerned with the case of 1:1 electrolytes such as KCl, such that the central ion was K^+ or Cl^-, and a was 0.1-0.5 nm. Initially they defined their model in terms of point charges, and thus the peak position of

$$\frac{dq}{dr} = 4\pi r^2 \rho = -ze\kappa^2 re^{-\kappa r} \quad (13)$$

corresponds to 1/κ. As they defined it, "1/κ measures the length within which the charge density of the ion atmosphere reduces to one e^{th} part" (Debye & Huckel, 1923a). This

corresponded to the Helmholtz description of a "double layer" at an electrode in an electrolytic solution. However, attaching any special, physical meaning to the distance $1/\kappa$, or considering the "double layer" to be a discrete entity is misleading. Both $1/\kappa$ and the "double layer" are concepts which facilitate the math rather than tangible properties.

Note that the area under each curve in Figure 2.1 is the same. This distribution of solvent ions, *differing from the bulk*, is termed the ion atmosphere. Its presence is a key feature which must be dealt with in describing electrophoretic transport. Furthermore, the theories describing this atmosphere and ionic transport are limited to dilute solutions. As the right hand diagram of Figure 2.1 shows, a "dilute solution" implies that the distance between central ions is large relative to 1/k so that no overlap of the central ion atmospheres occurs. The central ion can thus be treated as an isolated ion whose atmosphere is unperturbed by other nearby macroions.

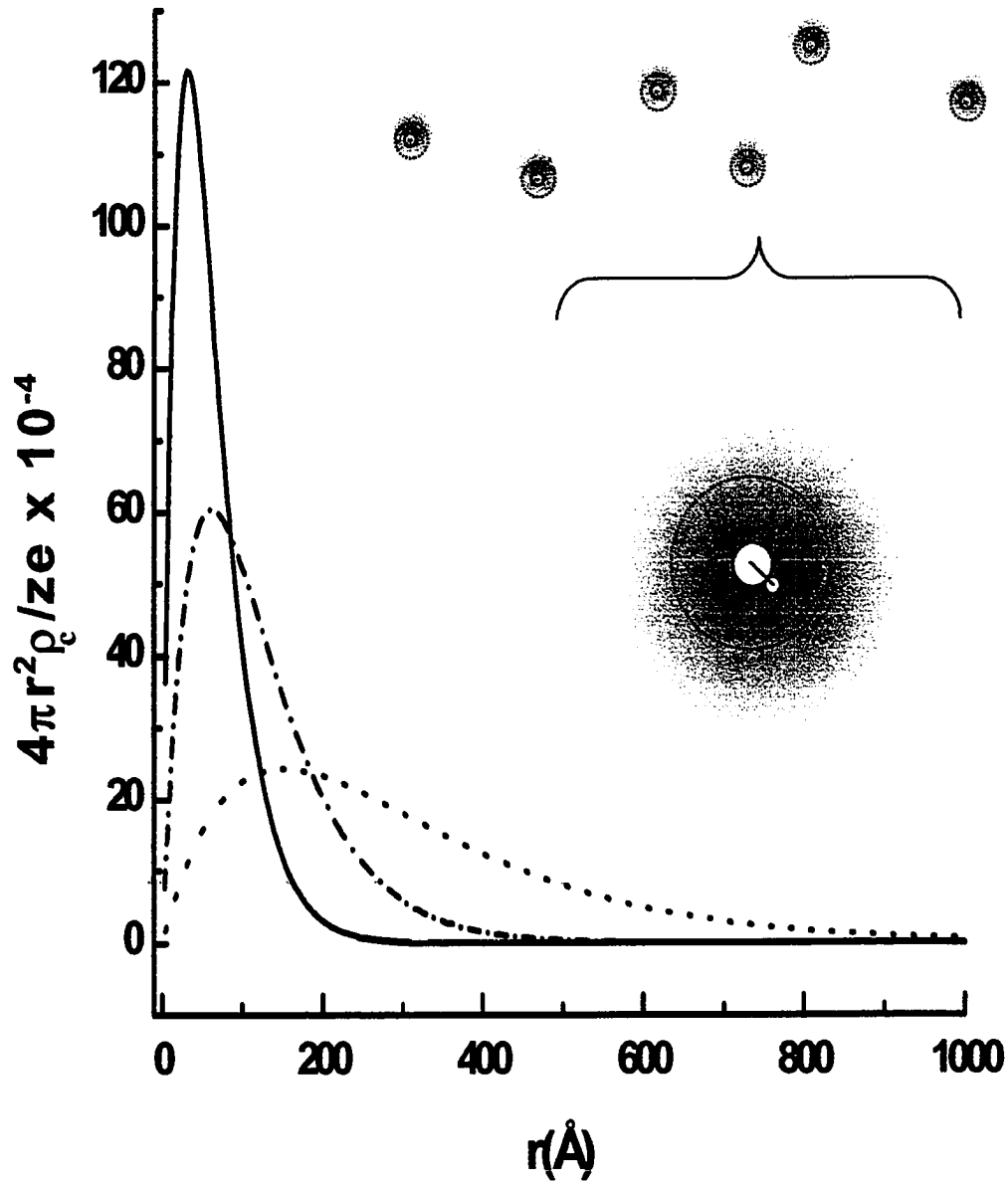

Figure 2.1. dq/dr calculated for an arbitrary central ion. A collision diameter of 3 X 10^{-8} cm was used in the Debye-Hückel model. The values of dq/dr are normalized to net charge. The results are for —— 0.01, —·— 0.0025, and ····· 0.0004 M ionic strengths. The diagram to the right shows the model imposed boundaries. The solid line represents the collision diameter. The dotted circle, represents 1/κ, which changes with ionic strength.

If thermal forces are now considered, M perfoms a random walk, meandering through the bulk hydrogen-bonded water structure and the ions therein. Near the surface of M, the electrostatic forces are substantial. In fact, the strength of the ion-dipole interaction between M and the water molecules in its immediate vicinity is greater than the hydrogen bonding forces between the water molecules in bulk solution (Bergethon & Simons, 1990). Some of the water molecules at the surface of M surface become immobilized and there is a loss of entropy. Therefore, as M wanders, this solvation sheath travels with the macroion. For every water molecule that drops off, another binds within a matter of picoseconds. Thus, the effective radius of the macroion is increased to a hydrodynamic radius. Additionally, to return to the concept of the ion atmosphere, it is possible that some counterions may approach M close enough to form what is called an ion pair. This may constitute site binding or simply be a nonspecific, diffuse binding, both of which contribute to the net valence of the macroion M. The total mobile unit, thus far, is a dynamic unit consisting of a central macroion M, site bound ions, possibly diffusely bound ions, and a hydration sheath all contained within a poorly defined radius. At this radius, sometimes called the outer Helmholtz plane, a new potential, the zeta potential (ζ), is defined. The Helmholtz plane, like the double layer and Debye distance, should be viewed as a construct useful for developing the mathematics of electrophoretic theory, rather than a real entity. With no directional force acting on the central macroion, the counterion distribution both inside and outside this plane is still described by the Poisson-Boltzmann equation.

If M now moves in response to an electric field, there is a change in the ion atmosphere relative to the central macroion which gives rise to two non-conserved forces. First, the mobile counterions, due to their countercharge, flow in a direction opposite that of M. The momentum transferred to M by this counter flow causes a retarding force called electrophoretic retardation. Furthermore, the tendency of the ion atmosphere and M to move in opposite directions distorts the time average shape of the ion atmosphere from its equilibrium distribution, leading to a dipole moment not described by the Poisson-Boltzmann equation. This gives rise to an additional retarding force called the asymmetry effect (also called ion relaxation).

These phenomena were first described by Debye-Hückel-Onsager theory in modeling conductivity (Onsager & Fuoss, 1932). In this case, the retarding effect for a two species system (eg. K^+ and Cl^-) was described as resulting from the interaction of the respective ionic atmospheres leading to an increase the resistance to current flux. Thus, for the equivalent conductance (Λ) of a 1:1 electrolyte,

$$\Lambda = \Lambda^\circ - k\sqrt{c} = \Lambda^\circ - (A + B\Lambda^\circ)\sqrt{c} \qquad (14)$$

where Λ° is the equivalent conductivity at infinite dilution, c is the concentration, and k is an empirical constant (known as the Onsager slope) that incorporates both the electrophoretic (A) and asymmetry (B) effects. While Kohlrausch had previously described the square root dependence of conductance, it was Debye, Hückel, and Onsager who elaborated on *k*. Their work can be cast in terms of the equivalent conductance (in cgs units) of just the anion (λ_-) such that

$$\lambda_- = \lambda_-^0 - \left(\frac{z_- eF\kappa}{1800\pi} + \frac{e^2\kappa}{6\varepsilon k_B T} z_- z_+ \frac{2q}{1+\sqrt{q}} \lambda_-^0 \right) = \lambda_-^0 - \left(\frac{41.25}{\eta(\varepsilon T)^{1/2}} z_- + \frac{1.4\times10^6}{(\varepsilon T)^{3/2}} z_- z_+ \frac{2q}{1+\sqrt{q}} \lambda_-^0 \right) \sqrt{I} \qquad (15)$$

where F is the Faraday and

$$q = \frac{z_+ z_-}{z_+ + z_-}\left(\frac{\lambda_+^0 + \lambda_-^0}{z_+\lambda_+^0 + z_-\lambda_-^0}\right) \qquad (16)$$

Though these same historical terms often are used in descriptions of the electrophoresis of biological molecules, there are some differences that should be kept in mind: 1) the central ion is no longer one of the salt ions, 2) the ions have a finite size which is ignored in Equations 14-16 and 3) Equation 15 is, in theory, only valid for 1:1 electrolytes and for I < 0.001 M (Friedl et al., 1995) (Li et al., 1999).

In an attempt to reconcile these facts, Li and co-workers recently reapproached Debye-Hückel-Onsager theory using the Pitts equation to account for the effect of ionic size. They found

$$\lambda_- = \lambda_-^0 - \left(\frac{41.25}{\eta(\varepsilon T)^{1/2}} z^2 + \frac{1.4\times10^6}{(\varepsilon T)^{3/2}} z_- z_+ \frac{2q}{1+\sqrt{q}} \lambda_-^0\right)\frac{\sqrt{I}}{1+Ca\sqrt{I}} \qquad (17)$$

such that C is the first term in equation (12) and the electrophoretic effect now has a second order dependence on valence which has been noted both by Pitts and Li (Pitts, 1953). Neither, however, provides a physical explanation of its source. Interestingly, Edsall and Wyman give the same expression without the second order dependence (Edsall & Wyman, 1958). Nonetheless, the equation clearly predicts a weaker dependence of mobility ($\mu=\lambda F$) on ionic strength compared with the predictions from Equation 14. A comparison of the Equations 15 and 17 in the context of T4 lysozyme electrophoretic results is presented in Section 4.7.

As Bull pointed out, "the electrophoresis of a particle is closely related to the motion of a simple ion in an electrical field; ion conductance and electrophoresis are two aspects of the same phenomenon" (Bull, 1964). Thus, during the same years Onsager

was developing conductivity theory, Henry formulated equations for the electrophoretic effect in terms of the description of electrophoresis given in Smoluchowski's 1903 work. Contributions from Booth, Overbeek and Wiersema led to a more comprehensive treatment of mobility during the middle of the century (see section 4.5 for the detailed description of these) (Booth, 1950; Overbeek, 1943; Overbeek, 1950). Nevertheless, the complexity of the equations which govern the ion distribution, ion velocities, electrostatic potential and the hydrodynamic flow field around a particle in an applied electric field, called for something which conveniently became available around this time: the computer. O'Brien and White were amongst the first to develop a numerical solution and computer algorithm for solving the problem of electrophoresis (O'Brien & White, 1978). They decomposed the process of electrophoresis into two simpler cases: 1) calculation of the force required to move the particle in the absence of an applied field and 2) calculation of the force required to hold the particle stationary in the presence of a field. Their work is the basis for the boundary element model developed by Allison (Allison et al., 1997; Durant et al., 2002).

Allison, although making use of their two case scenario, takes the problem one step further by incorporating detailed crystallographic coordinates describing the shape of the protein and the position of its charges. The boundary element (BE) model details, in the context of T4 lysozyme, are discussed in Section 4.4.3. Previous work with the BE model was done using hen egg white lysozyme (HEL) (Allison et al., 1997) and some important aspects of those results are discussed here. Initially, ignoring ion relaxation, HEL mobilities were calculated by numerical solution of both the *linear* PB (to obtain the electrostatic potential) and Navier-Stokes equation *at a molecular surface* with an

exclusion radius of 0.45 nm (corresponding to a diffusion coefficient of 10.6 x 10^{-7} cm^2/s). The results did not agree with experimental values except at pH 6 (the results were given for pH 2-6). Mobilities were then recalculated by solution of the linear PB *at a molecular surface* (exclusion radius of 0.30 nm) and of the Navier-Stokes equation *at a Stern surface* (exclusion radius of 0.45 nm) but still ignored ion relaxation. Inclusion of this Stern layer, which "contains solvent and mobile ions that move with the polyion as a rigid body", gave somewhat better agreement, at least for pHs near neutrality (Allison & Tran V., 1995). Allison and coworkers, however, in readdressing the problem later, concluded that instead of using the Stern surface, the discrepancies could best be overcome by treating the electrostatics at the level of the *full* PB and including the effects of ion relaxation (Allison et al., 1997). It is important to note that the *molecular surface* at which the *full* PB was solved was defined for an exclusion radius of 0.45 nm, corresponding to the original Stern surface. However, by model definition, the *molecular surface* is considered "impermeable to penetration by salt and mobile ions" which is contradictory to the original justification for choosing 0.45 nm. The net valence is often more than the simple sum of the side chain charges and includes whatever charge might lie in the as yet ill-defined shell around the macroion where the PB should be solved. The *effective* valence as measured by MCE then, is purely a consequence of the nonconserved forces. Were electrophoretic and asymmetry effects to be absent and $\kappa a << 1$, $z_{eff}\, e$ would equal ζDa or, if small ions were not contributing to the electrokinetic potential, equal ze. However, at present these nonconservative effects cannot be eliminated. The work described in this dissertation has been designed to explore the

much less well understood area of intermediate κa values. This is an area particularly important to biological macroions.

CHAPTER III

MATERIALS AND METHODS

3.1 Protein Preparation

3.1.1 T4 Lysozyme Purification

E. coli strain RRI containing the various clones (courtesy of Brian Matthews) were stored at -80°C. In order to produce sufficient amounts of each mutant, a protocol was adapted from the literature (Dao-pin et al., 1991; Tsugita & Inouye, 1968). Protein samples were pure with respect to size and charge as assessed by SDS polyacrlyamide gel electrophoresis and capillary electrophoresis.

Wild Type (WT) and Single (SM), Double(DM), Triple Mutants (TM):

For the WT, SM (R119E), DM (K16E/R154E) and TM (R119E/K135E/K147E) proteins, frozen bacteria were streaked onto LB ampicillin plates and grown overnight at 37°C. The plates were then kept at 4°C until used, which was within 2 days in all cases. A single colony from the plate was used to both inoculate 100 mL of LBH broth (per liter: 10 g tryptone, 5 g yeast extract, 5 g NaCl, 1 mL of 1M NaOH, and 100 ug/mL ampicillin) and initiate a lysis plate as described below. The inoculated culture was grown overnight (10-14 hrs) at 37°C, after which it was diluted into 3 L of LB broth (per liter: 12 g tryptone, 5 g yeast extract, 10 g NaCl, 1 g glucose). The 3 liter cultures were then grown at 37°C on a shaker for aeration until the A_{595} reached 1.2-1.3. Samples were taken hourly and diluted for measurement such that the absorbance reading was less than

0.4. Growth to an A_{595} of 1.2 generally took about 5 hours. At this point, the incubator temperature was reduced to 30°C and 700 mg of isopropyl-1-thio-β-D-galactopyranoside (IPTG) was added (giving 0.2 mg/mL IPTG concentration) to induce lysozyme expression. After 1.5 hours, the cells were harvested by centrifugation at 15,000 g for 20 min at 4°C.

The yellow-orange supernatant was discarded except in the case of WT and SM preps where there was a significant amount of lysozyme in the supernatant. In this case the supernatant was dialyzed against nanopure water until the conductivity was below 1.5 mmhos/cm (newer units: mS/cm). Dialysis generally took overnight.

Concurrently, the pellet was resuspended in 100 mL of lysis buffer (0.1 M sodium phosphate pH 6.5, 0.2 M NaCl, 10 mM $MgCl_2$, 1 mM $CaCl_2$, and 1 mL of 0.5 M EDTA per 100 mL solution) and stirred at 4°C overnight. After this time, 1 mg of DNase I (Sigma Lot # 89H7606) and 1 mL of 1 M $MgCl_2$ were added to reduce the viscosity. The solution was stirred for 2 more hours at room temperature. The lysate was centrifuged for 80 minutes at 39,000 g to remove debris. The resulting supernatant was just slightly yellow. The pellet was discarded. The supernatant was either dialyzed, as described above or diluted to reduce the ionic strength. Both supernatants were treated identically thereafter.

The Pharmacia FPLC system was used to purify all samples. A Pharmacia XK26/20 column (18-1000-72) was packed with 50 mL of CM Sepharose Fast Flow (17-0719-10) beads (50 mg/mL gel binding capacity for Ribonuclease A) according to the manufacturer's directions. The weak cation exchange column was washed with 1X column volume (CV) of 100 mM NaOH , 3X CV of 1 M NaCl , and lastly 3X CV of

buffer A (10 mM sodium phosphate, pH 6.5 measured at 4°C or adjusted for). Once the post column pH and conductivity matched the pre-column values, the sample pH was adjusted to 7.0 with dilute HCl and loaded onto the column by using either a Pharmacia Superloop or direct application if the volume was larger. Once loaded, the sample was eluted with a salt gradient at a flow rate of 5-10 mL/hr, where the high ionic strength buffer was10 mM Phosphate, 300 mM NaCl pH 6.5. Initially, a 500 mL linear gradient was used, but the protocol was optimized in later purifications after the desired peak positions were identified. Optimization generally led to slopes (%gradient/mL) of 0.2-0.3 during elution of the desired protein and higher slopes prior to and after in order to reduce the length of the run and minimize the quantity of buffer consumed. Protein fractions, identified by absorbance at 280 nm, were each tested for activity as described below. The fractions with activity were pooled and dialyzed overnight against the buffer (50 mM sodium phosphate, pH 5.8 at 4°C) used as the initial buffer for the strong cation exchange step described next.

A Pharmacia HR 5/10 column (18-0384-01) was packed with 2 mL of Source 15 Sepharose Fast Flow (17-0944-10) beads (25 mg/mL gel or greater binding capacity) according to the manufacturer's directions. This strong cation exchange column was washed with 1X column volume (CV) of 100 mM NaOH , 3X CV of 1 M NaCl , and lastly 3X CV of buffer (50 mM sodium phosphate, pH 5.8). The dialyzed sample was loaded onto the column and eluted with a salt gradient, using a flow rate of 1 mL/min where the high ionic strength buffer was 50 mM sodium phosphate, 500 mM NaCl, pH 5.8. Optimization generally led to slopes (%gradient/mL) of 0.3-0.5 during elution of desired protein. Higher slopes were used prior to and after for the reasons described

above. Protein fractions, identified by absorbance at 280 nm, were each tested for activity as described below. The fractions exhibiting activity were pooled and concentrated to 2-5 mg/mL. Samples were stored in 50 mM sodium phosphate, 150 mM NaCl, 0.02 % sodium azide at pH 6.3. Yields ranged from 5 to 30 mg protein depending on the mutant.

Quadruple Mutant (QM):

Because of the low charge of the quadruple mutant protein (K16E/R119E/K135E/K147E) it cannot be purified by the same means as the other mutants. The strength of the interaction with the anionic column media (whether carboxylic or sulfonic acid) is insufficient for separation. Therefore, the procedure for QM purification differs from that given above following the first centrifugation.

After the initial centrifugation, the pellet was passed through a French press. The resulting solution/gel was centrifuged at 20,000 g for 30 min to remove debris. Ammonium sulfate was ground and added to the supernatant to give a 40% solution at 4°C. The solution was placed on ice for 15 min and then centrifuged at 15,000 g for 15 min and the pellet discarded. The T4 protein was precipitated from the supernatant by increasing the ammonium sulfate concentration to 80%. After 15 min at 4°C the solution was centrifuged at 10,000 g for 30 min and the supernatant discarded. The pellet was dissolved in 5 mL of 200 mM sodium phosphate buffer, pH 7.0.

A Pharmacia HiPrep 16/60 Sephacryl S100 gel filtration column (17-1165-01/ bed volume 120 mL) was equilibrated with same 200 mM sodium phosphate buffer. The sample was concentrated using Millipore UltraFree® Biomax centrifugal filter devices to 2-8% of the bed volume, loaded onto the column, and eluted with 10 mM potassium

phosphate, 150 mM KCl, pH 7.0 at 0.5 mL/min. The peak containing lysozyme eluted in about 9 hrs. The lysozyme-containing fractions were identified by their activity. These fractions were pooled and the QM lysozyme precipitated by adjusting to solution to 85% ammonium sulfate at 4°C. After centrifugation, the pellet was dissolved in an equal volume of the phosphate buffer. The sample was reapplied to the Sephacryl S100 gel filtration column and eluted as described before, resulting in a sample judged pure by SDS-PAGE and CE. This solution was concentrated and dialyzed into the storage buffer described above for the other proteins.

Lysis Plates:

These were used to test for transformed colonies. A lawn of E. coli RR1 transformed with an ampicillin-resistance-conferring plasmid (YRP7 Plasmid – courtesy of Dr. Clyde Denis) was grown on LBH glass plates containing ampicillin. The cells were killed by exposure to UV light and chloroform. Colonies believed to contain T4 lysozyme were subsequently innoculated onto these plates and incubated at 32°C. The plates were monitored for 4-48 hrs for the formation of halos indicative of lysozyme producing colonies.

The lysis plates were prepared by adding 100 uL of 50 mg/mL IPTG to each LBH plate (10 g tryptone, 5 g yeast, 5 g NaCl, 1 mL of 1 M NaOH, 15 g agar, 20 ug/mL thymine, 100 ug/mL ampicillin). This was overlain with a mixture of 0.5 mL of log or stationary phase cultures of the RR1/YRP7 and 2.5 mL of molten LBH soft agar (10 g tryptone, 5 g yeast, 5 g NaCl, 1 mL of 1 M NaCl, 7 g agar, 100 ug/mL ampicillin). The plates were incubated for 8-12 hrs at 37°C and then subjected to 60-120 seconds of UV irradiation (4 W, 254 nm) at a distance of 15 cm. One mL of chloroform was then placed

in the lids of the inverted plates and left at room temperature for 8-12 hrs in a fume hood. The plates were stored at 4°C until used.

Activity Assays:

These were used to asses the lysozyme content of fractions collected from the various columns used in the purification process.

Microcucuss Luteus - Initially, a protocol with *Micrococcus luteus* (previous name *Micrococcus lysodeikticus*) was used to identify T4 containing fractions. This method called for the addition of sample to a suspension of *Micrococcus luteus* (0.1 M potassium phosphate, pH 7.0; A_{280} = 0.8) and monitoring the decrease in turbidity at 450 nm as the lysozyme lysed the cells. This method, however, gave very limited lysis. E. coli cells are 300 times more sensitive and were therefore used utilized in later assays.

Escherichia coli - Glycerol stocks of DH5α E. coli (E. coli kindly supplied by Dr. Eric Schaller) were prepared according to Current Protocols in Protein Science, 1998, Section 5.2.6, vol. I. Five mL of nutrient broth (Sigma N7519, Lot 39H0536) was inoculated from glycerol stocks. This was grown overnight at 37° C to stationary phase (A_{600}=1.34). The cells were then diluted ten-fold and grown for about 5 hours longer, at 37° C on a shaker, until the A_{600}=1.4. The cells were pelleted and resuspended in 50 mM Tris-HCl, pH 7.0. This procedure was repeated three times. The suspension was placed in the freezer for one week. As reported by Tsugita, the assay does not work if the cells have not been frozen (Tsugita & Inouye, 1968). The cells were then aliquoted into 1.5 mL, preweighed microtubes and lyophilized over 2 days. The yield was about 600 mg of cells. These were stored at room temperature in a desiccator.

A standard activity solution (11 mg lyophilized E. coli, 10 mL of 50 mM Tris-HCl, pH 7.0) was prepared on the day of assay. The solution was diluted as needed to reach an $A_{350} \cong 0.8$ (Tsugita & Inouye, 1968). Three mL of the solution was placed in a cuvette and the decrease in the A_{350} was recorded every 10 seconds after 10-200 uL of sample was added. The activity varies with mutant. For example, in one experiment WT caused the A_{350} to decrease by 3.3/min·mg while SM caused a decrease of 5.2/min·mg. As has been reported, however, activities of T4 lysozyme are not always reproducible (Walter Baase, personal communication) and measurement of reaction rates as a function of substrate is not possible due to limited solubility of bacterial cell walls (Dao-pin et al., 1991). Therefore, this assay was used only qualitatively to distinguish lysozyme containing fractions.

3.1.2 Ribonluclease Sa

Ribonluclease Sa WT and mutant proteins were kindly supplied by Dr. Nick Pace (Texas A&M University). Their purification was done by Stephanie Newsom (Texas A&M University, Department of Medical Biochemistry and Genetics). The mutants used were designated 2K (D17K/E41K) and 5K (D17K/E41K/D1K/D25K/E74K). A molar extinction coefficient of 12,045 M^{-1} cm^{-1} at 280 nm was used in concentration calculations.

3.1.3 α-Chymotrypsin

α-Chymotrypsin was purchased from Sigma (C-7762, lot 27H7010). The samples were 3X crystallized and used as supplied.

3.2 Instrumentation

3.2.1 Membrane Confined Electrophoresis (MCE)

The membrane confined electrophoresis apparatus allows measurement of both mobility and effective valence. The MCE instrument has been described previously (Ridgeway et al., 1998; Laue et al., 1991; Laue et al., 1996). Briefly, macroions are confined in a 2x2x4 mm quartz cuvette whose ends are sealed with semi-permeable membranes as shown in Figure 3.2.1.1. An electric field (E) is established between the membranes, and either a moving boundary (for mobility measurements) or the formation of a steady-state gradient (for valence measurements) is monitored using an imaging spectrophotometer. This work will focus on the steady state method. A 10 mL/hr buffer flow past the analysis chamber provides constant solvent conditions for electrophoresis. Though the flow past each membrane was matched as best as possible, previous work showed that a mismatch does not have a large effect on the resulting concentration distribution ($\sigma \pm 5\%$ in the extreme mismatch) for the range of fields used in these experiments (Wooll, 1996). It is important to note that the results presented in this dissertation are the first which were all obtained using a 0.4 cm long (instead of 0.2 cm) cuvette. This provides more data points per experiment for Nonlin fits. The prototype device used is shown in Figure 3.2.1.2.

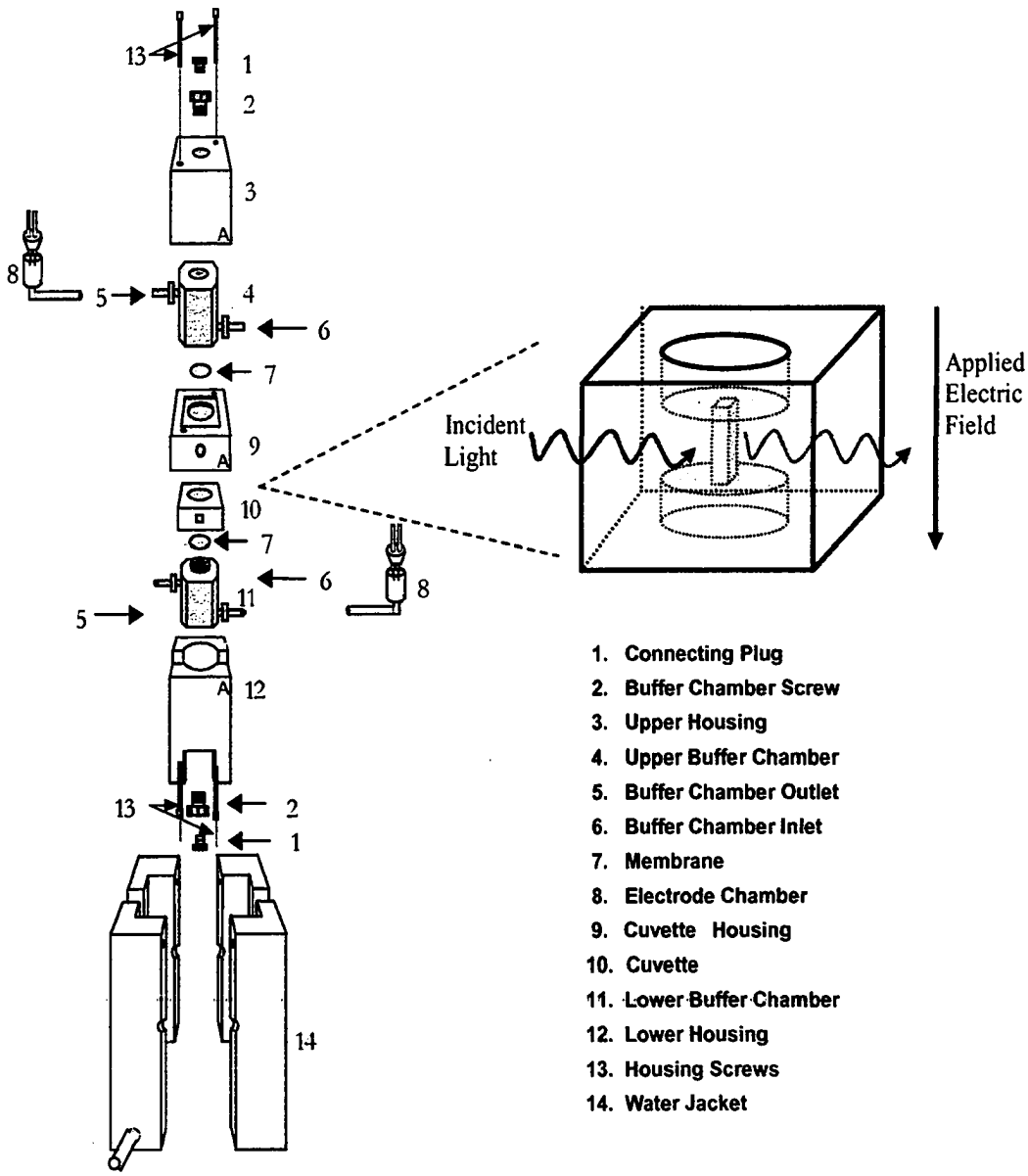

Figure 3.2.1.1: The MCE water-jacketed system. Above left shows the components of the set up (left-hand detail done by Daryl Lyons). The quartz cell (10) which confines the macroion (yellow) is shown in detail on the right with the membranes (gray) shown on top and bottom.

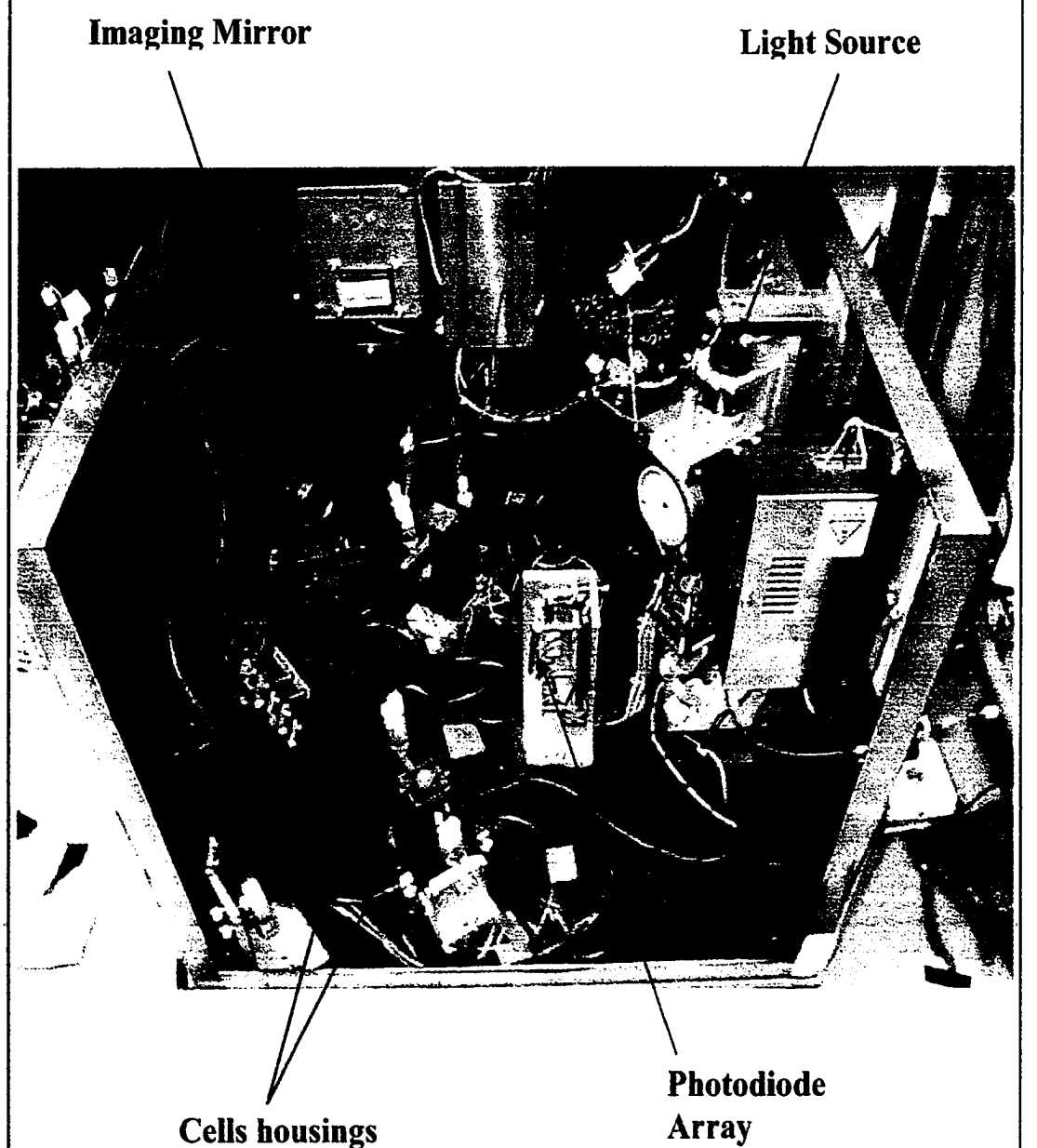

Figure 3.2.1.2: The MCE prototype used in this work. The light source can be seen on the right and the two cell housings on the left. Center is the photodiode array. The device is covered during measurement to exclude room light.

Steady-state electrophoresis is analogous in many respects to sedimentation equilibrium. A concentration gradient of the macroion is established down the cell due to an externally applied force. Due to the concentration gradient, there is a diffusional back-flow which eventually balances the electrophoretic flow. Because current is passing through this system, however, the result is a steady-state concentration gradient and not an equilibrium gradient. It is this flow of current which complicates the theory beyond that of centrifugation (discussed in Section II).

Determination of mobility (u) and valence (z_{eff}) from steady-state measurements

At steady state, all system properties, including the concentration gradient of any membrane-confined species, are invariant with time. For a system with a single-species macroion component, the equation describing the macro-ion concentration gradient at steady state is

$$c = a_o e^{\sigma_c (x - x_0) - 2B^* M c} \quad (18)$$

where x is the position in cm; x_0 is the arbitrary reference position; c is the macro-ion concentration at x; $a_0 = c_0 e^{2B^* M c_0}$ where c_0 is equal to c at x_0; σ_c, in units of cm^{-1}, is the exponential coefficient that characterizes the steady-state concentration gradient in the limit as c approaches zero; M is the molar mass, in g/mol, of the macro-ion; and B^* is the apparent second virial coefficient that accounts for the apparent influence of c on the exponent of Equation 18 (Laue et al., 1990). That influence can include, but *is not limited to*, the effect that c has on the thermodynamic nonideality of the system. For example, a shallow gradient of the small mobile ions will result in a shallow gradient in

the electric field. This may alter the macroion concentration distribution in a manner analogous to the effects of thermodynamic nonideality (Moody & Shepard, 2002). Fitting data to a model that includes B^* allows for such a gradient and improves the accuracy of the determination of σ_c.

The time needed for the concentration distribution to reach steady state (generally 8-9 hrs) was judged using MATCH (courtesy of Dr. David Yphantis, available at the RASMB archive: ftp://www.bbri.org/rasmb). Absorbance readings were truncated at each end to remove points distorted by reflections from the membranes. Typical results are shown below in Figure 3.2.1.2. Using data from systems judged to be at steady state, nonlinear least squares analysis was used to determine σ_c (Laue et al., 1991; Laue et al., 1996). For each protein, σ_c was determined for a minimum of 5 fields. In all cases, the data fit adequately to a model consisting of a single, nonideal species (i.e. B^* nonzero). Diagnostic graphs of σ_c as a function of E and σ_c/E as a function of E were constructed to test for bulk solvent flow (see Results, Figure 4.1.4.3). Tests for bulk fluid flow were also conducted using the neutral molecule, rhodamine dextran, as described previously (Laue et al., 1991).

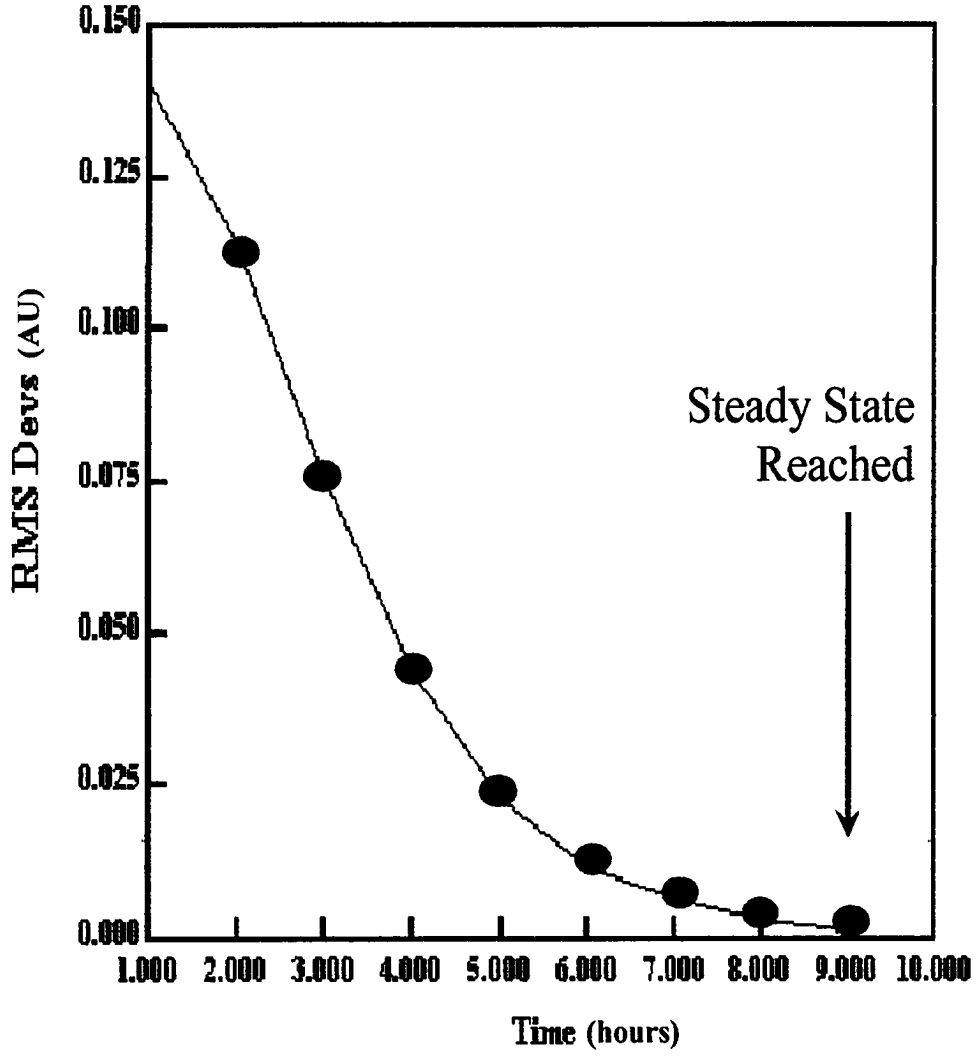

3.2.1.3: Approach to SSE. Steady state is reached after about 9 hours for T4 lysozyme in this representative plot. All SSE measurements were taken after a minimum of 10 hrs.

The effective charge in protonic units is defined as

$$z_{eff} = \frac{RT\sigma_c}{EF} = \frac{k_B T\sigma_c}{Ee} \qquad (19)$$

where R is equal to 8.314 J/mol·K, F is the Faraday constant in C·mol, E is the electric field in V/cm. The mobility is then calculated by the relation

$$\mu = \frac{k_B T\sigma_c}{fE} \cdot \text{constant} = \frac{z_{eff} e}{f} \cdot \text{constant} \qquad (20)$$

where f is the ordinary translational frictional coefficient and the constant is 10^7 erg/C·V. Therefore, while valence determinations by SSE do not require any prior knowledge, mobility calculations from SSE data do require independent hydrodynamic experiments. Conversely, calculations of valence from mobility determinations require an independent assessment of f.

3.2.2 Capillary Electrophoresis

Capillary zone electrophoresis (CZE) was used to both check for sample purity and to measure mobility. Capillary isoelectrophoric focusing (CIEF) was used to verify the isoelectric point (pI) of purified proteins.

Both techniques were carried out on a P/ACE 5510 apparatus (Beckman Coulter, Fullerton , CA) equipped with UV absorbance detection. The data collected at 214 nm were analyzed using the P/ACE Station program version 1.2. For CZE, purity checks were usually done at a single field and the mobility was calculated by

$$\mu = \frac{l_t l_d}{Et} - \mu_{EOF} \quad (21)$$

where l_t is the total length of the capillary in cm, l_d is is the length of the capillary to the detector window in cm, t is the time in seconds required for a sample to pass the detector window after injection, and μ_{EOF} is the mobility of the neutral marker. For results using multiple fields, the mobility (μ) was calculated by plotting sample velocity (V_{EOF} subtracted from the apparent sample velocity) as a function of field strength (see Figure 4.1.3.2 in Results as an example). The slope of a linear least squares fit of these data is the sample mobility, and an estimate of the precision is reported as the error of the slope. This procedure provides a better assessment of the accuracy of the mobility than single field calculations. While the precision of the mobility calculated by this method is ~10%, the reproducibility of the mobility at any given field is within 1 to 4 %, which is in the range typically reported for CE errors (Stellwagon et al., 1997). The CE effective charge was then calculated from the relation

$$z_{eff} = \frac{\mu f}{e \cdot \text{constant}} \qquad (22)$$

3.2.3 Analytical Ultrcentrifugation

Sedimentation velocity experiments were conducted to 1) determine the diffusion coefficient, D, 2) confirm the hydrodynamic characteristics of the mutants were unchanged in the ionic strength range used in the MCE experiments and 3) to further verify sample homogeneity. The sedimentation of a particle can be described by the following equation

$$\frac{s}{D} = \frac{M\left(1-\bar{v}\rho\right)}{RT} \qquad (23)$$

where s is Svedberg, M is the anhydrous molecular weight, $\bar{\nu}$ is the partial specific volume, ρ is the density of the solution. Sedimentation velocity experiments were conducted using a Beckman Coulter XLA analytical ultracentrifuge with absorbance detection. Data were edited using WinReedit and analyzed using WinNonlin (both programs are available at ftp://alpha.bbri.org/rasmb/spin). The programs Dc/DtPlus (courtesy John Philo, Allied Protein Science) and SEDFIT (courtesy Peter Schuck, NIH) were used to fit the data.

Sedimentation equilibrium experiments were used to 1) verify the molecular weight of the purified species, 2) assess the thermodynamic nonideality of the system and 3) in the case of α-chymotrypsin, to determine the association constant. The program WinNONLIN (courtesy David Yphantis, University of Connecticut) was used to fit all data (ftp://alpha.bbri.org/rasmb/spin/ms_dos/uconn_auf/).

3.2.4 Dynamic Light Scattering

A Protein Solutions DynaPro was used to measure the hydrodynamic radius (Rh) of the proteins. For particles of <5% of the wavelength of incident light (2nm/830nm<1%), the intensity of scattering is given by Lord Rayleigh's equation (van Holde et al., 1998). Because of the sinusoidal dependency of intensity, the angle between the incident monochromatic, plane polarized light and the direction of detection of scatter is 90°. The data was analyzed using DYNAMICS® version 4.0 software.

3.3 Experimental

3.3.1 Buffers and Membranes

As buffers are critical to these experiments, a thorough documentation is included here.

Table 3.3.1.1: Buffer Properties.

Buffer	Formula	pK_{a1}	pK_{a2}	FW
BTP	$C_{11}H_{26}N_2O_6$	6.8	9.0	282.3
Tris	$C_4H_{11}N_1O_3$	8.1	-	121.1
BT	$C_8H_{19}N_1O_5$	6.5	-	209.2
KAcetate	$C_2H_4O_2$	4.8	-	98.2

Table 3.3.1.2: Buffer Compositions.

Buffer	**mM BTP**	**mM KCl**	**pH**
1	10	10	7.5*
2	10	20	7.5
3	10	40	7.5
4	10	80	7.5
5	10	100	7.5*
6	10	150	7.5*
	mM Acetate	**mM KCl**	**pH**
7	10	100	4.3
8	10	200	4.3
	mM BT	**mM KCl**	**pH**
9	10	100	7.5

*Some AUC experiments were done in this buffer at other pHs as will be noted in the discussion. Many MCE experiments were also done at other pHs but this was before the small ion gradient problem at these pHs was demonstrated. Thus, these results are not presented.

Buffer pH was determined using an Orion 520A pH meter. Adjustments to pH were made with same-ion species acid or base. Specific conductance was measured with a VWR 1054 conductivity meter and a platinum (> 5 mS/cm) or gold (< 5 mS/cm) probe.

The meter was calibrated prior to measurement using VWR calibration standard solutions (Lot # 23226-625). For convenience the properties of the buffers used are given in Table 3.3.1.2 above. The materials used to make the buffers are given in Table 3.3.1.3 below.

Table 3.3.1.3: Buffer Material List.

Buffer/Salt	Dates Used
BTP Sigma Lot # 24H5704	10/14/00-07/15/01
BTP Sigma Lot # 90K5428	07/16/01-02/20/02
Tris J.T.Baker Lot # N30597	10/14/00-02/22/02
BT Fisher Lot # 934477	10/14/00-02/22/02
KCl J.T.Baker Lot # N12353	10/14/00-05/26/01
KCl J.T.Baker Lot # V05615	05/27/01-08/08/01
KCl J.T.Baker Lot # V15596	08/09/01-12/10/01
KCl J.T.Baker Lot # N12333	12/11/01-02/20/02
KAcetate Fisher Lot # 004987	12/14/01-01/25/02

The membranes used were either SpectraPor or BioDesign. In either case, the membranes were initially boiled in 1mM EDTA, 2% $NaHCO_3$ for 10 minutes and then rinsed in deionized H_2O. In addition to this, the membranes used in some experiments were stirred overnight in 0.1 M MES, 1 mM 1-ethyl-3-(3-dimethylaminoproply) carbodiimide, 1 mM ethanolamine, pH 4.5. The treatment, similar to that used in surface plasmon resonance coupling, neutralizes any residual carboxyl groups on the dialysis membranes as shown in Figure 3.3.1.1.

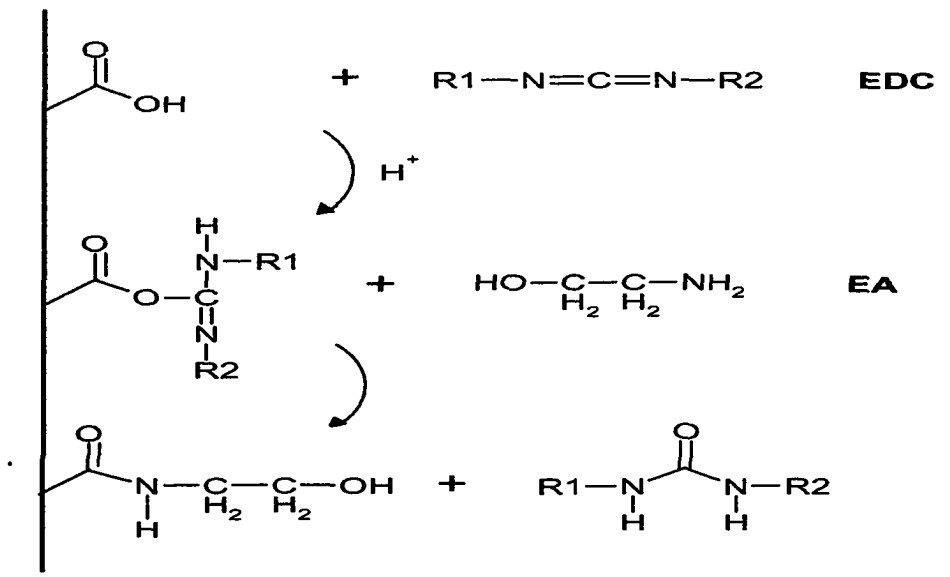

Figure 3.3.1.1: Membrane Neutralization. The EDC activates the carboxyl, forming an ester. Subsequent coupling with the nucleophilic amino group of EA releases EDC as a soluble urea derivative

3.3.2 T4 Lysozyme

Analytical Ultracentrifugation

In all experiments using T4 lysozyme a partial specific volume of 0.74 g/ml was used (Tsugita & Inouye, 1968). Calculation of this quantity with Sednterp also gave 0.74 g/mL. The measured density for buffers 1,5 and 6 was found to vary by less than 0.5% and thus the average value of 1.003 ± 0.003 g/ml was used. The density measurements were made at 20 °C using a DMA02D Mettler/Paar Precision Density Meter. The average measured viscosity of buffers 1, 5 and 6 was 1.013 cp. The viscosity was measured at 20 °C on an Anton Paar Automated MicroViscometer (AMVn).

Sedimentation Velocity

All experiments were done at 60,000 rpm, 20°C using a four-hole, titanium rotor and sedimentation velocity cells assembled with 12-mm double-sector charcoal-filled epon centerpieces.

Table 3.3.2.1: Sedimentation Velocity Experiments with T4 Lysozyme.

#	Experiment[a]	Sample[b]	Buffer[c]	Concentration (mg/mL) Sedfit
1	070600/134420	WT*	6 (pH 7.0)	0.93
2	110100/110012	WT	5	0.87
3	013001/130747	SM	5, 6	0.70, 0.74
4	042401/164704	SM	1 (pH 6.5), 9 (pH 6.5), 5 (pH 6.5)	0.17,0.22, 0.22
5	042301/103420	SM	1 (pH 6.5), 9 (pH 6.5), 5 (pH 6.5)	0.56, 0.46, 0.40
6	042001/163059	SM	1 (pH 6.5), 9 (pH 6.5), 5 (pH 6.5)	0.68, 0.46, 0.38
7	041901/183353	SM	1 (pH 6.5), 9 (pH 6.5), 5 (pH 6.5)	1.21, 1.05, 1.22
8	013001/130747	TM	5	0.62

[a]Experitmental date and number
[b]WT* is the cysteine free wild type variant (C54AC97T)
[c]Numbers refer to those given in Table 3.3.1.2

Sedimentation Equilibrium

All experiments were done at 20°C using 3 mm, long columns with quartz windows.

Table 3.3.2.2: Sedimentation Equilibrium Experiments with T4 Lysozyme.

#	Experiment[a]	Sample[b]	Buffer[c]	rpm x 1,000
1	071600/163835	WT*	6 (pH 7.0)	18, 25, 36
2	110900/153655	WT	5	18,25,36

[a]Experitmental date and number
[b]WT* is the cysteine free wild type variant (C54AC97T)
[c]Numbers refer to those given in Table 3.3.1.2

Dynamic Light Scattering

Experiments were done at 20 °C in either 10 mM sodium phosphate, 150 mM KCl, pH 7.5 or 10 mM BTP, 100 mM KCl, pH 7.5. After dialysis against the appropriate buffer, samples were passed through a 20 μm filter before measurement. Triplicate measurements in each buffer were taken. Protein concentrations ranged from 0.7 to 1.2 mg/ml.

Capillary Electrophoresis

CZE was carried out at 20 °C with an eCap® bare silica or neutral capillary. Benzyl alcohol (0.001%) was used as an EOF marker. Capillaries were 27 or 37 cm in total length (20 or 30 cm to detector) with internal diameters of 50 μm. Voltages within the linear range of Ohm's law plots were used (beyond this range Joule heating becomes a problem). Samples were dialyzed overnight against the running buffer. Final sample concentrations were generally 1 mg/mL. Capillaries were rinsed at 20 psi for 2 min with deionized water and 5 minutes with running buffer before each run. A 2-4 second hydrodynamic sample injection time at 0.5 psi was used. For a 37 cm capillary under these conditions, 3.3 ng of sample was injected in a 3 second injection (see Appendix for details).

The CIEF was done according to directions in the Beckman CIEF Kit (477490). In brief, a 27 cm neutral capillary was installed, rinsed with 10 mM phosphoric acid for 2 minutes (20 psi), 0.2 μm filtered deionized water for 10 minutes, and then filled with an ampholyte/protein solution. The ends of the capillary were placed in the analyte (91 mM phosphoric acid) and catholyte (20 mM NaOH). The proteins were then focused by applying an electric field of 500 V/cm (13.5 kV for the 27 cm capillary) for 2 minutes after which the proteins were mobilized past the detector by additionally applying a low pressure (0.5 psi). The protein markers used were ribonuclease A, carbonic anhydrase II, β-lactoglobulin A, and a cholecystokinin (CCK) flanking peptide whose pIs were 9.45, 5.90, 5.1, and 2.75 respectively.

Membrane Confined Electrophoresis

Experiments were conducted at a controlled temperature of 20.0 ± 0.1 °C using16 μL of a solution containing 1.5-2.5 mg/mL protein. The cuvette was siliconized with 10% Surfacil in toluene before each loading. This creates a hydrophobic surface that eliminates preferential interaction of cations with the walls of the cuvette. Samples were dialyzed against the experimental buffer after being loaded into the MCE. Electric fields covering the broadest possible range were used. However, the range is limited to those fields which do not 1) produce too shallow a gradient (low fields), 2) too steep a gradient (high fields) or 3) cause Joule heating (high fields). The fields used were randomized temporally.

Table 3.3.2.4: MCE Experiments with T4 Lysozyme.

#	Sample[a]	Buffer[b]	E (V/cm) Range
1	WT*	1	0.05-0.40
2		5	0.20-0.60
3		6	0.10-0.50
4	WT	1	0.05-0.35
5		5	0.25-0.60
6		6	0.15-0.50
7	SM	1	0.10-0.24
8		5	0.25-0.50
9		6	0.15-0.45
10	DM	1	0.10-0.40
11		5	0.20-0.55
12		6	0.20-0.70
13	TM	1	0.20-0.60
14		5	0.70-1.10
15		6	0.20-1.00
16	QM	1	0.25-0.60
17		5	NA
18		6	NA

[a]WT* is the cysteine free wild type variant (C54AC97T)
[b]Numbers refer to those given in Table 3.3.1.2

3.3.3 Ribonuclease Sa

Analytical Ultracentrifugation

Sedimentation Velocity

Table 3.3.3.1: Sedimentation Velocity Experiments with RNase Sa.

#	Experiment[a]	Concentration (mg/mL)	Buffer[b]
1	061501/125632	0.61	5
2	061601/130140	0.49	5
3	061701/145400	0.25	5

[a]Experitmental date and number
[b]Numbers refer to those given in Table 3.3.1.1.

Dynamic Light Scattering

Experiments were done at 20 °C in 10 mM BTP, 100 mM KCl, pH 7.5. After dialyzing against the appropriate buffer, samples were passed through a 20 μm filter before measurement. Protein concentrations of 1-2 mg/mL were used.

Capillary Electrophoresis

CZE was carried out at 20 °C with an eCap bare silica or amine coated capillary. The current was reversed in the case of the negatively charged WT and the 2K mutant. Benzyl alcohol (0.01%) was used as an EOF marker. Capillaries were 27 to 47 cm in total length with an ID of 50 um. Voltages within the linear range of Ohm's law plots were used. Samples were dialyzed overnight against the running buffer. The amine coated capillaries were regenerated by rinsing (5 min, 20 psi each) with 1 M HCl, water, 1 M NaOH, water again and amine regeneration solution (Beckman Coulter 477433, Lot # S107169) at the beginning of each day. Between data collection, the capillary was rinsed at 20 psi with 0.1M NaOH, water, amine regeneration solution (each for 1 min) and running buffer (2 min). This produced both a very stable baseline and current. A 3

second hydrodynamic sample injection time at 0.5 psi was used. Depending on the capillary length and voltage, a run lasted between 15 and 50 min.

Memebrane Confined Electrophoresis

MATCH indicates steady-state is reached after about 9 hours.

Table 3.3.3.2: MCE Experiments with RNase Sa.

Sample	Buffer[a]	E (V/cm) Range
WT	5	0.10 - 0.50
2K	5	0.25 - 0.60
5K	5	0.25 - 0.50

[a]Numbers refer to those given in Table 3.3.1.2.

3.3.4 α-Chymotrypsin

Analytical Ultracentrifugation

Sedimentation Equilibrium

The sample was determined by Match to be at equilibrium after 25 hours. Interference optics and sapphire windows were used in all cases. Because of the much higher association constant expected at 200 mM salt, lower protein concentrations were used than in the case of 100 mM salt.

Table 3.3.4.1: Sedimentation Equilibrium Experiments with α-Chymotrypsin.

#	Experiment[a]	Buffer[b]	Concentration (mg/mL)	rpm X 1,000
1	121401/152558	7	1.0,0.3,0.1*	32, 34, 36*
2	011502/165454	7	7.0, 2.3, 0.3	20, 32, 42
3	011502/165454	8	1.0,0.3,0.1	20, 32, 42

[a] Experitmental date and number

[b] Numbers refer to those given in Table 3.3.1.2

*Admittedly, this is too narrow a range in rpm and the concentrations are a bit low to expect a significant dimer population. However the desire was to reproduce exactly the experiments of Ford and Winzor.

Dynamic Light Scattering

Experiments were done at 20 °C in 10 mM potassium acetate, 100 mM KCl, pH 3.9. After dialyzing against the appropriate buffer, samples were passed through a 20 μm filter before measurement. Protein concentration used was 1 mg/mL.

Memebrane Confined Electrophoresis

The membranes were equilibrated with running buffer for 20 min prior to loading sample. The results were obtained in three experimental phases and have thus been grouped as experiment 1, 2, and 3 as described below.

Table 3.3.4.2: MCE Experiments with α-Chymotrypsin.

Experiment	Concentration (mg/mL)	Buffer	E (V/cm) Range
1	1.2	7	0.10 - 0.30
2	7.0	7	0.05 - 0.20
2	1.0	8	0.10 - 0.30
3	2.7	8	0.10 - 0.40

Experiment 1

Measurements in 100 mM KCl were made from the same stock as that used to do the AUC experiments. Thus, channel A of AUC experiment 121401/152558 is identical with that used here. Derivatized BioDesign (Prep #3: 10/20 EDC/EA) membranes were used.

Experiment 2

In this case, samples used in MCE were taken directly from the AUC cells (channel A, the most concentrated) once the sedimentation equilibrium (Experiment 011502/165454) run was complete. Derivatized BioDesign (Prep #3: 10/20 EDC/EA) membranes were used for all the 200 mM data and most of the 100 mM data. For the final 2 MCE measurements at 100 mM KCl, the BioDesign membranes stock was depleted and

Spectrapor Biotech (lot #31260, 8K MWCO) membranes were used instead. These membranes behave similarly to those of BioDesign in nitrate tests (Sue Chase, personal communication, see Appendix).

Experiment 3

Only data from samples in 200 mM KCl was collected. An initial protein concentration of 4.5 mg/mL was used but was lowered to 2.7 mg/mL after observing precipitation. A test for small ion gradients with nitrate was done at that time (see Appendix).

3.4 pK_a Values

In order to calculate the formal charge, it is necessary to have estimates of the pK_a values of the titrable groups. Calculation of pK_a's is complicated by their dependence on ionic strength, temperature, macroion charge, and the potential for ion pair formation (Matthew et al., 1985). Consequently, there is uncertainty in the calculated formal charge.

For T4 lysozyme, I attempted to estimate the uncertainty by calculating the formal charge using various estimates of the pK_a values. The formal charge is reported as an average of three calculations at pH 7.5 and the error estimated for the 95% confidence level. The pK_a values used are given in Table 1. The set 1 values are taken from D. E. Anderson (1992 thesis dissertation). The set 2 and set 3 values are general textbook values (Segel, 1976) combined with the NMR values for His31 and Asp70, which are believed to form a salt bridge (Anderson et al., 1990; Anderson, 1992). The values used for RNase Sa were from Laurents et al. (Laurents et al., 2003). No pKas are available for the 2K protein and the WT values overestimate the observed pI of 3.5 by 0.4 units.

Table 3.4.1: pK_a Values for T4 Lysozyme Valence Calculations

SET 1			
Residue	pK_a	Residue	pK_a
Glu5	3.8.	Asp72	3.4
Asp10	0.4	Asp89	4.0
Glu11	5.4	Asp92	2.5
Asp20	3.6	Glu108	4.6
Glu22	3.8	Asp127	3.4
His31	9.05	Glu128	3.7
Glu45	3.8	Asp159	3.4
Asp47	3.0	Arg	12
Asp61	3.6	Lys	12
Glu62	2.9	Tyr/Csy[a]	-
Glu64	4.4	N-term	7.35
Asp70	0.5	C-term	3.9

[a] Cys and Tyr are not considered titrable in this set

SET 2		SET 3	
Residue	pK_a	Residue	pK_a
Asp70	0.5	Asp70	0.5
His31	9.1	His31	9.1
Asp	3.9	Asp	4.5
Arg	12.5	Arg	12.0
Cys	8.3	Cys	9.3
Glu	4.2	Glu	4.6
Lys	10.5	Lys	10.4
Tyr	10.1	Tyr	9.7
N-term	7.3	N-term	7.3
C-term	3.9	C-term	3.9

Table 3.4.2: pK_a Values for RNAse Sa Valence Calculations

Residue	pK_a (WT/5K)	Residue	pK_a (WT/5K)
Asp1	3.44/Lys	Asp79	7.37/6.06
Glu14	5.02/2.83	Asp84	3.01/2.98
Asp17	3.72/Lys	His85	6.35/6.09
Asp25	4.87/Lys	Asp93	3.09/3.00
Asp33	2.39/2.12	Lys	10.5
Glu41	4.14/Lys	Tyr[a]	11.5/11.13
His53	8.27/7.39	Arg	12.0
Glu54	3.42/2.26	Csy	disulfide bond
Glu74	3.47/Lys	N-term	9.14/7.30
Glu78	3.13/3.02	C-term	2.44/2.36

[a] For WT protein, Tyr30 pKa = 11.30, Tyr49 = 10.6, and all other Tyr were given as 11.5 or greater. No measurements were made for the 5K and so an average of the WT values was used.

3.5 Limiting Molar Conductivity

The limiting molar conductivity of BTP, needed in the BE modeling, can be described by the equation

$$\frac{1}{\Lambda}=\frac{1}{\Lambda^{\infty}}+\frac{c\Lambda}{K_D\Lambda^{\infty 2}} \qquad (24)$$

where the molar conductivity of the electrolyte (Λ) is equal to $\frac{k}{c}$, c is the molar concentration, k is conductivity, K is the equilibrium constant, and Λ^{∞} is the molar conductivity of the electrolyte at infinite dilution (Castellan, 1983). Because there are multiple conducting species of BTP at pH 7.5, the situation is more complex than with Tris for example. The limiting molar conductivity of each electrolyte is

$$\Lambda^{\infty}=\frac{\sum_i c_i \nu_i \lambda_i^{\infty}}{c_{salt}} \qquad (25)$$

where λ^{∞} is the limiting molar conductivity of species *i*, c is the concentration, ν_i is the stoichiometric coefficient of species *i*, and the (*i*) ion species accounted for are $BTP2H^{+2}$, $BTPH^{+1}$, and Cl^- with 83% of the solution in the basic form ([B]/[A]=5.012). The conductivity measurements (k) were made using a gold probe at 23 °C with a VWR 1054 meter. The conductivity of water (k_w) was subtracted from the measurements.

CHAPTER IV

RESULTS

4.1 T4 Lysozyme

In addition to the electrophoretic results, several other pieces of information were necessary to meet objectives set forth in the introduction. Sedimentation velocity experiments were conducted to 1) determine the diffusion coefficient, D, 2) confirm that the hydrodynamic characteristics of the mutants were unchanged in the ionic strength range used in the MCE experiments and 3) to verify sample homogeneity. Sedimentation equilibrium experiments were used to 1) verify the molecular weight of the purified species, 2) assess the magnitude of thermodynamic nonideality that affect MCE experiments and 3) in the case of α-chymotrypsin, to determine the association constant. Density, viscosity and dynamic light scattering measurements provided parameters used in the application of the DHH, Booth and BE models.

4.1.1 Analytical Centrifugation

Sedimentation Velocity

The data were in many cases fit with both DcDtPlus and a newer program, Sedfit, as is shown in Table 4.1.1.1. Loading concentrations were determined from best fit A_{280} values (analysis program: Sedfit) using an extinction coefficient of 1.28 mL/mg-cm and a pathlength of 1.2 cm. No concentration dependence of the fitting parameters was observed indicating that neither hydrodynamic nor thermodynamic nonideality was

significant. Thus, D is apparently independent of concentration in the range of concentrations used. The partial specific volume ($\bar{v}$) used in fitting was 0.74 mL/g (Tsugita & Inouye, 1968). Fits using Sedfit with the SM data in 10 mM BTP, 100 mM KCl gave an average sedimentation coefficient (s) of 1.94 ± 0.06 s and an average translational diffusion coefficient of 10.2 ± 0.7 x 10^{-7} cm^2/s (95% confidence interval for both). These values are highlighted in Table 4.1.1.1. This value of D was used in subsequent calculations of mobility and in BE modeling. The diffusion coefficients for WT and TM proteins in the same buffer were within error of the SM results and thus it was concluded that, as expected, the mutations did not lead to variations in the hydrodynamics of the macromolecule. The average diffusion coefficients for SM in 10 mM BTP with either 10 mM KCl or 150 mM KCl (9.4 x 10^{-7} cm^2/s and 9.5 x 10^{-7} cm^2/s cm^2/s respectively) were within error of those at 10 mM BTP, 100 mM KCl. Therefore, in the range of 10 to 150 mM KCl, no ionic strength dependence of the diffusion coefficient was observed. Our hydrodynamic data are consistent with T4 lysozyme crystallographic studies at low, medium and high ionic strengths, which showed the crystal structures were very similar (Bell et al., 1991).

Additionally, D was calculated by combining the sedimentation velocity and sedimentation equilibrium data, using the equation $D = sRT/M_b$, where R is the gas constant, and M_b is the buoyant molar mass determined from $M_b = \sigma RT/\omega^2$ (Laue, 2002). Here, σ is the exponential coefficient for the concentration gradient in the analytical ultracentrifuge and ω is the angular velocity. This method circumvents uncertainty associated with $\bar{v}$ and gives a diffusion coefficient within error of the above value (10.2 ± 0.6 x 10^{-7} cm^2/s).

Table 4.1.1.1: Sedimentation Velocity Results for T4 Lyszoyme.

#	Sample	Buffer	Conc. (mg/mL)	Fitting Program	S ($\times 10^{-13}$ s)	rms	D ($\times 10^{-7}$ cm^2/s)	MW (g/mol)
1	WT*	6 (pH 7.0)	0.93	Sedfit	1.86	7.72E-3	9.03	18,586
				DcDtplus	1.73	6.18E-2	8.78	18,750
2	WT	5	0.87	Sedfit	1.96	1.02E-2	9.00	19,705
				DcDtplus	1.78	7.10E-3	9.73	17,380
3	SM	5	0.70	Sedfit	1.86	4.24E-3	9.46	17,740
		6	0.74	Sedfit	1.86	9.96E-3	9.54	18,960
4	SM	1 (pH 6.5)	0.17	Sedfit	2.01	6.03E-3	8.03	22,570
		9 (pH 6.5)	0.22	Sedfit	1.84	5.14E-3	10.66	15,558
		5 (pH 6.5)	0.22	Sedfit	1.95	4.78E-3	10.06	17,507
5	SM	1 (pH 6.5)	0.56	Sedfit	1.90	6.93E-3	8.47	20,259
				DcDtPlus	1.99	1.20E-3	11.42	16,680
		9 (pH 6.5)	0.46	Sedfit	1.96	5.92E-3	9.14	19,404
				DcDtPlus	1.86	7.98E-3	13.26	13,410
		5 (pH 6.5)	0.40	Sedfit	1.94	5.22E-3	9.81	18,063
				DcDtPlus	1.86	5.18E-3	14.38	12,340
6	SM	1 (pH 6.5)	0.68	Sedfit	1.95	8.51E-3	8.95	19.645
		9 (pH 6.5)	0.46	Sedfit	1.98	3.45E-3	10.77	16,586
		5 (pH 6.5)	0.38	Sedfit	1.95	3.98E-3	10.86	16,212
7	SM	1 (pH 6.5)	1.21	Sedfit	1.90	8.35E-3	9.91	17,354
		9 (pH 6.5)	1.05	Sedfit	1.92	8.08E-3	9.19	18,919
		5 (pH 6.5)	1.22	Sedfit	1.91	2.89E-2	10.16	16,987
8	TM	5	0.62	Sedfit	1.94	3.94E-3	9.61	18,247
				DcDtPlus	1.69	6.98E-3	9.50	16,960
						Average:	9.99	16,878
						Average Sequence:		18,611

Sedimentation Equilibrium

As shown in Table 4.1.1.2, the measured molecular weights were in good agreement with the molecular weights of 18,601 and 18,633 calculated from sequence for WT* and WT, respectively.

Table 4.1.1.2: Sedimentation Equilibrium Results for T4 Lysozyme.

#	Sample[a]	Buffer[b]	Global Molecular Weight (g/mol)	RMS
1	WT*	6 (pH 7.0)	17,087 (15,677-20,152)	1.49E-2
2	WT	5	18,189 (17,308-19,041)	1.16E-2

[a]WT* is the cysteine free wild type variant (C54AC97T)
[b]Numbers refer to those given in Table 3.3.1.2.

4.1.2 Dynamic Light Scattering

The average radius (2.07 nm) of T4 lysozyme WT, determined from three experiments in each buffer, was used to calculate the translational diffusion coefficient of $10.37 \pm 0.56 \times 10^{-7}$ cm^2/s (95% confidence interval assuming no error in viscosity of 1cp).

Table 4.1.2.1: Hydrodynamic Radius as Measured by DLS for T4 lysozyme.

R_H (nm)	10 mM NaPhosphate, 150 mM NaCl	10 mM BTP, 100 mM KCl
1	2.12	2.10
2	2.03	2.08
3	2.06	2.02
Average:	2.07 nm	2.07 nm

4.1.3 Capillary Electrophoresis

CIEF

The pIs measured by focusing are given in Table 4.1.3.1. The results were in fair agreement with the average value of Sednterp predictions using the pK_a sets 2 and 3 (see Table 3.4.1). Unfortunately, the WT lysozyme value had to be extrapolated from the standards instead of being interpolated, as with the others, because the highest reference marker pI was 9.45 (RNase A). Only one literature values for these mutants could be found for comparison. Dao-pin et al. simply state that for WT lysozyme, "the isoelectric point is above pH 9.0" (Dao-pin et al., 1991).

Table 4.1.3.1: Isoelectric Points of T4 Lysozyme.

protein	pI measured	pI Sednterp
WT	~10.0	9.8
SM	9.6	9.6
DM	*	9.3
TM	8.6	8.8
QM	*	*

* pI not measured

CZE

The experimental results for I = 0.11 M are shown in Figure 4.1.3.1. The slopes from these velocity vs. field plots were used in calculating the valences given in Section 4.6 (Table 4.6.1). Only the two lower ionic strengths were amenable to absolute mobility measurements by CE due to problems associated with linearity of the field with increased current. This problem is illustrated in Figure 4.1.3.2, where an Ohm's law plot shows the limit to be about 50 μA in the case of 10 mM BTP, 100 mM KCl, pH 7.5 using a 20 cm neutral capillary. The upper limit of linearity was increased to some extent by

lengthening the capillary. However, for 10 mM BTP, 150 mM KCl, pH 7.5 the limit of linearity was below a voltage that the machine could maintain for any length of time. The principle cause for the difficulty is thermal; it is difficult to maintain a constant temperature profile across the capillary when significant power is being dissipated. Several attempts were made to conduct experiments at this ionic strength, but in all cases, the voltage cut out after only a of couple minutes. Figure 4.1.3.3 shows the significant boundary skewing that occured for the higher charged proteins on a bare capillary. The skewing results from protein interaction with the negatively charged capillary wall. A neutral capillary was therefore used to measure the WT and SM mobilities. The neutralization of the bare silica capillary is accomplished with a polyacrlyimide coating which is hydrophilic and does not interact with proteins or DNA. The eCap® neutral capillaries produced good peak shapes, but required significantly longer run times because the EOF was significantly reduced.

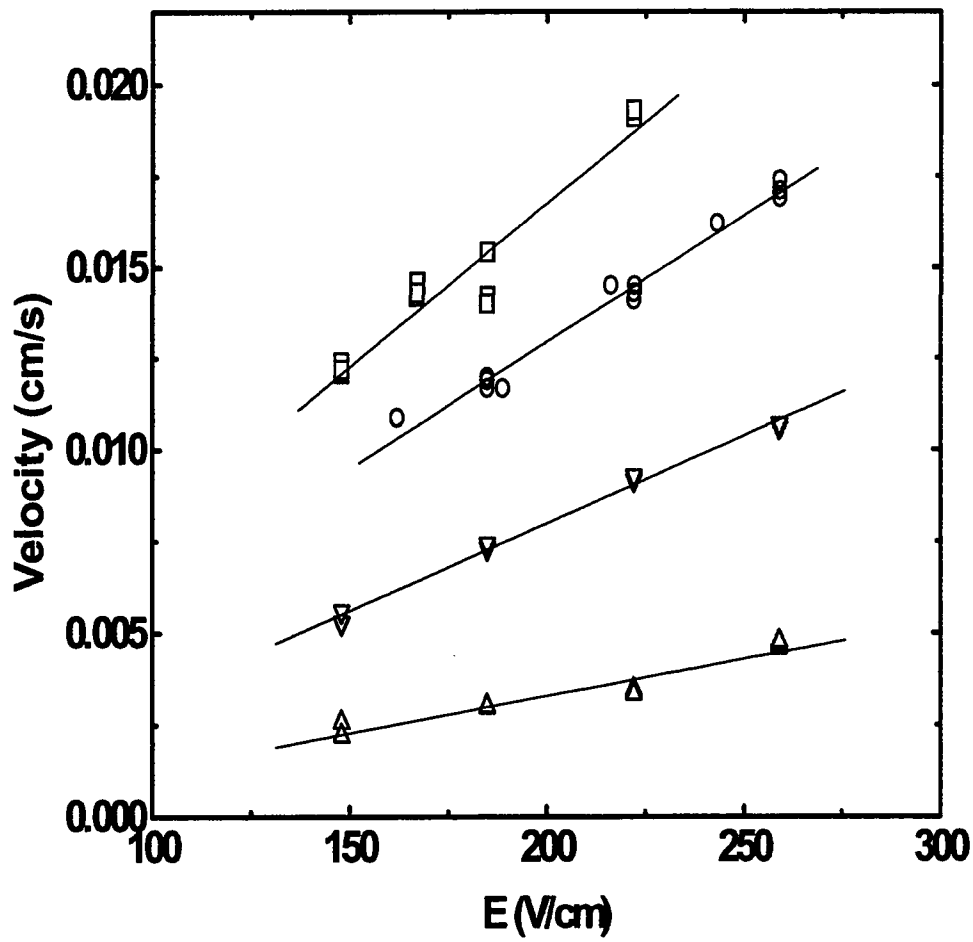

Figure 4.1.3.1: Capillary electrophoresis of T4 lysozyme. Results are given for □ WT (N=15), ○ SM (N=14), ▽DM (N=12), and △TM (N=12) in 10 mM BTP, 100 mM KCl, pH 7.5 (20° C).

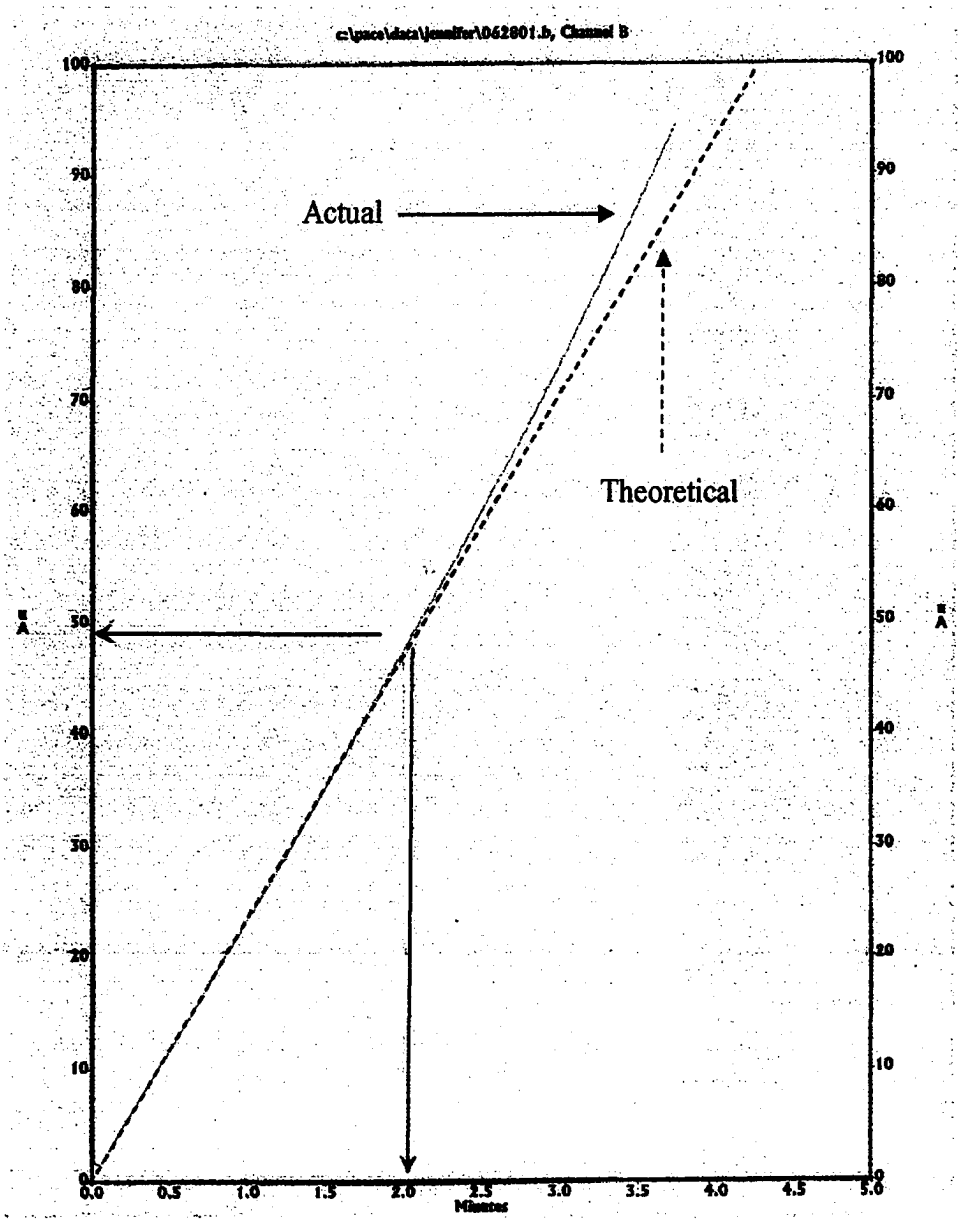

Figure 4.1.3.2: Ohm's Law plot showing the limits of CE linearity. The plot is for 10 mM BTP, 100 mM KCl, pH 7.5 in a 20 cm neutral capillary. The arrows indicate the approximate maximum current (and thus voltage) at which absolute mobility measurements could be made accurately.

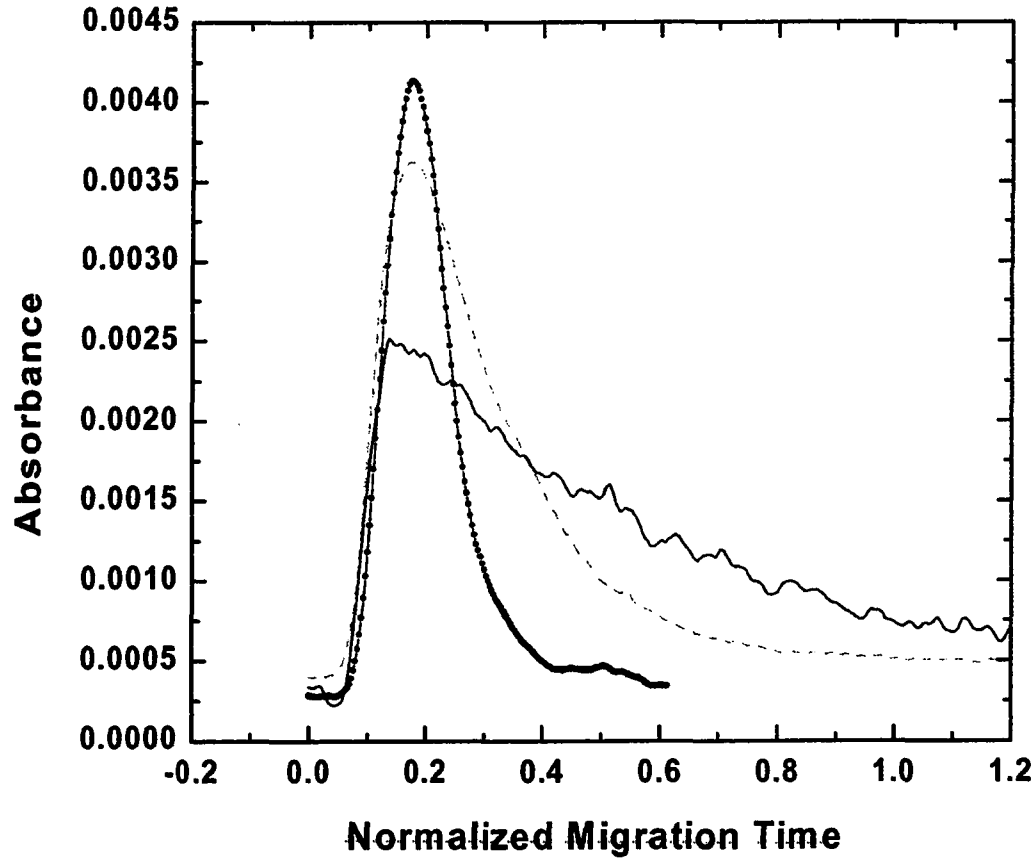

Figure 4.1.3.3: CE of T4 lysozyme on a bare silica capillary. Results are given for — WT , ----DM, and —o— TM in 10 mM BTP, 100 mM KCl, pH 7.5 (20° C). The migration time has been normalized for presentation purposes only.

4.1.4 Membrane Confined Electrophoresis

Samples were assayed for degradation when possible after MCE experiments. As is shown in Figure 4.1.4.1, no difference before and after experiments was seen in most cases. If heterogeneity was observed after an experiment, the experiment was repeated.

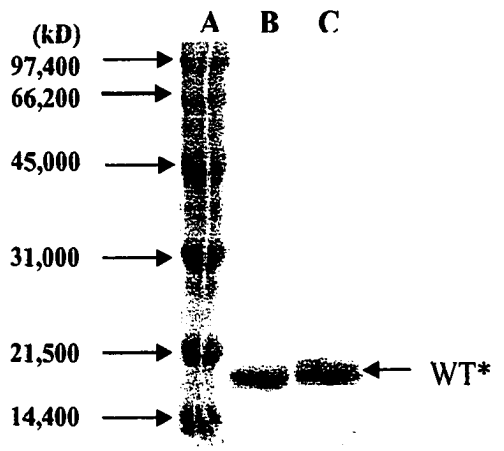

Figure 4.1.4.1. Lysozyme sample durability in MCE. A 15% acrylamide gel showing WT* before experiment (lane B) and after experiment (lane C). Standards (laneA).

A representative plot of the steady state lysozyme profiles obtained is given in Figure 4.1.4.2. The residuals indicate a good fit when nonideality (B*) is accounted for and, as Figure 4.1.4.3 shows, z_{eff}/z has a single value. As Figure 4.1.4.4 shows, the slopes of σ/E vs E plots were generally negligible, as was expected. This observation is consistent with sample homogeneity and an absence of bulk fluid flow (Laue et al., 1996). If there were a mixture of charges, at low fields the more highly charged protein contribution would be expected to dominate the steady state absorbance profile. This

would lead to higher σ/E values at the low fields and thus give negative slopes. However, there is no evidence of this in Figure 4.1.4.4. It should be pointed out that if the range of E were not large enough, heterogeneity would not be obvious. Thus, as broad a range as possible was used. The lower value of E, of course, is limited by gradient formation. Plots of z_{eff} vs. z at the various ionic strengths are summarized in Figure 4.1.4.5. The general trend of decreasing slope with increasing ionic strength was observed, and is expected from theory (Debye & Huckel, 1923b). A summary of the measured effective valences is given in Section 4.6 (Table 4.6.1).

Additionally, the MCE data was combined with CE data as shown in Figure 4.1.4.6. The slope of these velocity vs. field plots yielded a multi-instrument, global mobility. In all cases the linearity over this large range of fields was good and the intercepts were essentially zero. These global mobilities as a function of valence are shown in Figure 4.1.4.7. Recall that the slope of this graph may be compared with slopes predicted by various electrophoretic theories. Fitting the data, it is possible to extract an experimental estimate of the DHH value $f(\kappa a)/(1+\kappa a)$. The resulting line has an intercept near zero and a slope of 7.60×10^{6} s/g. Multiplying this slope by the frictional coefficient for T4 lysozyme (3.97×10^{-8} g/s), $f(\kappa a)/(1+\kappa a)$ is found to be 0.30. This is in good agreement with the slope of 0.32 predicted by DHH theory at I = 0.11 M (Debye & Huckel, 1923a). Note that the MCE velocities used in Figure 4.1.4.7 are from mobility experiments and not calculated from steady-state experiments, which are obtained at even lower fields. Nonetheless, the MCE mobility runs are conducted at fields significantly lower than those in the CE, providing a large test range.

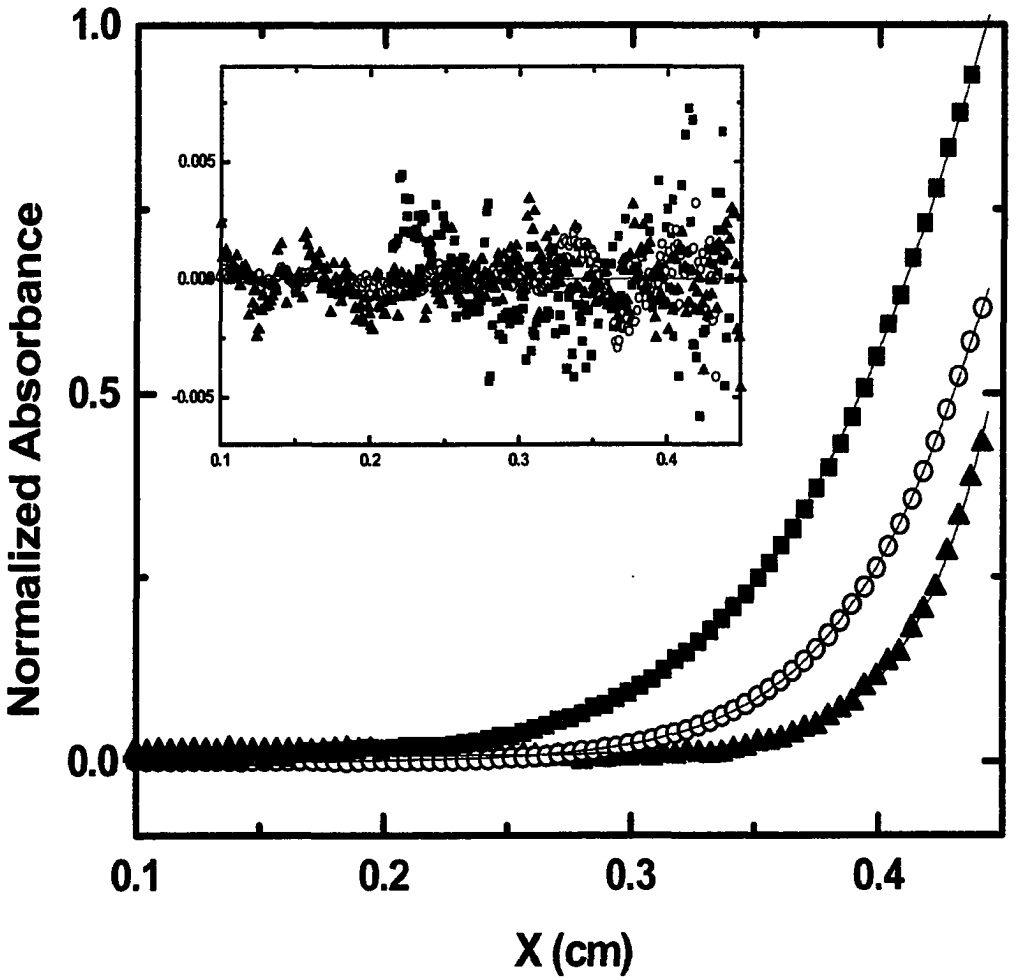

Figure 4.1.4.2: MCE steady state concentration gradients. Results are for T4 lysozyme ▲ WT (σ = 34.773 cm^{-1}), ○ SM (σ = 25.242 cm^{-1}) and ■ DM (σ = 19.972 cm^{-1}). Data were all acquired at a field strength of 0.4 V/cm in 10 mM BTP, 100 mM KCl, pH 7.5 (20° C). The absorbance has been normalized for presentation purposes only. The residuals of the Nonlin fits are shown inset.

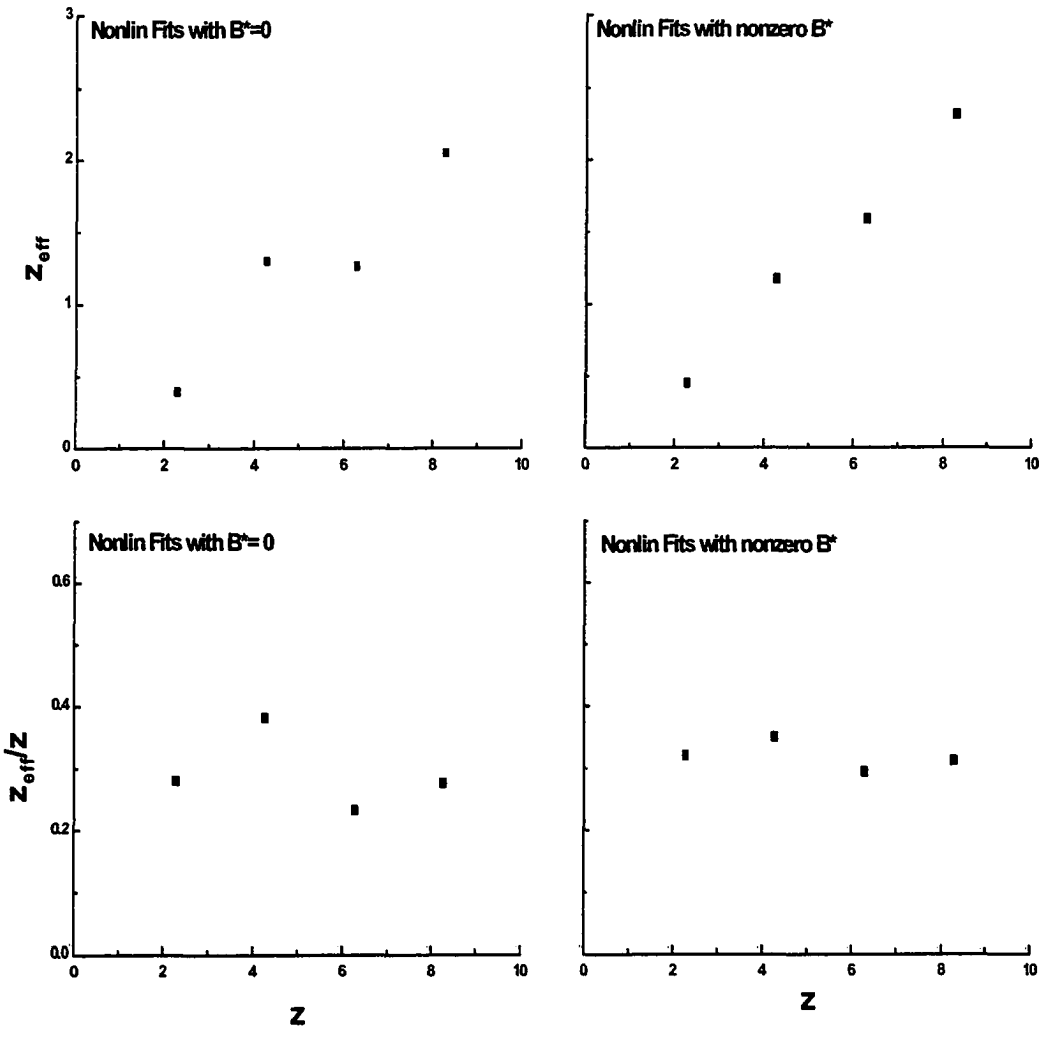

Figure 4.1.4.3: Inclusion of parameter B* in Nonlin Fits. All 4 plots are of 10 mM BTP, 100 mM KCl (pH 7.5) steady state data. For a given set of conditions with a series of charge mutants, z_{eff}/z is expected to have a single value as the lower right plot (with B* included as a fitting parameter) shows.

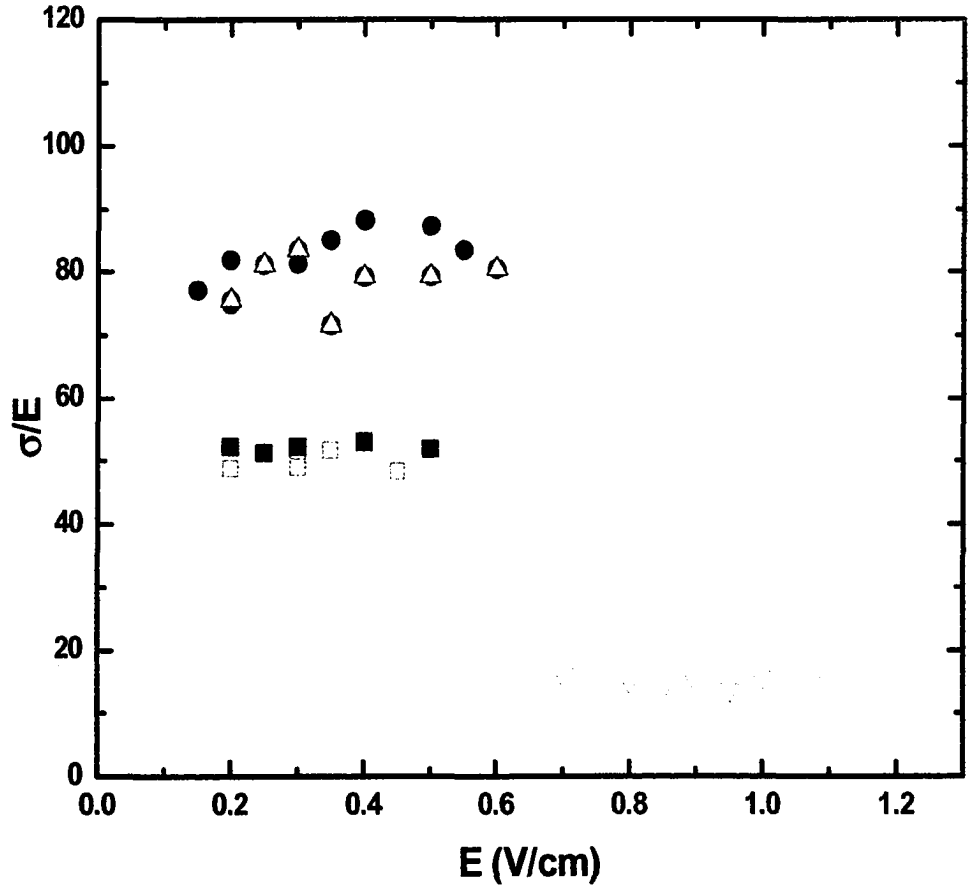

Figure 4.1.4.4: Representative Sigma/E vs E plot. The T4 lysozyme samples were in 10 mM BTP, 100 mM KCl, pH 7.5. The data points correspond to ● WT*, △ WT, ■ SM, □ DM and ▫ MCE steady state results.

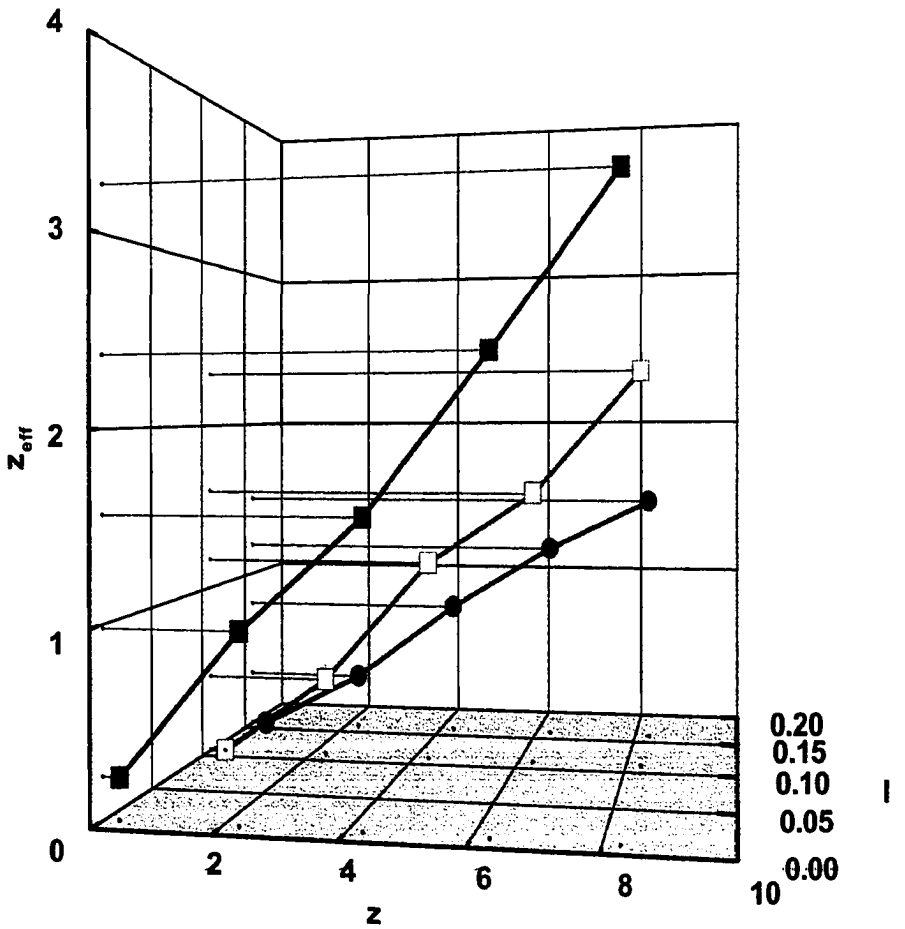

Figure 4.1.4.5: Summary of T4 lysozyme results in the MCE. Steady state results for ● I=0.16 M, □ I=0.11 M and ■ I=0.02 M. Notice the decrease in slope with increasing ionic strength.

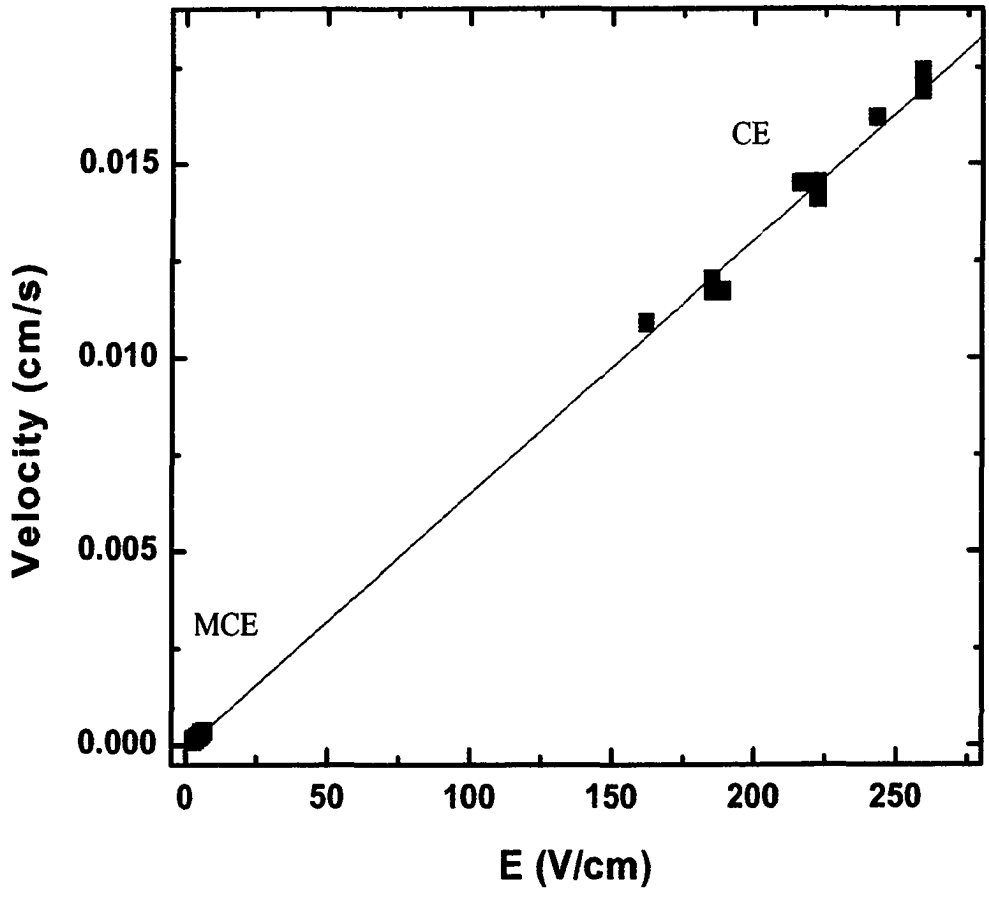

Figure 4.1.4.6: Representative plot of combined MCE and CE mobilities. SM lysozyme in 10 mM BTP, 100 mM KCl at pH 7.5. The slope gives a mobility of $6.56 \pm 0.05 \times 10^{-5}$ $cm^2/V \cdot s$ and y-intercept = -8.51 $\pm$ 8.06×10^{-5} cm/s (R=0.999).

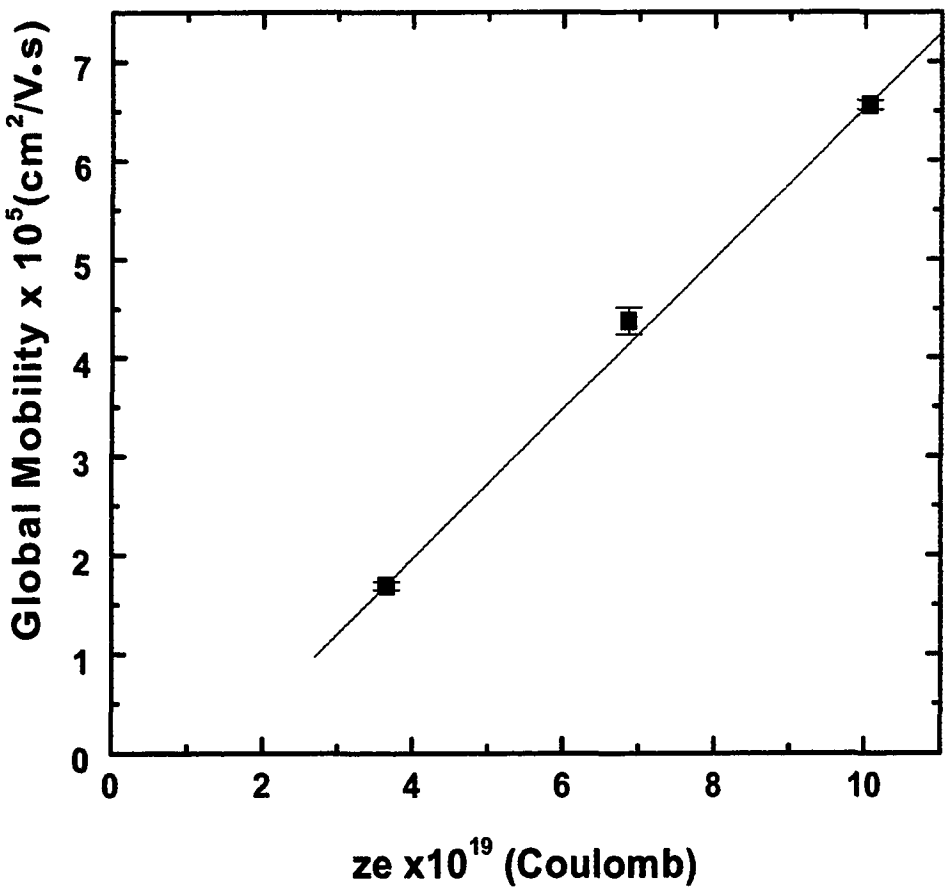

Figure 4.1.4.7: Instrumental global mobilities as a function of valence. SM, DM, and TM in10 mM BTP, 100 mM KCl at pH 7.5. The slope is $7.60 \pm 0.17 \times 10^{13}$ s/g and y-intercept = $-1.08 \pm 0.12 \times 10^{-5}$ $cm^2/V \cdot s$ (R=0.999) with weight of error bars taken into consideration. Unweighted, the slope is $7.60 \pm 0.44 \times 10^{13}$ s/g and y-intercept = $-1.00 \pm 0.33 \times 10^{-5}$ $cm^2/V \cdot s$ (R=0.998). Approximately 8-10 experiments from *each* type of instrument contribute to each of these points.

4.2 Ribonuclease Sa

As a second test molecule, the guanosine-specific ribonulease from *Streptomyces aureofaciens* was chosen. Except for being anionic, RNAse Sa is similar in size and charge to T4 lysozyme WT. The expectation was that the electrophoretic results would be in similar agreement with theory. Furthermore, the availability of a mutant (5K) with complete charge reversal allowed investigation of a broader valence range than with T4 lysozyme. As with T4 lysozyme, sedimentation velocity, DLS, CE and MCE data were obtained for RNase Sa.

4.2.1 Analytical Centrifugation

Sedimentation Velocity

The sedimentation velocity results are given in Table 4.2.1.1. A $\bar{\nu}$ of 0.74 ml/g was used in calculating the molecular weights which agree well with that calculated from sequence (10,575). The average diffusion coefficient of $12.93 \pm 0.42 \times 10^{-7}$ cm^2/s was used in subsequent calculations of mobility. Values of D for the 2K ($12.01 \pm 1.3 \times 10^{-7}$ cm^2/s) and 5K ($12.09 \pm 1.2 \times 10^{-7}$ cm^2/s) variants were within error of that for the WT. A speed of 60,000 rpm was used.

Table 4.2.1.1: Sedimentation Velocity Results for RNase Sa.

#	Conc. (mg/mL)	Fitting Program	S ($x10^{-13}$ s)	rms	D ($x10^{-7}$ cm^2/s)	MW (g/mol)
1	0.61	Sedfit	1.59	5.10E-3	13.08	10,971
		DcDtplus	1.38	1.27E-2	12.44	10,620
2	0.49	Sedfit	1.58	1.32E-2	12.82	11,088
		DcDtplus	1.32	4.88E-2	13.64	9,020
3	0.25	Sedfit	1.54	1.44E-2	12.82	10,865
		DcDtplus	1.51	1.42E-2	12.79	10,682
				Average:	12.93	10,541

[a] All experiments done with buffer 5 as given in Table 3.3.1.2.

4.2.2 Dynamic Light Scattering

The average RNase Sa radius determined from three experiments was 1.92 nm. Calculation of the translational diffusion from this value gives $11.17 \pm 0.57 \times 10^{-7}$ cm^2/s (95% confidence interval assuming no error on viscosity), which is in fair agreement with that obtained by centrifugation.

Table 4.2.2.1: Hydrodynamic radius as Measured by DLS for RNase Sa.

R_H (nm)	10 mM BTP, 100 mM NaCl
WT	1.84
2K	1.95,1.98
5K	1.92
Average:	1.92

4.2.3 Capillary Electrophoresis

Figure 4.2.3.1 shows the experimental results for I = 0.11 M. The slopes from velocity vs. field plots were used in calculating the valences given in Section 4.6 (Table 4.6.2). As can be seen in Figure 4.2.3.1, the precision of the bare capillary results (5K) is much greater than that for the amine coated capillary results with the 2K and WT. The amine coating degrades over time and must be regenerated. Even with this precaution taken, as described in Section 3.3.3, the precision of the measured velocities using the amine capillary was no better than ± 8%. Nonetheless, the 2K and WT (as well as 5K) intercepts were, within error, zero.

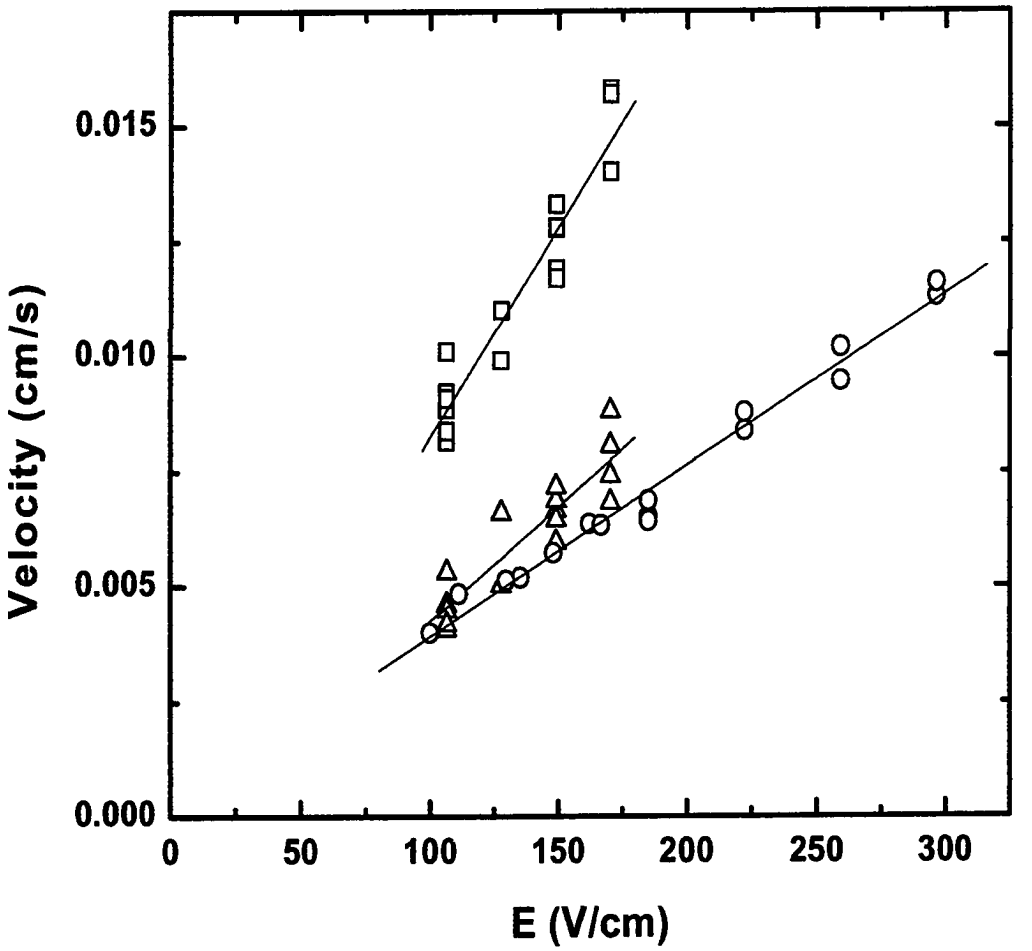

Figure 4.2.3.1: Capillary electrophoresis of RNase Sa. Results are given for □ WT (N = 17), △ 2K (N = 17), and ○ 5K (N = 16) in 10 mM BTP, 100 mM KCl, pH 7.5 (20° C).

4.2.4 Membrane Confined Electrophoresis

The use of the RNase Sa mutants provided an opportunity to not only extend the tested valence range from 8 (as with T4 lysozyme) to 10, but also to examine complete charge reversal. The results for RNase Sa (Table 4.2.4.1) in 10 mM BTP, 100 mM KCl at pH 7.5 are shown in Figure 4.2.4.1. Nonlin fits for both B* = 0 and B* included as a fitting parameter are given. Residuals of fits from the "black box" (lens based) prototype data were not improved with the additional parameter as they were in the "silver box" (mirror based) prototype.

Table 4.2.4.1: MCE Steady State Results for RNase Sa.

Sample	Prototype[a]	Membranes[b]	Nonlin fit RMS	z_{eff} from Global Sigma[c]
WT	1	untreated	2.806E-3 2.350E-3	-1.75±0.02 -1.61±0.06
	1	treated	5.047E-3 4.799E-3	-1.81±0.11 -2.10±0.27
	2	treated	3.512E-3 3.415E-3	-1.59±0.13 -1.93±0.33
Global (all data, B* = 0)			4.016E-3	-1.72±0.01
2K	1	untreated	4.658E-3 4.605E-3	-0.82±0.02 -0.85±0.05
5K	1	untreated	2.013E-3 2.011E-3	0.72±0.01 0.72±0.02
	1	treated	2.442E-3 2.082E-3	0.67±0.01 0.61±0.03
	2	treated	1.940E-3 1.398E-3	0.62±0.02 0.68±0.04
Global (all data, B* = 0)			3.666E-3	0.71±0.01

[a] The "black box" prototype is designated 1 and the "silver box" prototype is 2.
[b] See Section 3.3.1 for details on treatment of the SpectraPor membranes.
[c] The upper values are for B* held at zero and the lower are with B* as a fitting parameter.
[d] The overall global zeff from the WT and 5K cumulative data sets was used in Table 4.6.2.

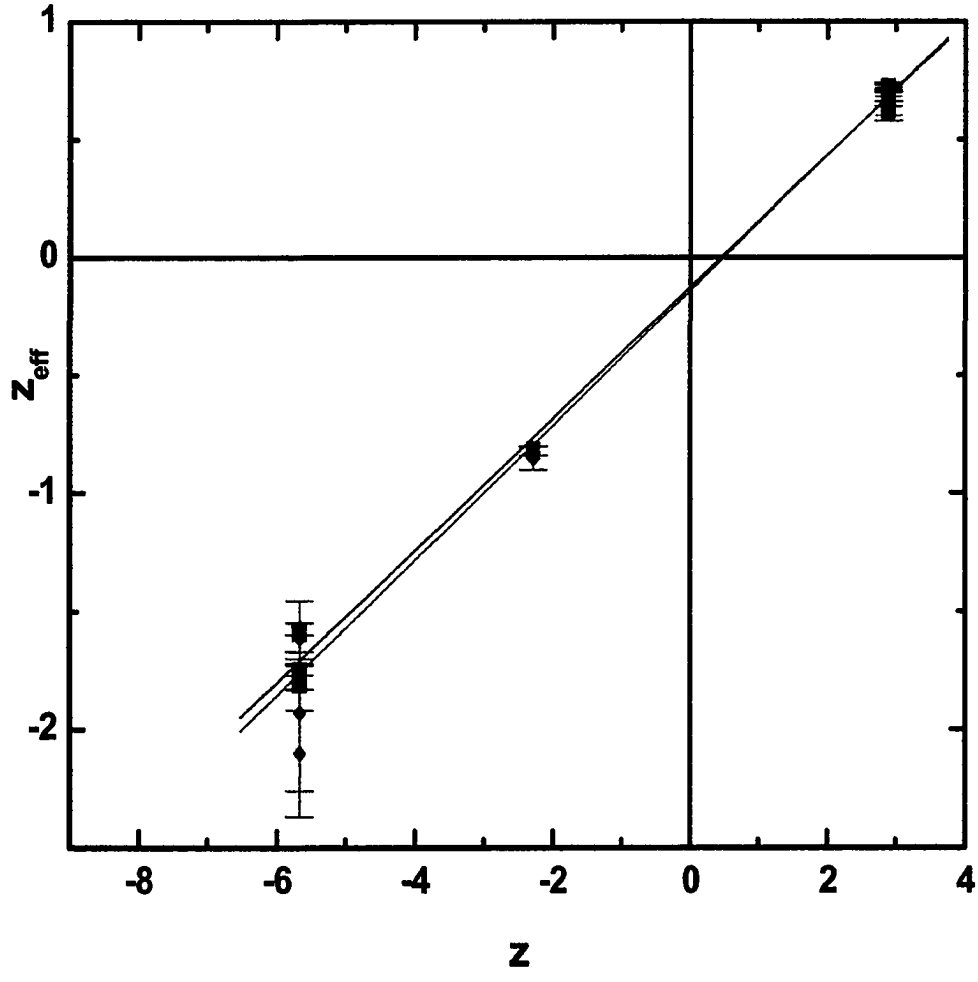

Figure 4.2.4.1. RNAse Sa steady state results. The samples were in 10 mM BTP, 100 mM KCl, pH 7.5. ■ is for an ideal fit with B* held at 0 (slope = 0.28 ± 0.01, intercept = -0.14 ± 0.01) while ◆ includes B* as a fitting parameter (slope = 0.28 ± 0.01, intercept = -0.12 ± 0.02) in Nonlin.

4.3 α-Chymotrypsin

In addition to the work with monomeric T4 lysozyme and RNase Sa, a two-species macroion component, α-chymotrypsin and its dimer, was studied. One goal of MCE development is to provide a tool that will allow assessment of the role of valence in macromolecular association. The protein, α-chymotrypsin, has been proposed to be a model system for studying self association (Ford & Winzor, 1983). It was hoped 1) that the centrifugation experiments of Ford and Winzor could be repeated to verify the amount of dimer expected in the MCE under a given solution condition, 2) to measure the steady state concentration gradient of the monomer-dimer equilibrium, and 3) to extract the charge stoichiometry of the system for comparison to that reported by Ford and Winzor (Ford & Winzor, 1983). The results, unfortunately, are not clear but have been included as they may be of use in future work in this area.

4.3.1 Analytical Centrifugation

Sedimentation Equilibrium

The objective was to verify that self association results in a sufficient dimer population under conditions amenable to MCE steady state experiments. The data reported in Table 4.3.1.1 were fit for two species. Table 3.3.4.1 gives the experimental conditions. A $\bar{\nu}$ of 0.736 ml/g was used (Ford & Winzor, 1983). The association constant (K_a) measured in 100 mM KCl in the first experiment was10 fold smaller than that reported by Ford and Winzor under the same conditions. With salt concentrations above 100 nM, the association was reportedly stronger and thus this was explored as well (Tellam et al., 1979). The result obtained in 200 mM KCl was much closer to the

reported literature values. High salt, however, poses difficulties for electrophoresis measurements as will be discussed.

Table 4.3.1.1: Sedimentation Equilibrium Results for α-Chymotrypsin.

#	Buffer[a]	Global Molecular Weight (g/mol)	RMS x 10^2	B x 10^4 (fringe^{-1})	K_d (μM) measured	K_d (μM) reported in literature
1	7	26,464	3.97	1.00	2331	286[1]
2	7	26,601	6.77	9.68	1203**	
3	8	25,000*	2.71	35.0	16.27	10.50[2], 5.71[3], 18.18[4], 11.42[5]

*Held sigma at expected value for MW 25,000 as given by Ford and Winzor.
**This value is taken from an average of lnKs returned from global analysis with separate Ln Ks fit for. Furthermore, there is some evidence of aggregation in this run as the Ln Ks increased with speed and decreased with dilution.
[a]Numbers refer to Table 3.3.1.2
[1] Ford and Winzor (1983)
[2] Winzor (1964)
[3] Winzor (1967)
[4] Horbett and Teller (1974)
[5] Tellam, Jersey and Winzor (1979)

To convert the association constant, $K_{OBS,AUC}$, obtained from the AUC interference experiments to comparable values in the MCE, a molar dissociation constant was using

$$K_d = \left[\frac{K_{OBS,AUC} M_a^{i-1}}{i} \left(\frac{Y_T}{C_T} \right)^{i-1} \right]^{-1} \quad (26)$$

where M_a is the monomer molar mass of α-chymotrypsin, i is the degree of association, and. for a 12 mm pathlength and a wavelength of 670nm, 3.25 is the specific fringe displacement (Y_T/C_T) in units of fringe·L/g (Laue et al., 1984).

4.3.2 Dynamic Light Scattering

The average radius obtained was in good agreement with the 2.44 nm reported by Ford and Winzor (Ford & Winzor, 1983). Their value was based on a sedimentation velocity $s_{20,w}$ value of 2.4S for monomeric α-chymotrypsin.

Table 4.3.2.1: Hydrodynamic Radius as Measured by DLS for α-Chymotrypsin.

R_H (nm)	10 mM KAcetate, 100 mM KCl, pH 3.9
1	2.29 nm
2	2.41 nm
3	2.50 nm
Average:	2.40 nm

4.3.3 Membrane Confined Electrophoresis

As with T4 lysozyme and RNase Sa data, α-chymotrypsin MCE data from multiple fields was combined to give a global NONLIN fit. The goal was to use the association constant obtained from sedimentation experiments and fit for a value of sigma (see Equation 19) and N (the stoichiometry). Holding LnK at the AUC measured value (converted to the corresponding MCE value) reduced the number of fitting parameters, allowing NONLIN fits for sigma and N simultaneously. These values are given in Table 4.3.3.1 below. Table 3.3.4.2 gives the experimental conditions.

The observed association constant obtained from MCE, $K_{OBS,MCE}$, can be converted to a molar dissociation constant using

$$K_d = \left[\frac{K_{OBS,MCE}\, l \in}{2} \right]^{-1} \qquad (27)$$

where 0.2 is the MCE path length (l) and ϵ is the molar extinction coefficient of α-chymotrypsin. The molar extinction coefficient of the dimer is assumed to be 2 times that of the monomer and thus the result is divided by 2. The K_d obtained from AUC data (Equation 26) was used to solve for $K_{OBS,MCE}$ (Equation 27) and in NONLIN fits of the MCE data, LnK was fixed at this value.

Table 4.3.3.1: MCE Steady State Results for α-Chymotrypsin.

Experiment	Ionic Strength (M)	Global Sigma (cm^{-1})	N	LnK	RMS
1	0.10	7.85 (7.73-7.95)	2.0 (1.4-2.7)	-2.4	2.95E-3
2	0.10	No fit*	-	-	-
2	0.20	5.57 (5.42-5.73)	2.0 (1.4-2.6)	2.5	1.91E-3
3	0.20	6.67 (6.35-6.99)	2.0 (1.9-2.2)	2.3	4.58E-3

*The resulting SSE concentration gradient was S-shaped and could not be fit with NONLIN. Although this was the highest protein concentration used, it seems unlikely that the range of linearity of the device is at fault as scans at 250 and 300 nm (where the absorbance is 0.9 and 0.6) show the same shape.

It should be pointed out that there is no precedent for the above method: this is the first attempt to determine stoichiometry by an electrophoretically-established steady state concentration gradient. Although an N = 2 is to be expected according to Ford and Winzor (Ford & Winzor, 1983), the resulting confidence intervals associated with N are too broad to say with certainty that charge σ scales with stoichiometry upon α-chymotrypsin dimerization. Also effective valences do not agree well with theory, as Table 4.6.3 shows. However, as has been pointed out there may be some inherent difficulties in using NONLIN in this manner if σ does not scale with stoichiometry (Moody & Shepard, 2002). Future work should be directed at sorting out both the experimental and fitting difficulties.

4.4 Limiting Molar Conductivity

To verify that Equation 24 would give an accurate value of Λ° (see Section 3.5), data taken from a 1979 determination of the Λ° for Tris by Klein and Bates were plotted (Klein & Bates, 1979). They used a much more complex equation, called the full Pitts equation, to fit the data and found the limiting molar conductivity of $TrisH^{+}$ to be Λ°= 29.72 S·cm^2/mol at 25° C (Pitts, 1970). If their data instead is fit to the more simple Equation 24 as is shown in Figure 4.4.1, the result is 27.61 S· cm^2/mol. It was then determined whether our equipment could reproduce this result. As is shown in Figure 4.4.1, measurements made with a VWR 1054 conductivity meter were in good agreement with their data. A linear fit of this experimental data yields Λ°= 28.37 S ·cm^2/mol at 23 °C, which is only 4.5% below the value reported with the full Pitts equation.

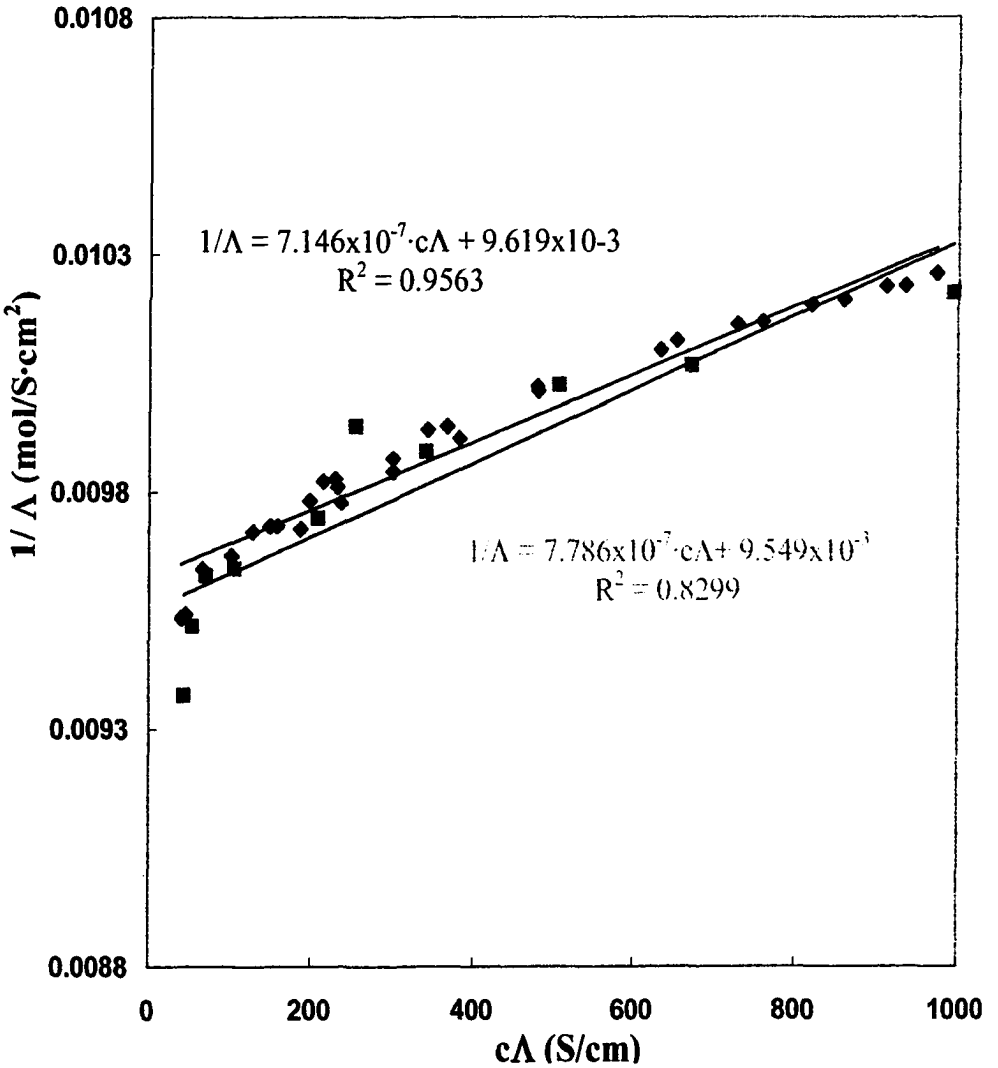

Figure 4.4.1. Limiting molar conductivity of $TrisH^+$ as found by Equation 26. The above plot is for data collected ♦ by Klein et. al, 1979 and ■ by J. Durant, 2001 (Exp080801).

As shown in Figure 4.4.2, the limiting molar conductivity of BTP was measured in two ways: 1) by adding concentrated BTP solution to distilled water as was done by Klein (1979) and 2) by diluting a sample initially 0.1 M. Although the results are slightly different, the y-intercept values are within 1% of each other. The calculation was made originally with the assumption that at infinite dilution, $\lambda^{\circ}_{BTP^{+2}} = 2\lambda^{\circ}_{BTP^{+1}}$. This gives $\lambda^{\circ}_{BTP^{+1}} = 26.95$ S·cm^2/mol and $\lambda^{\circ}_{BTP^{+1}} = 26.02$ S·cm^2/mol. The average of these was used in the BE modeling. Later, however, it was found that $\lambda^{\circ}_{BTP^{+2}} = (2)^2 \lambda^{\circ}_{BTP^{+1}}$. This results in a lower average value of 20.96 S·cm^2/mol (30% lower than above average). Because the earlier value was used in the modeling, this leads to a slight overestimate in the retarding effects due to the ion atmosphere. However, because BTP is such a minor component of the solution, the difference in the BE estimate is likely to be negligible. The limiting molar conductivity results are consistent in that BTP^{+1} is a slightly bulkier cation and has a greater potential for hydrogen bonding (6 OH groups) than $TrisH^{+1}$ and therefore one might expect $\lambda^{\circ}_{BTP^{+1}}$ to be slightly smaller than that of $TrisH^{+1}$.

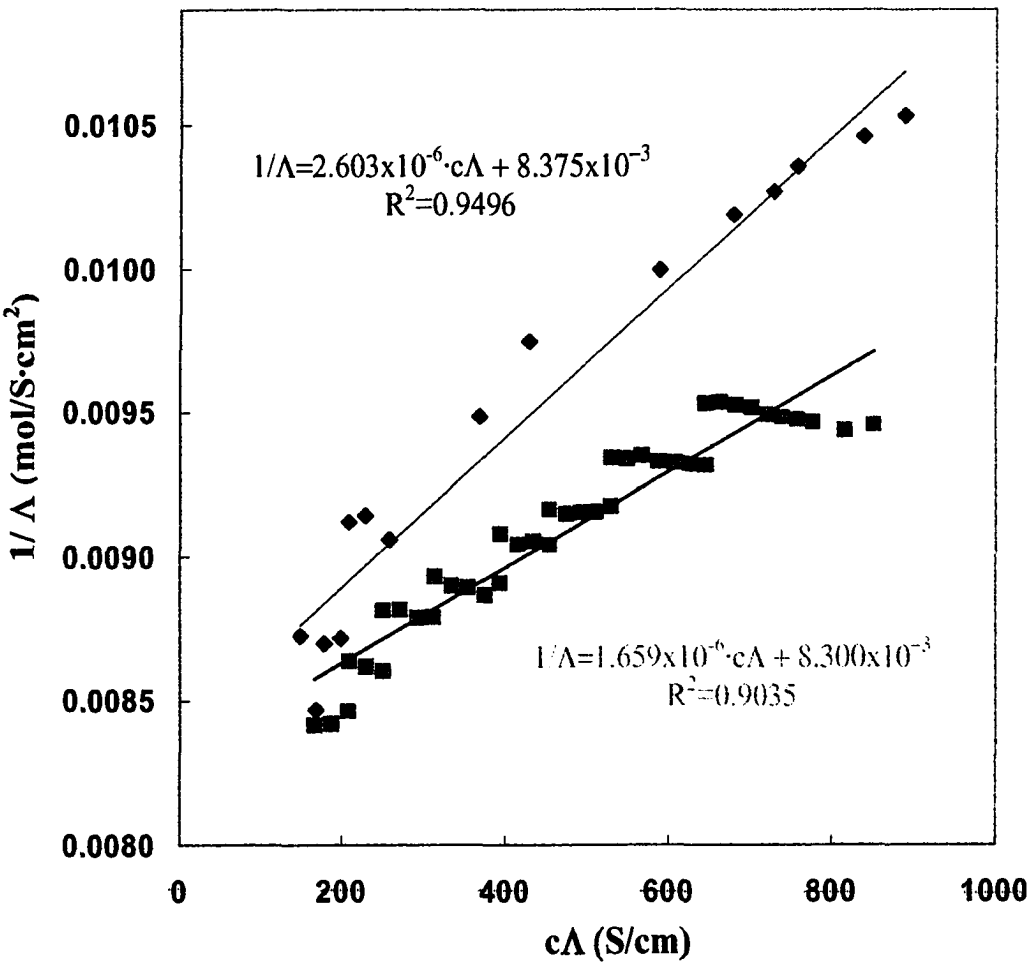

Figure 4.4.2. Limiting molar conductivity of BTP. The experiments were done at a constant pH of 7.5: ♦ (Exp081401) BTP diluted and ■ (Exp082001) BTP added to distilled water.

4.5 Model Calculations

The equation for mobility first given by Smoluchowski in 1903 is

$$\mu = \frac{v}{E} = \frac{\varepsilon_0 \varepsilon \zeta}{\eta}\left(\frac{1\,\mathrm{m}}{100\,\mathrm{cm}}\right)\left(\frac{10^7\,\mathrm{erg}}{\mathrm{C}\cdot\mathrm{V}}\right) \quad (28)$$

and was thought to be valid for an electrically insulating particle of arbitrary shape (Smoluchowski, 1903). Debye and Hückel, however, concluded 20 years later that

$$\mu = \frac{v}{E} = \frac{2\varepsilon_0 \varepsilon \zeta}{3\eta}\left(\frac{1\,\mathrm{m}}{100\,\mathrm{cm}}\right)\left(\frac{10^7\,\mathrm{erg}}{\mathrm{C}\cdot\mathrm{V}}\right) \quad (29)$$

was the correct expression (Debye & Huckel, 1923b). The discrepancy between these equations remained unresolved for nearly a decade.

4.5.1 Debye-Hückel-Henry Model

In 1931 Henry reconciled the above discrepancy with the expression

$$\mu = \frac{v}{E} = \frac{2\varepsilon_0 \varepsilon \zeta}{3\eta} f(\kappa a)\left(\frac{1\,\mathrm{m}}{100\,\mathrm{cm}}\right)\left(\frac{10^7\,\mathrm{erg}}{\mathrm{C}\cdot\mathrm{V}}\right) \quad (30)$$

which can be rewritten in terms of valence (see Equation 9) to give

$$z_{eff} = z\frac{f(\kappa a)}{(1+\kappa a)} \quad \text{for } e\zeta / k_B T << 1 \quad (31)$$

where f(κ*a*) is termed Henry's function. While Smoluchowski had taken the particle as insulating, Debye and Hückel had assumed the particle to have the same electrical conductivity as that of the medium. This lead Smoluchowski to describe the applied field as distorted near the particle surface and, thus, the lines of electrostatic force ($\vec{F} = q\vec{E}$) as tangential. Debye and Hückel took the lines of force to be parallel to the x-axis (i.e.

unperturbed). Additionally Smoluchowski assumed that the "double layer" thickness (see Chapter 2) was "small compared with the radius of curvature"of the particle (i.e. the particle was large and the ion atmosphere small) (Henry, 1931). Henry reexamined electrophoretic theory but removed the restrictions on conductivity and double layer thickness that Smoluchowski had imposed and was thus able to bridge both theories with the correction f(κ*a*). Henry's solution for f(κ*a*) is a discontinuous function given by the bracketed term in the expressions

$$\mu = \frac{ze}{6\pi\eta a}\left(\frac{1}{1+\kappa a}\right)\left[\left(\frac{3}{2}\right)1 - \frac{3}{\kappa a} + \frac{25}{\kappa^2 a^2} - \frac{220}{\kappa^2 a^2} + \ldots\right]\left(\frac{10^7 \text{ erg}}{\text{C}\cdot\text{V}}\right) \quad (32)$$

$$\mu = \frac{ze}{6\pi\eta a}\left(\frac{1}{1+\kappa a}\right)\left[1 + \frac{\kappa^2 a^2}{16} - \frac{5\kappa^3 a^3}{48} - \frac{\kappa^4 a^4}{96} + \frac{\kappa^5 a^5}{96} - \left(\frac{\kappa^4 a^4}{8} - \frac{\kappa^6 a^6}{96}\right) e^{\kappa a} \int_{\infty}^{\kappa a} \frac{e^{-t}}{t} dt\right]\left(\frac{10^7 \text{ erg}}{\text{C}\cdot\text{V}}\right) \quad (33)$$

where $t = \kappa a$ (the first equation is taken from Henry while the second is in the form given by Cann) (Henry, 1931; Cann, 1970). The first expression is valid for $\kappa a \geq 25$ and the latter for $\kappa a \leq 5$. Because the function is discontinuous for some intermediate κ*a* values, the data was fit to a polynomial function bridging the gap and is given at the top of Figure 4.5.1.1. The standard deviation associated with values from this fit is ± 0.003 and no improvement is seen for higher order fits. The constants for this function are given in Table 4.5.1.1. The value of Henry's function can therefore be found for any κ*a*.

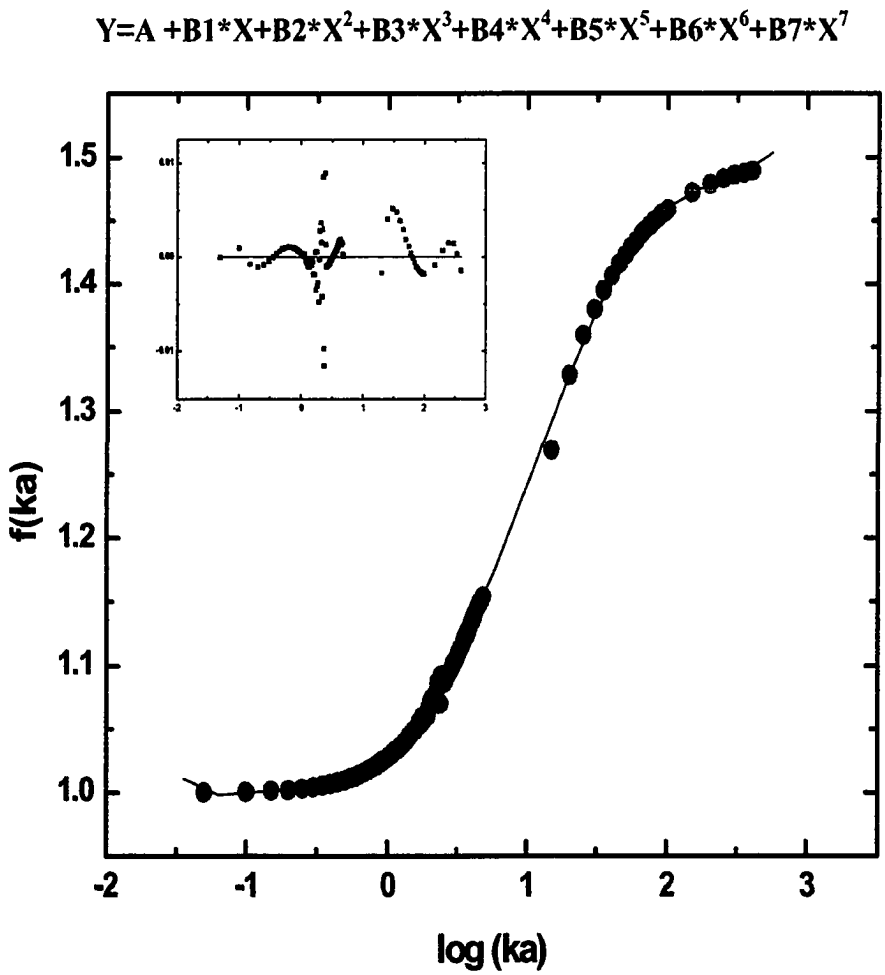

Figure 4.5.1.1. Henry's function (f(ka)) as a function of ka values. The values in red • are those from Equation 32 and 33. The result can be fit by the given polynomial (residuals inset). The constants are given in the Table 4.5.1.1. $R^2 = 0.9995$.

Table 4.5.1.1. Polynomial Constants to Fit of Henry's Equation.

Parameter	Value	Error
A	1.02625	6.2105E-4
B1	0.09252	0.00211
B2	0.12693	0.0034
B3	0.03999	0.00521
B4	-0.04013	0.00443
B5	-0.0102	0.002
B6	0.00796	0.00197
B7	-9.33572E-4	4.12311E-4

* Note that the error on B5 -B7 is 20% or greater.

Because several ionic strengths were used experimentally, the ionic strength dependence of the $1/1+\kappa a$ term in Equation 31 was calculated and is shown in Figure 4.5.1.2 for a macroion with the given collision diameter, $a = 2.197 \times 10^{-7}$ cm, corresponding to T4 lysozyme. The $1/1+\kappa a$ value was adjusted accordingly for the RNase Sa ($a = 2.047 \times 10^{-7}$ cm) and α-chymotrypsin data ($a = 2.527 \times 10^{-7}$ cm). Based on these $1/1+\kappa a$ and $f(\kappa a)$ values, predicted values of effective valence can be calculated for the various experimental conditions used. These are summarized in Tables 4.6.1 and 4.6.2 (Section 4.6).

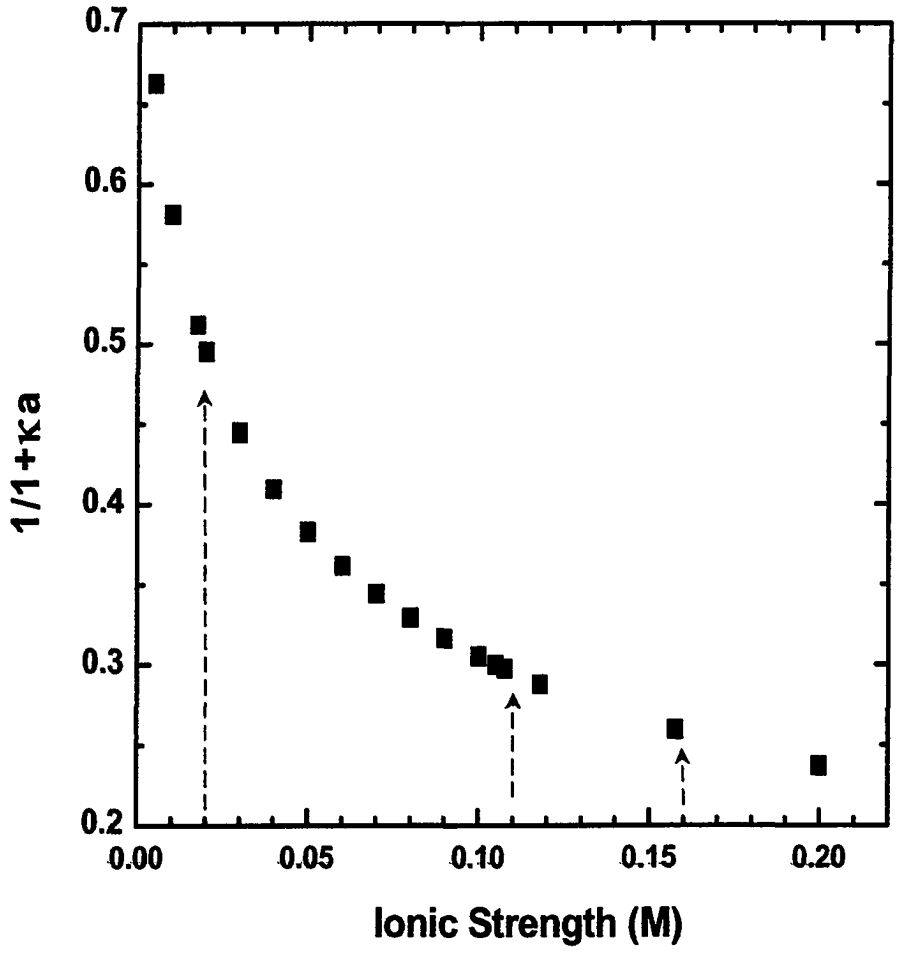

Figure 4.5.1.2. 1/1+κ*a* dependence on ionic strength for *a* = 2.19 nm. This *a* is the collision diameter for T4 lysozyme in the calculations. The ionic strengths used (arrows) cover more than a two fold change in 1/1+k*a*.

4.5.2 Booth Model

Smoluchowski also assumed that the applied field can be modeled as simply being superimposed on the field due to the electric double layer without causing any distortion in the ion atmosphere. However, as Henry noted, "it is certain that the application of an external field and the motion of the particle will disturb the symmetry of the ionic atmosphere, but it is not easy to estimate the magnitude of the error thus introduced" (Henry, 1931). Nineteen years later, after two years of revisions (the paper was first received in 1948 but not published until 1950), Booth was able to write an expression (Equation 34) which included an estimate of the asymmetry effect (Booth, 1950; Tanford, 1961).

$$z_{eff}e = ze\frac{f(\kappa a)}{(1+\kappa a)} + \sum_{v=2}^{\infty} z^{v}\frac{e^{2v-1}}{a^{v-1}(\varepsilon k_B T)^{v-1}}\left(X_v^{\mp}(\kappa a;q_v) + Y_v^{\mp}(\kappa a;q_v) + Z_v^{\mp}(\kappa a;q_v;q_v^{*})\right) \qquad (34)$$

In essence, the term on the far right accounts for the fact that the ion atmosphere is perturbed from its equilibrium distribution during electrophoresis. The terms $X_v^{\ddagger}$, $Y_v^{\ddagger}$ and $Z_v^{\ddagger}$ are complicated functions of κa, the valences and the mobilities of the small electrolyte ions. For example

$$Z_4^{\mp} = q_4^{*}Z_4(\kappa a) = \frac{\varepsilon_0 \varepsilon k_B T \sum_{i=1}^{s} n_i w_i^{-1} z_i^3}{e^2 \pi \eta \sum_{i=1}^{s} n_i z_i^2} Z_4(\kappa a) \qquad (35)$$

where

$$w_i = \frac{\lambda^{\infty}}{z^2 Fe} \qquad (36)$$

is the velocity of the ion under a unit force, λ^{∞} is the limiting molar conductivity, n_i is the concentration of the ion at a large distance from the particle (i.e. the bulk value concentration) and $Z_4(\kappa a)$ is taken from figure 1 of Booth's paper (Booth, 1950; Castellan, 1983). According to Booth, $X_2^{\ddagger} = Y_2^{\ddagger} = Z_2^{\ddagger} = X_4^{\ddagger} = Y_4^{\ddagger} = 0$. Calculations for intermediate dimensionless values of $X_3^{\ddagger}$, $Y_3^{\ddagger}$, $Z_3^{\ddagger}$ and $Z_4^{\ddagger}$ in the case of T4 lysozyme are given in Table 4.5.2.1 and 4.5.2.

Table 4.5.2.1 Values from Figure 1 of Booth's.

Ionic Strength (M)	0.02	0.11	0.16
$X_3(\kappa a)$	-1.7E-03	-7.0E-04	-5.4E-4
$Y_3(\kappa a)$	-1.5E-03	-5.8E-04	-4.3E-4
$Z_3(\kappa a)$	-8.1E-04	-2.2E-04	-1.5E-4
$Z_4(\kappa a)$	8.3E-05	4.6E-05	-2.7E-6

Table 4.5.2.2 Calculated q and q^* Values.

Ionic Strength (M)	0.02	0.11	0.16
q_3^*	1.89	1.06	1.01
q_4^*	2.00	3.39	0.24
q_3	1.57	1.09	1.06

As the above intermediate values of Equation 34 indicate, the corrections due to asymmetry are most significant at low ionic strengths where the ion atmosphere is most extended, and also for high valence. Final predictions of effective valence calculated using Booth's model are summarized in Tables 4.6.1 and 4.6.2 (Section 4.6).

4.5.3 Boundary Element Model

Overbeek derived the first general formulation of the coupled steady-state hydrodynamic, ion transport and electrodynamic differential equations, which he then

applied to the electrophoretic transport of a sphere of low charge in a weak external field.(Overbeek, 1943). In the last few years, Allison and coworkers (Allison & Tran V., 1995; Allison, 2002) have used the transport theories of Overbeek and Booth (Booth, 1950), as well as O'Brien and White (O'Brien & White, 1978), to develop a boundary element (BE) method that models the electrophoresis of infinitely dilute, rigid macro-ions of arbitrary size, shape and charge distribution. The model incorporates both structural and titration data, and applies the above mentioned transport theories to predict the electrophoretic mobility of macro-ions. The method has previously produced results that are in good agreement with the experimentally determined mobilities of hen egg white lysozyme (Allison et al., 1997), short duplex DNA fragments (Allison & Mazur, 1998; Mazur et al., 2001), and duplex DNA fragments of variable length (Allison et al., 2001).

As the schematic in Figure 4.5.3.1 shows, the T4 lysozyme protein is modeled as a plate structure based on the non-hydrogen coordinates obtained from the Protein Data Bank [2LZM]. The procedure used to construct detailed models of this type has been described previously (Allison & Tran V., 1995). Associated with each non-hydrogen atom is an atom exclusion radius, which is assumed to be constant for all atoms. Plated structures consisting of interconnected triangular platelets are constructed to completely enclose the protein. This represents the hydrodynamic shear surface, S_p. The experimental diffusion coefficient discussed in Section 4.1 is used to define the correct exclusion radius and thus, the distance from the center of mass to the plate position.

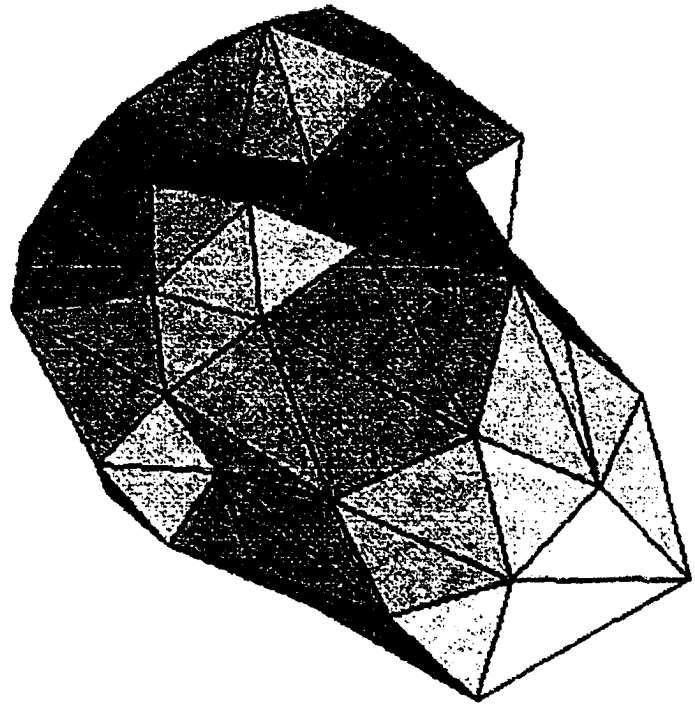

Figure 4.5.3.1 Plate model of T4 lysozyme based on crystallographic structure (2LZM). Figure was generated by Stuart Allison (Durant et al., 2002). Such a surface was used in the BE modeling.

For BE studies, it was necessary to know the small ion mobilities. These are related to the hydrodynamic radii, r, of the small ions by $\mu = ze/6\pi\eta r$, which, in turn are related to the limiting molar conductivities of the small ions, λ^{∞}.

$$r = \frac{Fe}{6\pi\eta}\left(\frac{100\,\text{cm}}{\text{m}}\right)^2\left(\frac{z^2}{\lambda^{\infty}}\right) \qquad (37)$$

where F is the Faraday (9.648 x 10^4 C/mol), z is the unitless valence, η is the viscosity (0.000895 Kg/m·s), λ^{∞} is in S·cm^2/mol and r is then in nm. The limiting molar conductivities of simple ions such as Cl^- can be found in standard references (1993). The limiting molar conductivity of BTP^+ had to be measured as described in Section 4.4. For K^+, Cl^-, and BTP^+, r = 0.125 x 10^{-7}, 0.127 x 10^{-7}, and 0.347 x 10^{-7} cm, respectively.

For T4 lysozyme in 10 mM BTP, 100 mM KCl, the results of detailed BE modeling with and without inclusion of the asymmetry effect are shown in Figure 4.5.3.2. As in the Booth model, the asymmetry effects are seen to be greatest at low ionic strength and high valance. Account is taken of the detailed charge distribution within the model proteins. Final predictions as calculated by Allison and coworkers using the BE model are summarized in Table 4.6.1 given in Section 4.6.

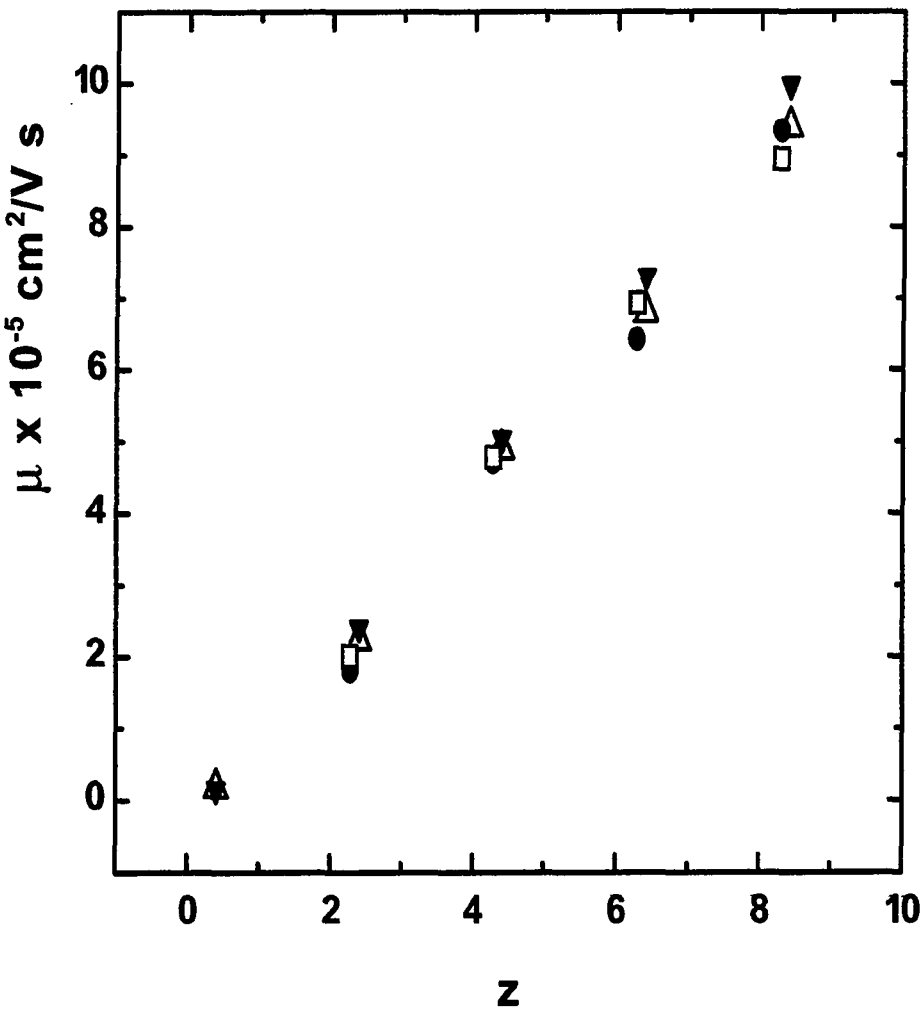

Figure 4.5.3.2 Asymmetry effect on boundary element modeling. The results are given ▼ without and △ with asymmetry effect included. Comparison with experimental results: ● SSE , □ CE. Data are for an ionic strength of 0.11 M.

4.6 Valence Summary

Using the formulas and measurements given previously, the following values were calculated for T4 lysozyme. For WT and all mutants:

I = 0.02 M, a = 2.20 nm, κa = 0.95, f(κa) = 1.00, and f(κa)/(1+κa) = 0.53,

I = 0.11 M, a = 2.20 nm, κa = 2.36, f(κa) = 1.08, and f(κa)/(1+κa) = 0.32, and

I = 0.16 M, a = 2.20 nm, κa = 2.86, f(κa) = 1.09, and f(κa)/(1+κa) = 0.28.

Table 4.6.1: Summary of Valence Results and Calculations for T4 Lysozyme.

T4	Experimental Measurements of Effective Valence		Predicted z^a	BE z^d	Model Predictions of Effective Valence		
	z_{eff}[b] SSE	z_{eff}[b] CE			z_{eff}[b] DHH	z_{eff}[b,e] Booth	z_{eff}[b,c] BE
I=0.02 M							
WT	3.25±0.20	*	8.28±0.48	8.402	4.22±0.14	3.92±0.14	3.80±0.14
SM	2.38±0.09	2.48±0.20	6.28±0.48	6.402	3.20±0.13	3.11±0.13	2.86±0.10
DM	1.56±0.13	1.60±0.15	4.28±0.48	4.402	2.18±0.12	2.19±0.12	2.13±0.08
TM	0.98±0.04	0.77±0.07	2.28±0.48	2.402	1.16±0.11	1.19±0.11	0.99±0.04
QM	0.22±0.05	0.17±0.05	0.28±0.48	0.402	0.14±0.11	0.15±0.11	0.15±0.00
I=0.11 M							
WT	2.31±0.20	2.21±0.23	8.28±0.48	8.402	2.66±0.09	2.55±0.09	2.33±0.08
SM	1.59±0.07	1.72±0.14	6.28±0.48	6.402	2.01±0.08	1.97±0.08	1.68±0.06
DM	1.17±0.11	1.18±0.09	4.28±0.48	4.402	1.37±0.07	1.36±0.07	1.21±0.04
TM	0.45±0.02	0.50±0.05	2.28±0.48	2.402	0.73±0.07	0.73±0.07	0.55±0.02
QM	No gradient	No mobility	0.28±0.48	0.402	0.09±0.07	0.09±0.07	0.04±0.00
I=0.16 M							
WT	1.50±0.19	*	8.28±0.48	8.402	2.32±0.08	2.23±0.08	2.11±0.07
SM	1.19±0.06	*	6.28±0.48	6.402	1.76±0.07	1.72±0.07	1.54±0.05
DM	0.80±0.10	*	4.28±0.48	4.402	1.20±0.06	1.19±0.06	1.14±0.04
TM	0.33±0.05	*	2.28±0.48	2.402	0.64±0.06	0.64±0.06	0.49±0.02
QM	No gradient	*	0.28±0.48	0.402	0.08±0.06	0.08±0.06	0.05±0.00

[a] Average formal charge was calculated from three sets of pK_a values as described previously. The error is estimated for the 95% confidence level. This is the value of z used in calculating z_{eff} for the DHH and Booth models.
[b] Given in proton equivalents.
[c] Includes asymmetry effects (IR). Error of μ_{BE}±3% on I=0.11 M data (as given by Allison) assumed for all I.
[d] These are the values of z used in the boundary element model.
[e] Because the functions for X,Y, and Z were not given explicitly by Booth, the error estimate for Booth's value can not be propagated through the term in parenthesis in Equation 34.
* Measurements could not be made either due to capillary wall adsorption or high current.

For RNase Sa at I = 0.11 M, a = 2.05 nm, κa = 2.20, f(κa) = 1.04, and f(κa)/(1+κa) = 0.33. For α-chymostrypsin at I = 0.10 M, a = 2.53 nm, κa = 2.69, f(κa) = 1.09, and f(κa)/(1+κa) = 0.30. For α-chymostrypsin at I = 0.20 M, a = 2.53 nm, κa = 3.71, f(κa) = 1.12, and f(κa)/(1+κa) = 0.24.

Table 4.6.2: Summary of Valence Results and Calculations for RNase Sa.

Sample	Experimental Measurements of Effective Valence		Predicted $z^{a,c}$	Model Predictions of Effective Valence	
	z_{eff}[b] CE	z_{eff}[b] SSE		z_{eff}[b] DHH	z_{eff}[b,c] Booth
I=0.11 M					
RNase Sa WT	-1.79±0.15	- 1.72±0.06	-5.67	-1.87	-1.81
RNase Sa 2K	-0.97±0.12	-0.82±0.02	-2.29 (-2.65)	-0.76	-0.73 (-0.84)
RNase Sa 5K	0.73±0.03	0.71±0.01	2.89 (2.49)	0.95	0.92 (0.79)

[a] Calculated from pK_a values taken from Laurents et al. (Laurents et al., 2003)
[b] Given in proton equivalents. For SSE, B*=0 Nonlin fits used.
[c] Values in parenthesis are for the case of the 5K His53 pKa = 6.0 instead of 7.4 as given by Laurents.

Table 4.6.3: Summary of Valence Results and Calculations for α-Chymostrypsin.

Sample	Experimental Measurements of Effective Valence	Predicted z^a	Model Predictions of Effective Valence
	z_{eff}[b] SSE		z_{eff}[b] DHH
I = 0.10 M			
α-chymostrypsin	1.98±0.03	11.00	3.25
	1.98±0.03	10.00[c]	2.95
I = 0.20 M			
α-chymostrypsin	1.16±0.02	11.00	2.62
	1.16±0.02	10.00[c]	2.38

[a] The average formal charges for α-chymostrypsin were calculated from pK_a's given by Marini and Wunch titration data (Marini & Wunsch, 1963). If use Segel pK_a's then get valence of 13-1=12 (Segel, 1976).
[b] Given in proton equivalents. B*=0 for SSE.
[c] Winzor asserts in several papers that he has observed binding of a single chloride ion to the monomer under these conditions and so results are presented with this possibility as well (Ford & Winzor, 1983; Wills & Winzor, 2001).

4.7 Ionic Strength Dependence of Mobility: Comparison of the Kohlrausch and Pitts Equations

As discussed in the Background section, the recent investigations of Li and co-workers provided the impetus for a similar investigation of the ionic strength dependence of mobility (Li et al., 1999). Two theoretical relationships between μ and I were examined for T4 lysozyme WT and TM proteins. These relationships, which incorporate the work of Kohlrausch (Equations 15) and of Pitts (Equation 17), are compared in Figure 4.7.1. To make this comparison, the MCE steady state measurements were converted to mobility (see Equation 20). Although the ionic strengths used are recognized to be above the expected limits of these theories, these relationships are often still used as first approximations of μ because of their simplicity (Li et al., 1999). As will be explained, it is the linearity and y-intercept of these equations which is of the greatest interest. The results are summarized in Table 4.7.1 below.

Table 4.7.1 The Predicted Valence of T4 Lysozyme from μ_∞

		Kohlrausch (Equation 15)		Pitts (Equation 17)			
	N[a]	$\sqrt{I}$[c]	Predicted Valence	$\sqrt{I}/(1+10.5\sqrt{I})$[c]	Predicted Valence	$\sqrt{I}/(1+7.2\sqrt{I})$[c]	Predicted Valence
		$\mu_\infty \times 10^{-5}$	z	$\mu_\infty \times 10^{-5}$	z	$\mu_\infty \times 10^{-5}$	z
BE							
WT	3	18.8±1.1	4.7	33.2±0.2	8.3	28.7±0.4	7.2
TM	3	5.0±0.4	1.3	9.21±0.2	2.3	7.9±0.2	2.0
MCE							
WT	9	15.6±0.6	3.9	28.7±2.1	7.2	24.6±1.6	6.2
TM	8	5.4±0.2	1.4	9.2±0.2	3.0	10.1±0.8	2.5

[a] N is the number of points used in the fit.
[b] z is the valence at zero ionic strength according to intercept of the indicated equation (Kohlrausch or Pitts).
[c] The abscissa of the used in Figure 4.7.1. Value of 10.5 and 7.2 for Ca (described in the Background section) are compared.

According to the theory, the y-intercept is the mobility of the salt ion at infinite dilution. This intercept can be converted to valence by the relation

$$z = \frac{\mu_\infty f}{e \cdot \text{constant}} \qquad (38)$$

where μ_∞ is given in $cm^2/V{\cdot}s$. In the present context, this intercept is interpreted as the mobility of the macroion (or valence) in the absence of any salt. However, if there are any intermolecular interactions (favorable or unfavorable), the intercept of plots such as those in Figure 4.7.1, could be skewed. That neither equation allows for the possibility of such interactions is not surprising given that, as discussed in the Background section, these were developed to describe the conductance of salt ions.

However, the steady state gradients in MCE may be altered by such interactions. If, for example, the macroions interact preferentially at high or low ionic strengths, there are unfavorable enthalpic contributions from charge-charge repulsion and an ideal fit with NONLIN would most likely return sigma values too low and too high, respectively. The value of μ_∞ (y-intercepts in Figure 4.7.1) would as a result be high in either case. It is generally only at higher concentrations that these solute-solute interactions are of concern. In all cases the steady state MCE data were fit for nonideality and based on comparable AUC B values, the source of B* was estimated to be primarily thermodynamic nonideality (as opposed to shallow ion gradients, for example, as discussed in Section 3.2.1). By fitting for B*, NONLIN effectively accounts for this concentration dependence of sigma, provided the model is appropriate. The value of μ calculated from steady-state results should therefore reflect that of an isolated marcroion.

The Kohlrausch equation predicts a linear relationship between mobility and the square root of ionic strength. Li et al. observed in their work, however, that the data plotted this way were not linear. In Figure 4.7.1 the BE values (A) exhibit the slight upward curvature observed by Li et al and a significantly better linear fit was obtained with Equation 17 (B). The standard deviation of a linear fit of the BE WT predictions drops from 7.1×10^{-6} $cm^2/V \cdot s$ using Equation 15 (A) to 5.4×10^{-7} $cm^2/V \cdot s$ (B) using Equation 17. Because the *same* set of formal valences was used to make the BE predictions, no salt-dependence in the resulting formal valence *should* be seen in this context. In other words, the intercept for WT and TM should correspond to the average formal valences of 8.28 and 2.28, which they do as is shown in Table 4.7.1. As discussed in Section 3.4, these formal valences have been calculated using combined textbook and titration data pK_a's. The titration data was not collected at multiple ionic strengths and extrapolated to zero ionic strength. There is therefore *no reason to assume* that these pK_a's are accurate at zero ionic strength. However, fitting these BE data provides a way to verify the method works before applying it to the experimental results (C and D). Furthermore, because the best fit for BE gives too large a C*a* value (10.5), this suggests the formal valences should change with ionic strength as discussed in the Section 5.2. The parameter C*a* in Equation 17 was expected to be 7.2, as calculated from Equation 17 (for B at 20° C) and the collision diameter of 22.0 Å. A value of 10.5 gives an *a* of 31.6 Å, which is 44% larger than expected. Li et al found their results overestimated *a* by 20% at most.

MCE values in Figure 4.7.1 (C) do not exhibit the slight upward curvature observed by Li et al (Equation 15). Neither, however, do they fit significantly better to

Equation 17 using the expected Ca = 7.2 (D). For example, the standard deviations of the WT fits are 6.8×10^{-6} $cm^2/V \cdot s$ (C) and 7.6×10^{-6} $cm^2/V \cdot s$ (D). It is possible, but unlikely, that an insufficient ionic strength range is the culprit. Li et al covered ionic strengths from 0.1 M down to 0.001 M, which is only an order of magnitude lower than that used in this work. The T4 lysozyme data actually encompass a greater overall range. At present, results with *Ca* equal to the best fit BE value (10.5) and expected value of 7.2 are shown in Table 4.7.1 for comparison. It was hoped that significantly better results would have been obtained with Pitt's results such that a reasonable *Ca* value could have been obtained from the experimental results. However, because there is no significant improvement in the fit of (D) over (C), it seems unproductive to pursue this at present. However, it can be said that both cases indicate that the formal valence does decrease as ionic strength decreases.

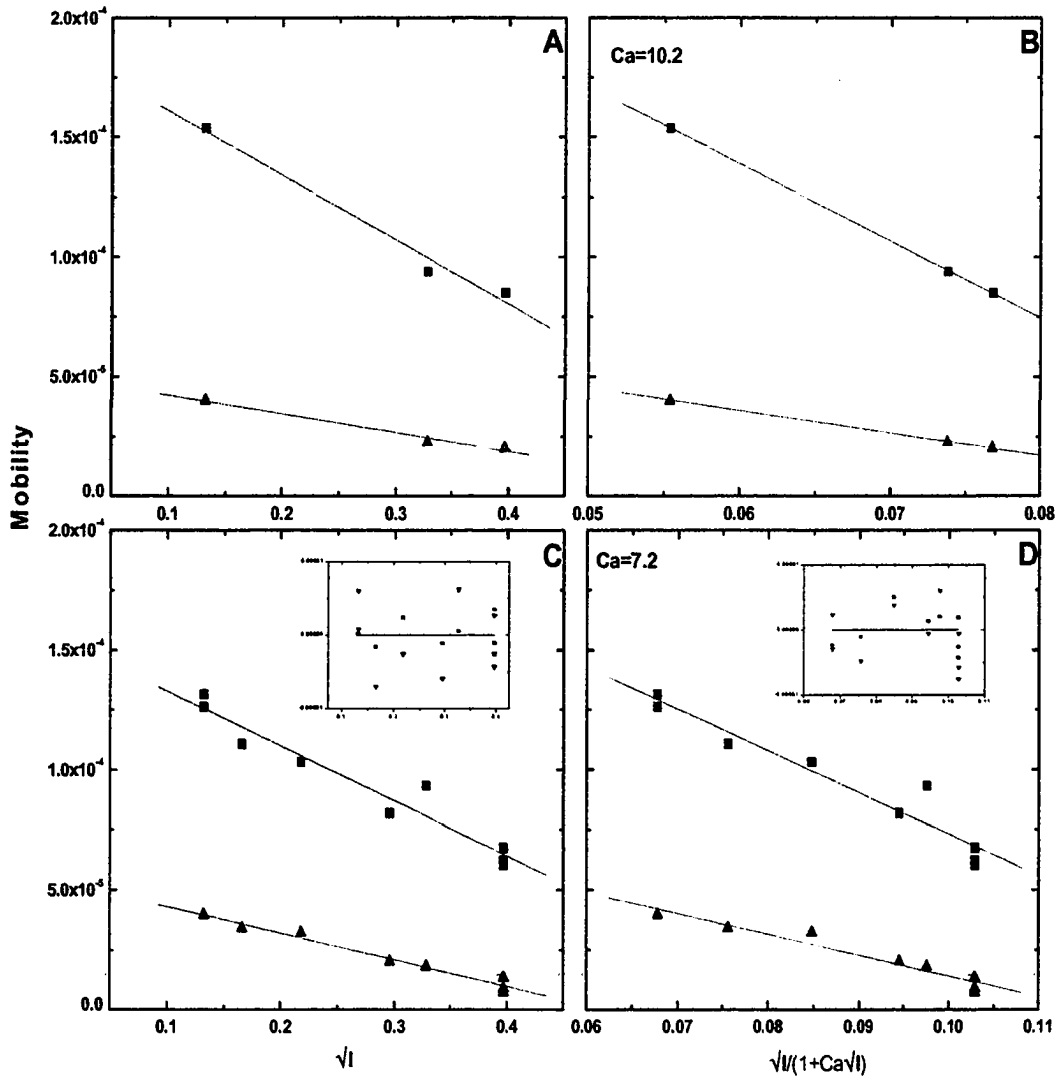

Figure 4.7.1: Dependence of Mobility on√I vs √I/(1+Ca√I).
Comparison of BE predictions (top) and MCE results (bottom) for ■ WT and ▲ TM. Equation 15 is used in A and C while Equation 17 is used in B (Ca=10.5) and D (Ca=7.2). Mobility is in cm^2/Vs. BE predictions were done only for I = 0.02, 0.11, and 0.16 M while experimental results were obtained for I = 0.02, 0.03, 0.05, 0.09, 0.11, and 0.16 M in the case of WT and TM.

CHAPTER V

DISCUSSION

Protein valence plays a role in stability, solubility, activity and is critical for designing and improving purification protocols. The magnitude of the contribution of valence to these properties is just beginning to be understood (Chapter 1). The intricacies of the microenvironment and its influence on valence are particularly daunting for a protein, where, compared to DNA, the type of and distance between charged groups is extremely variable. There are, it seems, few ways to experimentally access this value. The most direct means is electrophoretically. Free solution electrophoresis is an absolute, analytical method by which valence could be obtained. However, relating the electrophoretic result (whether it be μ or z_{eff}) to the valence has proven difficult for a number of reasons (Chapter 2). Nonetheless, there are a number of models (Section 4.5), of varying complexity, which attempt to do so. In obtaining free solution measurements, a relatively new technique, membrane confined electrophoresis (Section 3.2), was used along with the more established technique of capillary electrophoresis. T4 lysozyme (and its charge mutants) has served as the central model compound for testing several theories against experimental results. Some preliminary electrophoretic measurements with RNase Sa and α-chymotrypsin were also made.

5.1 Debye-Hückel Theory Applied to Macroions

One of the objectives of this work was to apply Debye-Hückel theory (with Henry's

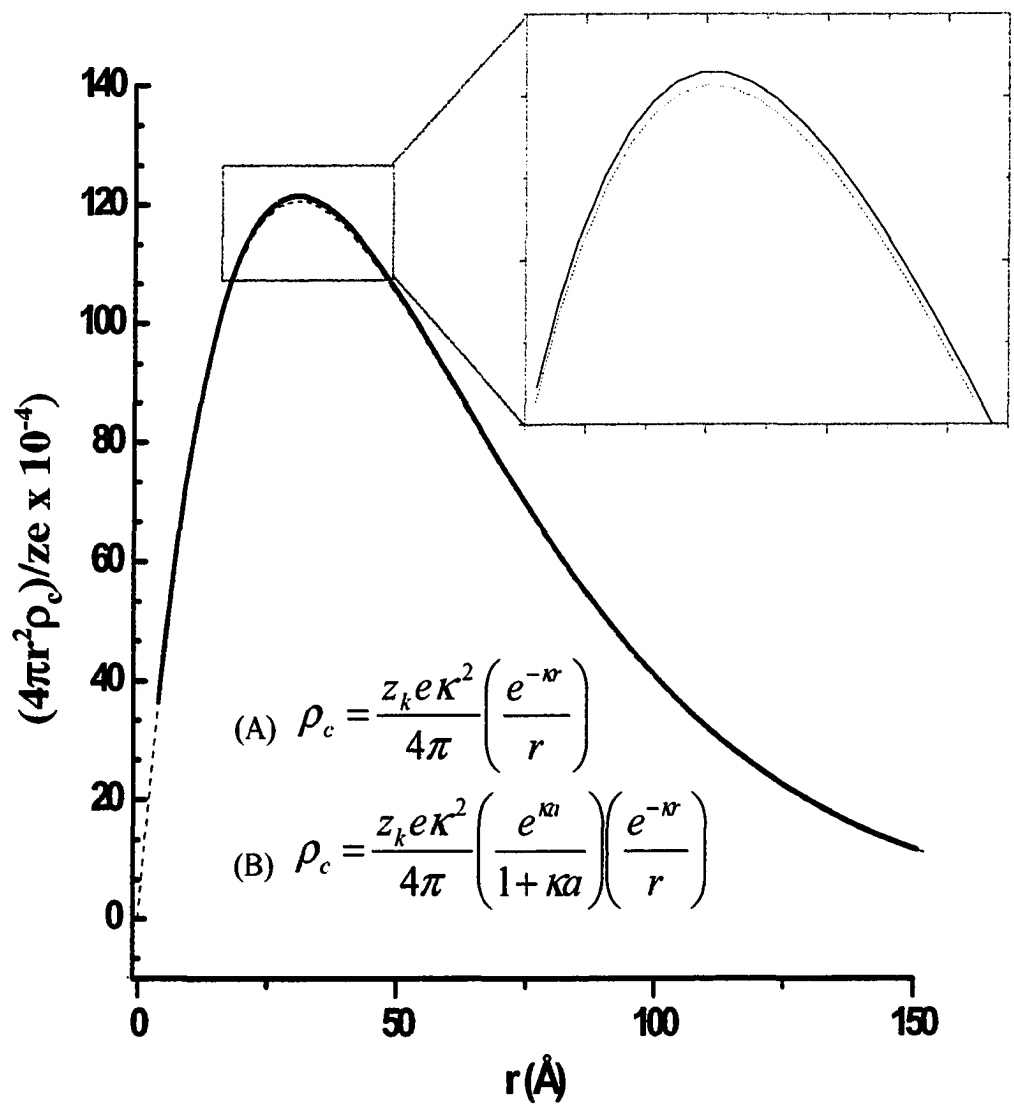

Figure 5.1.1: Point charge vs. finite charge. Excess negative charge over positive charge (dq/dr) at any distance r from the center of an arbitrary positive ion (I = 0.01 M). The red ···· is the solution of the DH model assuming a point charge approximation (Equation A) and thus is integrated from r = 0 to ∞. The black —— is the solution for an ion of finite size (Equation B, a = 3 X 10^{-8} cm) and is thus valid from r = a to ∞. Using the given integration limits, the area under both curves is 1.

correction) to T4 lysozyme and RNase Sa in order to determine the valence from the measured z_{eff}. The literature offers some conflicting information as to the nature of the parameters *a* and κ. For clarity, the interpretation of these used in this work is discussed here.

As discussed in Chapter 2, Debye and Hückel initially used a point charge as their central ion. As is shown in Figure 5.1.1 (red line), the excess counterion is found by integrating from zero to infinity. Recognizing that the point charge model (Equation A) was unrealistic in many cases, they changed the lower limit of integration to r = *a* in defining the charge density and thus the additional term, 1/1+κ*a*, arose (Equation B). This dissertation applied DH theory to the protein molecule as a whole (smeared charge assumption) and thus *a* is a key parameter in calculating the valence. In this work, the sum of the Stoke's radius of the protein and counterion has been used as the collision diameter. Unfortunately, this is, as yet, an ill-defined parameter and there is some disagreement in the literature, as to whether to include the counterion radius (Bull, 1964).

There is some confusion in the literature surrounding the definition of the Debye-length. Since it is a key term in Debye-Hückel theory, a brief discussion of its interpretation in this work is important. As described by Bull, "1/κ corresponds to the distance between two concentric spheres, i.e., between the central ion and the center of gravity of the ion atmosphere" (Bull, 1964). Furthermore, Wiersema defines κ as the "reciprocal *thickness* of the surrounding ionic atmosphere" (Wiersema et al., 1966). This would correspond to A in Figure 5.1.2. Eisenberg and Crothers, on the other hand, state that 1/κ is "the radius of the ion atmosphere" corresponding to B in Figure 5.1.2

Figure 5.1.2 The Debye length. (A) Definition of the 1/κ as given by Bull. Figure adapted from *An Introduction to Physical Chemistry*, p. 70 (Bull, 1964). (B) Alternative definition as given by Edsall and Wyman, p287, (Edsall & Wyman, 1958) as well as Eisenberg and Crothers, p356 (Eisenberg & Crothers, 1979).

(Eisenberg & Crothers, 1979). Both appear reasonable and it seems that some of the confusion may originate in the fact that both Helmholtz and Gouy-Chapman-Stern theory deal with ions at an electrified interface (e.g. electrode) in much the same way (Bergethon & Simons, 1990). This later work, originally developed by Gouy in 1910, predates the Debye-Hückel central ion theory. While it incorporates the idea of a finite (*salt*) ion size at an interface (and thus some region of linear potential decay called the Stern layer) the size of the interface has no meaning and the potential beyond the Stern layer drops off as $e^{-\kappa x}$ in a salt solution (Gouy, 1910). Similarly, with the Debye-Hückel theory for a point charge (considering spherical dimensions now), the potential drops off as $(e^{-\kappa r})/r$. However, in the Debye-Hückel finite (*central*) ion size model, the potential drops off as $(e^{-\kappa(r-a)})/r$.

As Tanford points out, at physiological ionic strength "1/κ becomes considerably smaller than the typical dimensions of the polyelectrolyte" (Tanford, 1961). For example, the 1/κ decreases from 9.6 nm at I = 0.001 M to 0.8 nm at I = 0.15 M. Thus the Debye length (in nm), as calculated from $1/\kappa = [(3.3/\text{nm})(I)^{1/2}]^{-1}$ (see Equation 12), corresponds to the *distance out from the (Stern) surface* until the charge density is reduced to 1/e of the value at the surface (dotted line in Figure 5.1.3). The correct interpretation of 1/κ in applying Debye-Hückel theory to a protein as a whole then must be as is shown in A of Figure 5.1.2. Indeed, when Debye-Hückel theory is applied in electrostatic modeling programs such as COGEN, the value of κ is zero inside the ion exclusion (Stern) layer (www.congenomics.com).

Figure 5.1.3 shows that as the size of the central ion increases from 3 Å (top plot, arbitrary ion) to 22 Å (bottom plot, TM lysozyme), the net charge of the ion atmosphere becomes greatest at the surface of the macroion and is given by the radial distribution function (dq/dr). Note that the areas under the red curves in Figure 5.1.3 are equivalent, as they should be. In other words, the volume of the *shell* extending from r = *a* to ∞, contains the correct amount of counter ion charge (q = -ze) to compensate that of the macroion (q = ze). This is because

$$q = \int_{r=a}^{r=r'} 4\pi r^2 \rho_c dr = -ze\,\kappa^2 \frac{e^{\kappa a}}{1+\kappa a} \int_{r=a}^{r=r'} r e^{-\kappa r} \qquad (39)$$

gives

$$q = -ze\left[1 - \frac{1+\kappa r'}{1+\kappa a} e^{-k(r'-a)}\right] \qquad (40)$$

upon integration, and at r' = ∞, q = -ze.

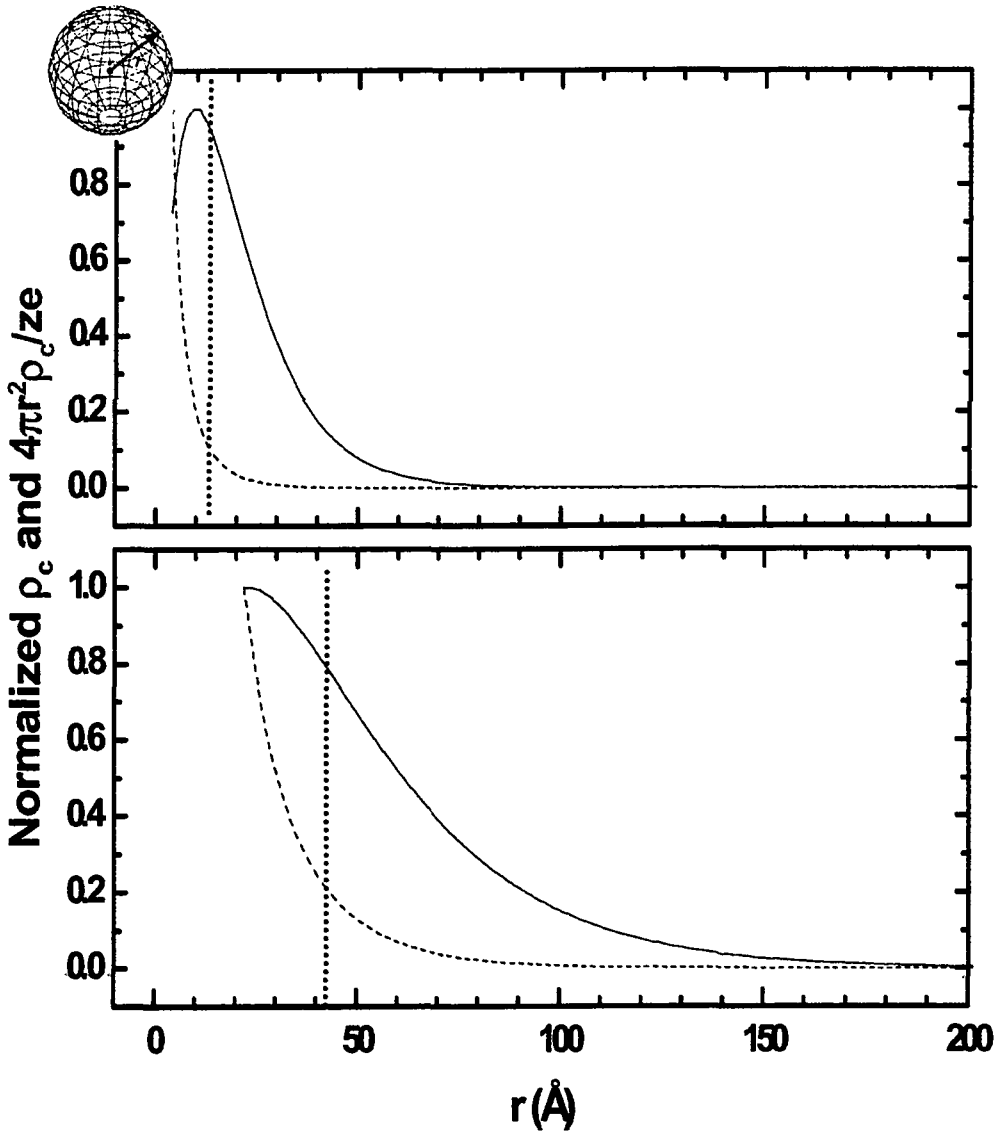

Figure 5.1.3 Normalized charge density and dq/dr. The dotted line (···) indicates where the density (---) falls to 1/e its value. This also corresponds to a distance of $1/\kappa$ from the surface of the ion. In the top plot the collision diameter was taken as 3.8 Å (3.8E-8 cm), $1/\kappa$ = 9.6 Å and $a + 1/\kappa$ = 13.4 Å. The bottom plot is for TM T4 lysozyme at I = 0.02 M. In this case a = 21.9 Å (2.19E-7 cm), $1/\kappa$ = 22.9 Å and $a + 1/\kappa$ = 44.8 Å. The valence was taken as 2.11 for both.

As expected, the T4 lysozyme and RNase Sa work is beyond the limits of applicability originally given by Debye and Hückel ($ze\psi << k_BT$ and $I < 0.001$ M such that $ka << 1$). However, it has been found in the past that Debye-Hückel theory works surprisingly better than expected, even well beyond its limits. For example, in the context of electrophoresis (which requires the additional considerations of the electrophoretic and asymmetry effects as discussed in Chapter 2), DH theory has been applied successfully to capillary electrophoresis of *Straphylococcus aureus* nuclease mutants at I = 0.06 M (Kalman et al., 1995) and α-lactalbumin at I = 0.10 M (Carbeck & Negin, 2001). Furthermore, the DLVO theory of colloidal interactions

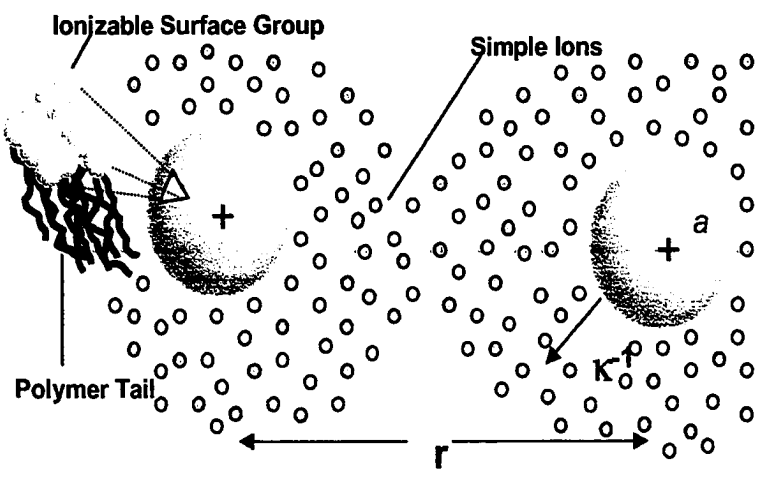

Figure 5.1.4 DLVO theory representation. Charge-stabilized colloidal suspension. The Debye length (κ^{-1}) is indicated for the salt solution (simple ions) surrounding the macroions. Figure adapted from Crocker and Grier (Crocker & Grier, 1998).

(Figure 5.1.4) also makes use of the work of Debye and Hückel (Verwey & Overbeek, 1948; Derjaguin & Landau, 1941). At a minimum, the Debye-Hückel theory is a good first approximation of the electro*static* behavior of ions. Additionally, it is by far the most tractable theory.

5.2 The Valence of T4 Lysozyme

Previous work indicates that the T4 lysozyme mutants used in this research are very similar in terms of structure and stability to that of the wild type T4 lysozyme (Dao-pin et al., 1991). The pK_a's of the changed residues are far removed from the pH at which the experiments were conducted. Additionally, all of the amino acid residues for which substitutions were made are solvent-exposed and very mobile (Dao-pin et al., 1991). These substitutions are shown in Figure 5.2.1.

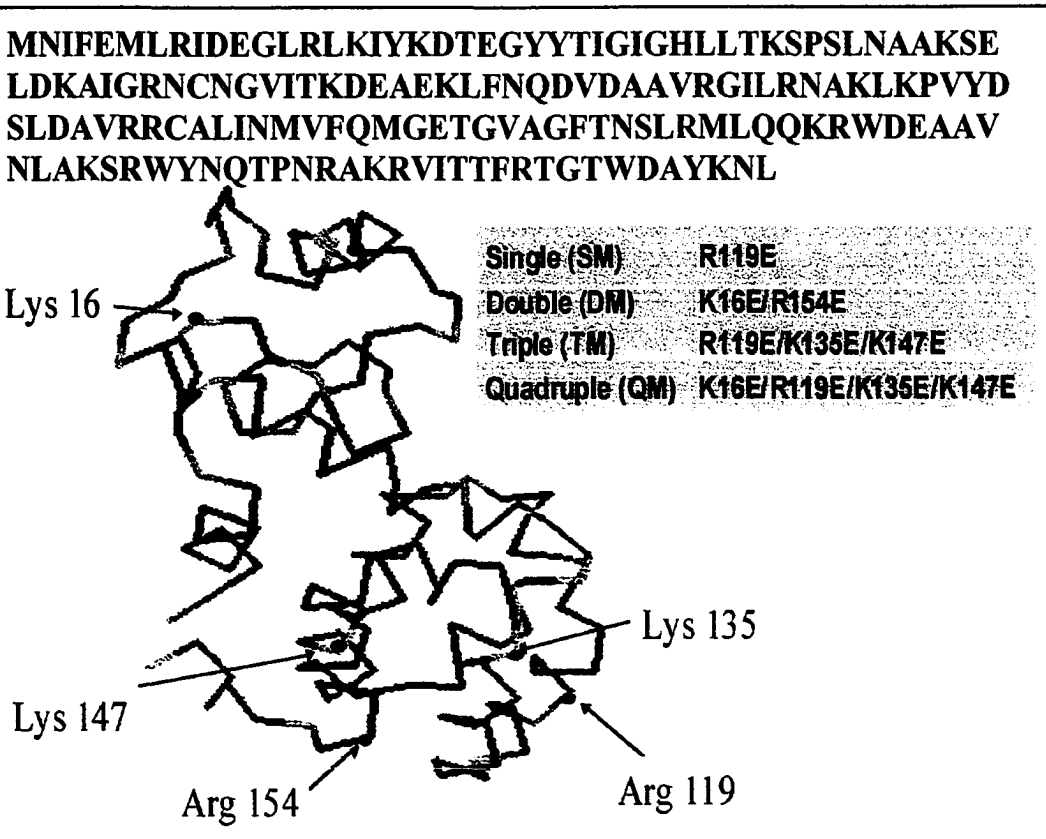

Figure 5.2.1. Identification of mutated residues of T4 lyszoyme. The WT protein has 164 amino acids and a MW of 18,633. Each red dot represents a mutated residue corresponding to the appropriate red letter in the sequence given above.

Debye-Hückel-Henry Model at I = 0.11 M

One of the virtues of the experimental protocol in this work is that by using a series of charge mutants in which the change in valence is known, one does not to have to necessarily know the value of the valence for given mutant protein. For example, in analyzing the results by the Debye-Hückel equation, $z_{eff} = z[f(\kappa a)/(1+\kappa a)]$, the value of z is poorly characterized. With a series of charge mutants however, we can examine $d(z_{eff})/dz = f(\kappa a)/(1+\kappa a)$. Therefore, even if the absolute values of z used in plots of z_{eff} vs. z are inaccurate, the slope should be accurate provided dz and *a* are unchanged for the mutants.

Considering first the Debye-Hückel-Henry model as described in Section 4.5.1, calculations of z_{eff} (using Equation 31 which relates valence to effective valence) can be compared with experimentally determined z_{eff} (Table 4.6.1). At I = 0.11 M, the WT T4 lysozyme is expected to have the greatest discrepancy due to it larger surface potential (~20 mV). Even so, the value of z_{eff} calculated from simple DHH theory is within 15% of experimental SSE values and 20% of values calculated from CE data as is shown in Figure 5.2.2. If instead the slope of z_{eff} vs z for all the SSE data is considered, the experimental result is within 7% of the predicted slope of 0.32 (see Equation 31, Section 4.5.1). In all cases, as expected, the DHH approximation yields higher values than those obtained experimentally. The overestimation by DHH theory results from the fact that their description of the "distribution of mobile ions in the fluid about the macro-ion is assumed to be that which exists at equilibrium in the absence of the applied field" (Tanford, 1961).

Booth Model at I = 0.11 M

Examination of the results in the context of Booth's work shows better agreement. Booth's equation as given by Tanford, was presented in section 4.5.2. Using Equation 34, the calculated z_{eff} values for WT are within 8% of SSE experimental values and 13% of those calculated from CE mobility. If again the slope for all the data is compared with that predicted by Booth's work (Figure 5.2.2), the results are within 1%. The improvement over the DHH model is attributable to the terms Y and Z (see Section 4.5.2) which describe the distortion of the mobile ion distribution by the applied field.

Boundary Element Model at I = 0.11 M

Making use of the boundary element model developed by Allison and coworkers, the discrepancy for WT is < 1% (SSE) and 5% (CE). The same trend is seen throughout the data. Although the overall experimental slope of z_{eff} vs z is 3% greater than BE predicts, the *individual* values track much closer than for any other model. These results are summarized in Figure 5.2.2 below.

The predictive ability of BE is particularly apparent upon examination of the behavior of the mutants with a smaller charge. Both SSE and CE show that the z_{eff}/z ratio decreases by about 20% for TM and most likely even more for QM (since experimentally no gradient or mobility was observed for QM). Although neither DHH theory nor the more complex work of Booth predicts this, BE modeling does. The results suggest that for structures with many charged groups but low net charge the mobility is sensitive to the charge distribution (Wiersema & Overbeek, 1967). The BE model by Allison predicts that if the placement of the three charge mutations of TM are changed, but that the protein still has the same formal charge, then z_{eff}/z changes from 0.23 (TM)

to 0.29 (L16E/L135E/L147E) to 0.25 (L16E/A119E/L135E). If z is reduced even further as in the QM protein, an even greater deviation in z_{eff}/z from the high charge value is predicted. In the limit of a pure quadrupolar charge distribution with z = 0, model studies show that the electrophoretic mobility is not necessarily zero (S. Allison, personal communication). Thus, the commonly held assumption that the isoelectric point and the point of zero electrophoretic mobility are the same is not strictly correct. Indeed, there is evidence in early literature which suggests that there may be a significant discrepancy between these two points, and that the discrepancy becomes greater as the ionic strength increases (Bull, 1964; Barnett & Bull, 1960).

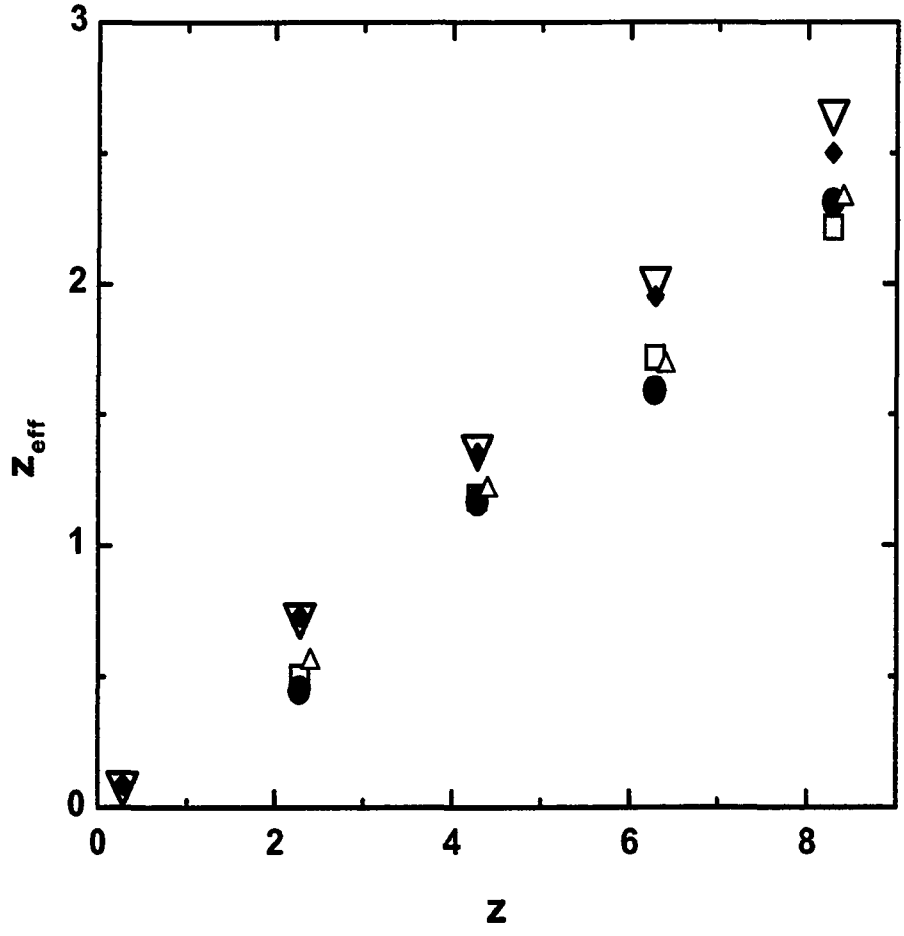

Figure 5.2.2: Model and experimental summary for at I=0.11 M. Effective charge as a function of formal charge for ▽ DHH, ♦Booth, ● SSE, □ CE and △BE results. DHH: Slope 0.32 ± 4.18E-17, yint 0 ± 2.14E-16. Booth: Slope 0.30 ± 0.01, yint 0.03 ± 0.03. SSE: Slope 0.30 ± 0.02 yint -0.21 ± 0.01. CE: Slope 0.29 ± 0.02 yint –0.15 ± 0.11. BE: Slope 0.29 ± 0.12 yint –0.12 ± 0.07.

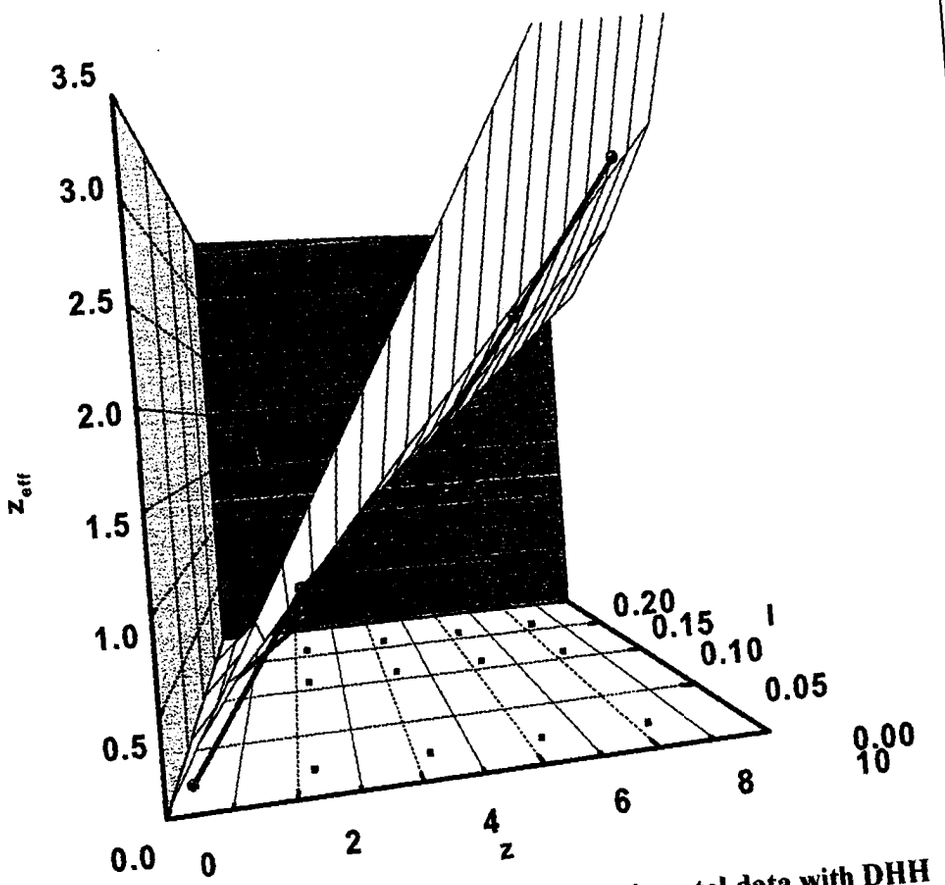

Figure 5.2.3: A 3D plot comparing MCE experimental data with DHH model. DHH model (yellow surface) shown with experimental steady state results at for I = **0.16, 0.11,** and **0.02** M. Below is another view.

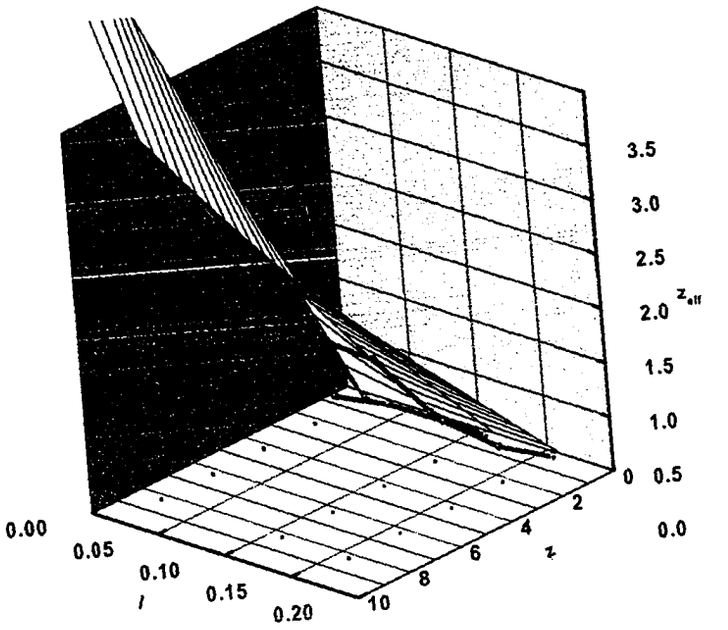

Ionic Strength Dependence of z_{eff}

When the results of using low and high ionic strengths are considered, some discrepancies are apparent. Considering only DHH theory first, in Figure 5.2.3 it is seen that this model is least predictive for the WT protein at the highest ionic strength where it overestimates the effective valence by 54%. Agreement between the predicted and measured z_{eff} is better at lower valence and ionic strength, where the overestimation for TM T4 lysozyme is only 18% at I = 0.02 M. If it is assumed that both $f(\kappa a)/(1+\kappa a)$ (0.28 at I = 0.16) and the measured z_{eff} values are correct, WT would have a predicted valence of 5.3, significantly lower than the formal valence used. Similarly, at an ionic strength of 0.02 M, the valence of WT would be 6.37. As Table 4.6.1 shows, z_{eff} predictions by the method of Booth are an improvement over those from DHH but they are still 20% higher for WT at I = 0.02 M, for example.

Because BE modeling was the most predictive at I = 0.11 M, further discussion shall focus on this model relative to the experimental results at the other ionic strengths (Figure 5.2.4). Because there is error in z as well as z_{eff}, standard linear regression is less appropriate. Thus a Model II regression was performed to get an error estimate of the BE and SSE slopes that would reflect this (Sokal & Rohlf, 1981). Even so the error does not bridge the difference as Table 5.2.1 shows, indicating that these are statistically different slopes.

Table 5.2.1: Model II Regression Error on SSE Slope.

I	BE	SSE
0.02	0.46 (0.39-0.52)	0.38 (0.33-0.43)
0.16	0.26 (0.23-0.30)	0.19 (0.16-0.22)

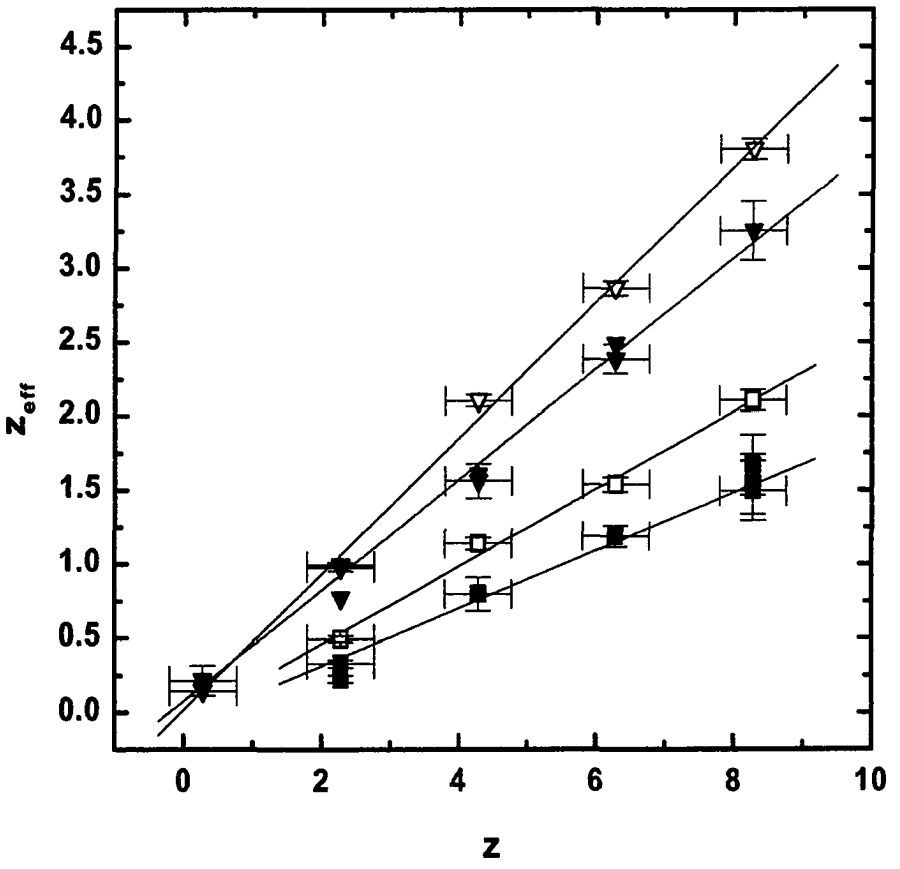

Figure 5.2.4: z vs. z_{eff} for higher and lower ionic strengths. Comparison of BE model predictions (white) with MCE (blue) and CE (red) experimental data. The results at I = 0.02 M are shown for ▽ BE (slope 0.46 ± 0.02, intercept 0.01 ± 0.13), ▼ MCE (slope 0.38 ± 0.01, intercept 0.08 ± 0.07) and ▼ CE (slope 0.39 ± 0.02, intercept -0.02 ± 0.09). The results at I = 0.16 M are shown for □ BE (slope 0.26 ± 0.02, intercept -0.06 ± 0.09) and ■ MCE (slope 0.19 ± 0.01, intercept -0.07 ± 0.07).

A. Comparison with Capillary Electrophoresis:

As seen in Figure 5.2.2, capillary electrophoresis results were in excellent agreement with MCE results at I = 0.11 M. It was postulated that this would be the case at other ionic strengths as well. By comparing MCE results to the more established technique of CE, it was hoped that some insight into the source of the discrepancy shown in Figure 5.2.4 might be gained. Unfortunately, due to limitations of the CE technique, absolute mobility measurements could only be made at the low ionic strength. However, at the low ionic strength (I = 0.02 M), experimental data from CE once again agreed well with MCE results (Figure 5.2.4). At high ionic strength, MCE steady state measurements were repeated to get 2 more global fits (a total of 18 individual measurements at 6 different fields) giving a precision of ±0.1. Therefore, although the MCE results are lower than the theoretical predictions in these two cases, it is believed not to be an instrumentation problem.

B. Other Possible Sources of Discrepancy:

Believing the instrument to be measuring z_{eff} accurately, several other possible sources of the discrepancy shown in Figure 5.2.4 were investigated. First, charge fluctuations could be responsible. Second, as discussed (Chapter 2), the BE model solves the PB at a molecular surface described as containing only the backbone charge as calculated from pK_a's. It is possible that some small ions are contained in this surface and contribute to the net valence (in which case the T4 valence and mobility could be reduced). Third, ionic strength altered pK_a's would give rise to differences between experiment and model. Because ionic strength effects on pK_a's are still as yet hard to model, BE predictions were all made with the same set of pK_a's (see Section 3.4).

Perturbation of the environment surrounding one or more of the charged residues, however, could shift their pK_a's.

Charge fluctuation-heterogeneity could arise from proton binding fluctuations as described by Linderstrøm-Lang or from temporary complex formation between the buffer and macroion. In order for this to be observable, the fluctuation would have to persist over a long time scale relative to the measurement (> 0.1 sec). According to Linderstrøm-Lang theory, the standard deviation in the net valence, $\overline{z^2}-(\bar{z})^2$, from proton binding can be estimated by the slope of the titration curve near the pH of interest such that

$$\frac{\partial \bar{h}}{\partial pH} = -2.303\left[\overline{z^2}-(\bar{z})^2\right] \qquad (41)$$

where $\bar{h}$ is the mean number of protons removed during titration ($\bar{h} = 0$ when the protein is fully protonated) (Edsall & Wyman, 1958). For WT T4 lysozyme at pH 7.5 this gives a deviation of approximately 3.4. Although this is significant, the time it takes to make a steady-state measurement is sufficiently long such that only the mean net valence would be measured. That is to say all the possible proton binding fluctuations that can occur, will occur during the time it takes to make a measurement such that multiple measurements will give the same result. This stems from the fact that H^+, which has a diffusion coefficient of 9.311E-5 cm^2/s, can traverse a T4 lysozyme molecule 20,000 times in the course of a 0.1 s measurement. If we could make instantaneous measurements, the valence estimate might vary by as much as ±3.4. As for buffer ion fluctuations, there is no way to exclusively estimate this possibility. Charge heterogeneity in general, which might also arise from sample impurities, for example, would show up in σ/E vs. E plots as discussed in Sections 3.2.1 and 4.1.4. Generally no

or very little slope was observed in these plots (see Figure 5.2.5 as an example). In some instances (second set TM, I=0.15 data) a small slope was observed for the B* fit data and not for the ideally fit data although the significance of this observation is unknown.

According to the Protein Data Bank (PDB) structures of the WT (2LZM) and single mutants K16E (1L42), R119E (1L44), K135E (1L45), K147R (1L46), and R154E (1L47), no ions are bound. The WT was crystallized in 1.05 M K_2HPO_4, 1.26 M NaH_2PO_4, 0.23 M NaCl, 1.4 mM β-mercaptoethanol at pHs between 6.7 and 7.0 for 2 years. It should be noted that the solvent molecule SOL168 of 2LZM was later redefined as a possible chloride (unfortunately this is *not* mentioned anywhere in the header file of 2LZM or its mutants in the Protein Data Bank). However, as Nicholson points out, "Lys 124 of an adjacent molecule [of T4 lysozyme] in the crystal structure is within 4.6 Å of the bound chloride ion [SOL168] and may contribute to its binding in the crystal lattice. The role of the chloride ion *in solution* is therefore uncertain" (Nicholson et al., 1991). It seems unlikely as well that small ion binding would occur at only the high and low ionic strengths. However, it may be possible that there are two different phenomena occurring at these extremes. Possibly, small ion binding diminishes the valence only at the high ionic strength. This is something to keep in mind in future work on T4 lysozyme.

The third possibility seems more likely and was experimentally testable. While the mutated residues do have pK_a's far removed from the experimental pH, the two cysteines and one histidine present in all of the T4 lysozymes do not. It is known that high salt favors ionization. The extent to which these changes occur, however, is something not well understood or predictable for proteins. Some progress has recently been made by Antosiewicz (Antosiewicz et al., 1996b). Ionic strength induced pK_a shifts

in T4 lysozyme could give rise to the changes in WT valence as shown Table 5.2.2 below.

Table 5.2.2: Possible pK_a Changes in T4 Lysozyme WT with I.

I (M)	HIS^{70}	CYS^{54}	CYS^{97}	Change from formal valence used in BE
0.02	0	0	0	-1
0.11	+1	0	0	0
0.16	+1	-1	-1	-2

A cysteine-free variant, WT*, was used to test this. Though a whole series of cysteine-free mutants would be needed to definitively prove this, only a WT* mutant was available. It was hypothesized that if the WT* was used in the low and high ionic strength solutions, the measured effective valence would be higher than that previously measured for WT. The BE predictions would then be in agreement with experimental results and the previous discrepancies could be attributed to a larger-than-expected ionic strength effect. Furthermore, just as the simple correction for ionic strength given by

$$\Delta pK_a = \log \frac{\gamma_{conj\ base}}{\gamma_{conj\ acid}} \qquad (42)$$

is dependent on the valence of the titrable group, it would be expected that the net protein charge would be a factor. The activity coefficient of the ion (γ) is found from the Debye-Hückel limiting law

$$\log \gamma = -0.509 z^2 \sqrt{I} \left(\frac{L}{mol} \right)^{1/2} \qquad (43)$$

As an example, ΔpK_a at I = 0.1 M is -0.32 for z = -1 and -0.53 for z = -2, but this is a simple point charge approximation developed such that the activity and ionic strength refer to the same ions; there is no "background" electrolyte as is the case in this work

(Segel, 1976). It is hoped that the more appropriate and complex modeling of Antosiewicz will eventually be available to the general user for the above purpose. Nonetheless, the ionic strength correction for a protein should follow the same trend as in Equation 42, diminishing with net valence. Thus the results observed could be explained in this manner.

However, using this WT* protein, it was found that the effective valence was not significantly greater in either case. The results are summarized below in Table 5.2.3. As expected, the results for WT and WT* at low ionic strength are in excellent agreement. The resulting z_{eff} for WT* was found to be within 1% of the value for WT. Measurements of WT protein were collected with untreated membranes while WT * with treated membranes (BioDesign, 1 mM EDC/EA). This confirmed that membranes were not a source of the discrepancy between model and MCE results. At high ionic strength the z_{eff} for WT* is 9% higher than for WT protein. However, the difference is within error of the NONLIN fit for WT and the precision of the instrument (Section 5.1). Diagnostic sigma/E vs E plots show no field dependence (Figure 5.2.5) and the post MCE WT* samples were pure with respect to charge as determined by CE measurements (Figure 5.2.6).

Table 5.2.3: Effective Valence of WT and WT* at Various I.

T4 Lysozyme	I=0.02 M	I=0.11 M	I=0.16M
WT	3.25±0.20	2.31±0.20	1.50±0.19
WT*	3.22±0.16	2.32±0.15	1.63±0.01
BE	3.8	2.33	2.11

Although it could obviously be a combination of factors, the observed discrepancy between the model and results is still predicted to lie in the formal valence

used. As has been discussed, there is greater error in determining the formal valence than in measuring the effective valence. The first set of pK_a's used was obtained at 10° C and an ionic strength of approximately 0.11 M (Anderson, 1992). Experimental evidence presented here suggests there are ionic strength dependent shifts but that the cysteine residues are not involved in the salt-dependent shifts at pH 7.5. However, at present, which pK_a's are shifted is uncertain. Table 5.2.4 summarizes the SSE/BE salt dependent valences for T4 lysozyme suggested by this work assuming that the MCE z_{eff} measurements are accurate, the BE model slope is correct, but that the formal valence is ionic-strength-dependent. This, of course, implies that dz is not constant with ionic strength.

Table 5.2.4: Valence of T4 Lysozyme at Low, Medium and High I.

T4 Lysozyme	I=0.02 M	I=0.11 M	I=0.16M
WT	7.1	8.0	5.8
SM	5.2	5.5	4.6
DM	3.4	4.0	3.1
TM	2.1	1.6	1.3
QM	0.5	-	-
Average dz:	1.7	2.0	1.5

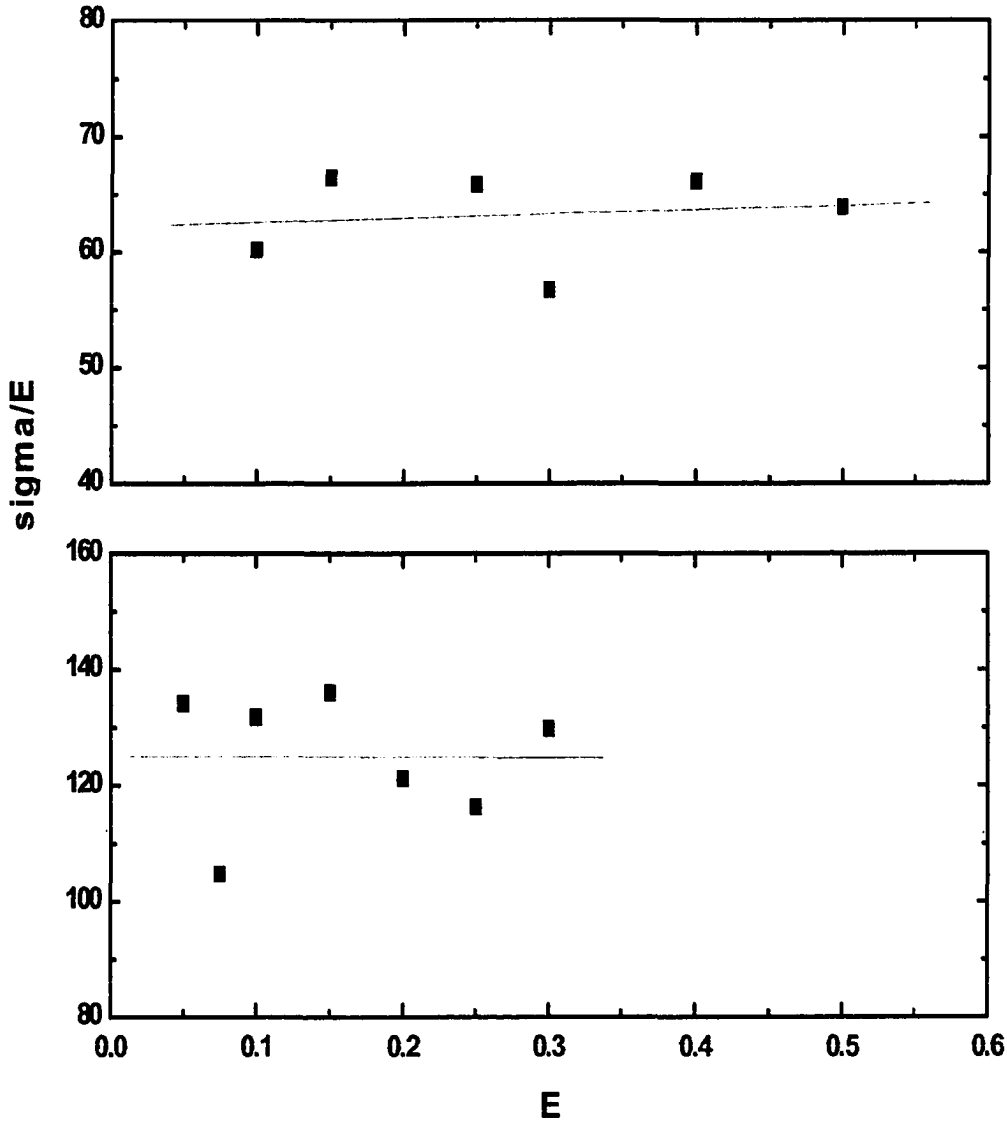

Figure 5.2.5: Sigma/E vs. E for WT* at high and low ionic strengths. For I = 0.16 M (top) the slope is 3.6 and for I = 0.02 M (bottom) the slope is -0.9.

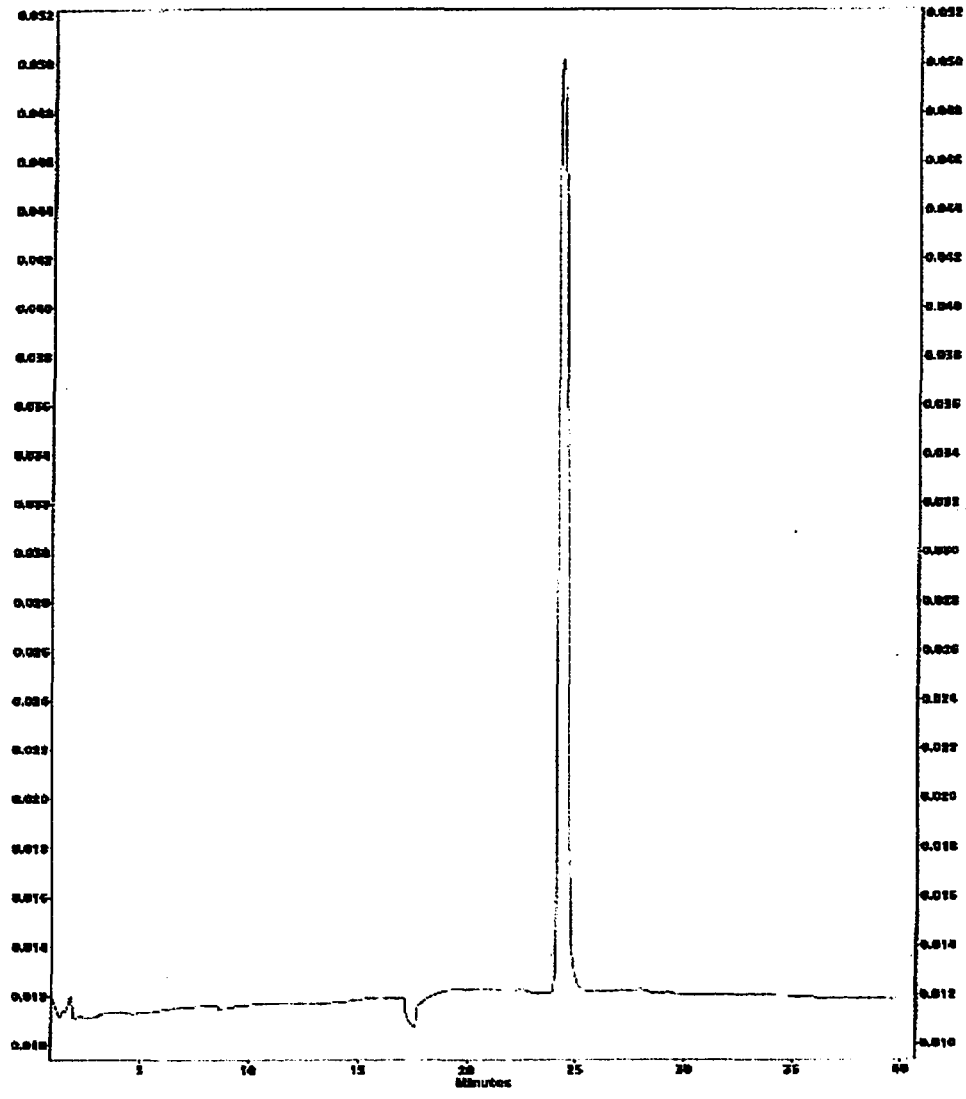

Figure 5.2.6: CE of WT* post MCE. The sample was removed from the MCE after 7 days of measurements at I = 0.16 M. Subsequently, CE mobility measurements were made on a neutral capillary at 4 KV using 0.01% BA as a neutral marker.

Mulitple pH experiments in the MCE

A large number of experiments were done at different pHs in the hopes providing more than 4 or 5 data points for the resulting z vs z_{eff} plots. However, the results were not given because, as we learned later, there is membrane interference at pHs other than 7.5. It should be noted that the residuals to these fits had a significant "W" shape. Another reason the multi-pH experiments did not work may be the result of a hydrodynamic radius change as Kalman and coworkers have discussed (Kalman et al., 1995). They found a strong pH dependence for *Staphylococcus aureus* nuclease charge mutants in the range 3 to 9. It is possible this occurs for the T4 mutant proteins as well. Though the ionic strength dependence of the hydrodynamic radius was verified for the results presented here and found to be invariant, the pH dependence was not. If these mulit-pH studies are readdressed in the future (as the membrane problem seems to be solved) this dependence should be investigated via AUC.

Summary

The use of T4 lysozyme WT protein and charge mutants allowed coverage of a more extensive charge range within a single set of experimental conditions than could be accomplished with pH changes. The differing response to the electric field is attributed solely to the change in charge due to the amino acid replacements and not to changes in shape. Similar experiments carried out by changes in pH would be limited in that multiple buffers would be needed to cover a substantial range in protein charge. This would introduce additional uncertainties, and at the extremes of pH, changes in protein frictional drag would be expected as denaturing pHs were approached. By using a series of charge mutants of a single protein, these concerns were eliminated. In analyzing the

mobility and charge of the various mutants of T4 bacteriophage lysozyme, several models were considered in order of increasing complexity. Linear evaluation and partial, nonlinear evaluation of the electrophoretic behavior of charged particles yielded, under many conditions, adequate approximation of electrophoretic behavior. However, detailed structural information combined with the electrostatic potential treated at the level of the full PB equation, including ion relaxation, yielded values that were the most representative of experimental results.

5.3 Ribonuclease Sa

MCE and CE results for RNase Sa in 10 mM BTP, 100 mM KCl (pH 7.5), given in Table 4.6.2, are plotted in Figure 5.3.1. As was found with T4 lysozyme, these two techniques are in excellent agreement.

The resulting experimental slope (0.29) for RNase Sa is within 15% of that predicted by simple DHH theory (0.33). Booth's model improves agreement, decreasing the theoretical slope to within 10%. Although T4 lysozyme results were in better agreement even with simple theory, there are a number of considerations unique to the RNase Sa results.

First, there are some aspects of the NMR titration results which should be kept in mind. NMR titrations measurements show large pKa shifts between the WT and 5K proteins (Laurents et al., 2003). These titrations studies further predict that the WT pKa values have the largest deviations from typical model compound pKa values as early (2001) MCE experiments had indicated. These NMR pKa values give a dz of 1.7 (a value of 2 would be expected if the WT, 2K, and 5K pKa values were the same). Unfortunately, no pKa values for the 2K protein are available and the average of the WT

and 5K pKa values were used as a reasonable first approximation. However, the resulting pI from these average pKa values is 5.5 which is significantly higher than the experimentally observed value of 4.6. The 5K NMR titration pKa values themselves also overestimate the experimental pI. Furthermore, while the structure is not expected to be significantly different, there is no crystal structure of the 5K variant verifying this. Interestingly, if the pKa valueof 5.95, calculated by Coulomb's Law (Laurents et al., 2003), for His53 is used in place of the NMR value of 7.39 for the 5K protein, the CE and MCE slopes are within 3% and 6%, respectively, of the Booth slope. It should also be pointed out that the NMR titrations were done at concentrations of 1-2 mM (~16 mg/mL). Although the ionic strength was 100 mM for the acid portion of the titration curve, no salt was added for the alkaline portion (N-terminus and tyrosines). At this concentration the distance between molecules is roughly 10 nm while the Debye length approaches 20 nm as the ionic strength drops below 5 mM and this may have had some affect on the results.

Second, recent work (with rhodamine-dextran and nitrate) to assess bulk fluid flow and background electrolyte behavior, has shown these to be affected differently depending on the direction of the current (Susan Chase, personal communication). These results show that for 10 mM BTP, 100 mM KCl, pH 7.5 no bulk fluid flow or NO_3^- gradient are present with the anode at the bottom of the cell (as in the T4 lysozyme MCE experiments). There is, however, a very slight NO_3^- gradient (particularly at higher fields) with the anode at the top of the cell (as in the RNase Sa WT and 2K MCE experiments). If this were a problem, one would expect only the WT and 2K proteins to be affected and this may contribute to the nonzero intercept observed.

Initially, all the RNase Sa data was collected on a different machine ("black box" prototype MCE) than that used for the T4 and α-chymotrypsin experiments (see Table 4.2.4.1 and the black triangles in Figure 5.3.1). As discussed in Section 5.5, measurements of the protein RNase A in the "black box" device gave a smaller sigma (17%) than in the "sliver box" prototype. If the difference between the two prototypes is taken into account, the resulting z_{eff} for RNase Sa are -2.05, -0.96 and 0.84. These give a slope of 0.29 ±0.01 which is much closer to the DHH and Booth predicted slopes of 0.34 and 0.33. To determine if instrument to instrument variation or membranes were a source of discrepancy, the RNase Sa WT and 5K experiments were repeated in both devices with treated SpectraPor membranes. In the case of B*=0, repeated experiments in the "black box" prototype were within 3% and 8%, respectively, for 5K and WT proteins. The "silver box" results were within 12% and 13% of the average "black box" results. Result from overall global values are given in Figure 5.3.1. While there is some instrument to instrument variation, the MCE results are reproducible and agree well with CE results. DHH and Booth predict slightly higher slopes for the RNase Sa proteins than those observed experimentally (Figure 5.3.1) if the NMR titration pKa values are used

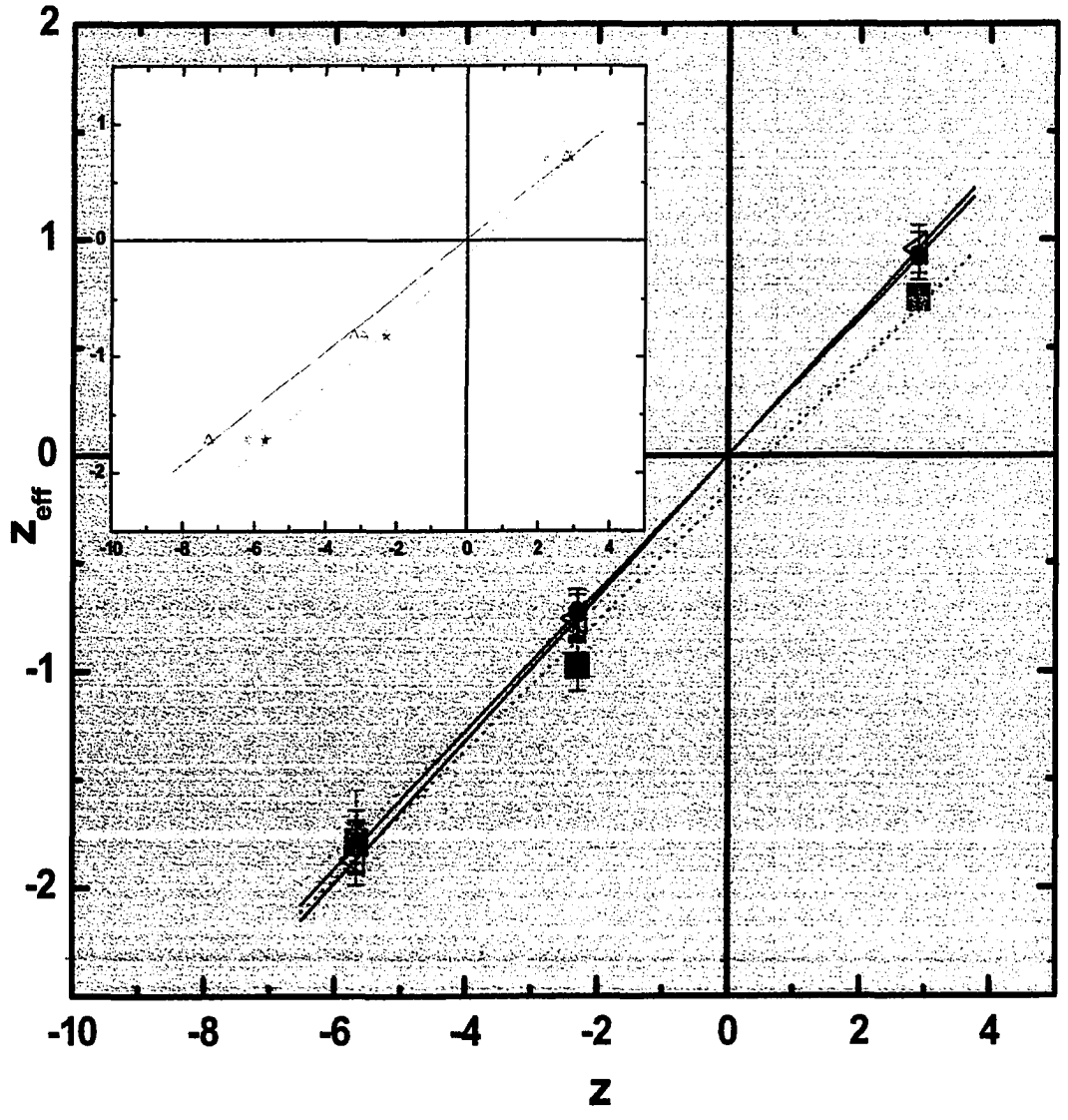

Figure 5.3.1: Comparison of CE vs MCE of RNase Sa. Using NMR titration pKa values, the results are shown for ■ CE (slope 0.30 ± 0.02, intercept -0.18 ± 0.09) and * MCE experiments (slope 0.29 ± 0.01, intercept -0.12 ± 0.03). All the experiments were done in 10 mM BTP, 100 mM KCl, pH 7.5 and the MCE z_{eff} calculated from global, ideal Nonlin fits. ◁ DHH theory predicts a slope of 0.33. ● Booth theory predicts a slope of 0.32. Also shown inset are the MCE results using model compound pKa values △ (slope 0.24 ± 0.01, intercept 0.01 ± 0.04) (Shaw et al., 2001)and using Coulomb's Law calculated pKa values ⁂ (slope 0.29 ± 0.01, intercept 0.05 ± 0.02) (Laurents et al., 2003).

5.4 α-Chymotrypsin

The initial objective was to measure the effective valence of α-chymotrypsin (Figure 5.4.1) at an ionic strength of 0.1 M and determine if charge was conserved upon dimerization. This ionic strength was chosen primarily because 1) this ionic strength had worked well for T4 lysozyme data and 2) this was the ionic strength Ford and Winzor used in their study of charge conservation for this dimer. However, initial AUC experiments could not reproduce their reported K_a of 3,500 M^{-1} (0.14 L/g) in 100 mM KCl. Instead, a value 10-fold smaller was observed.

Fitting the 100 mM MCE data for two species with NONLIN while holding the stoichiometry parameter (N) at 2, gave an LnK= -2.35. This MCE LnK (see Section 4.3.4 on conversion) corresponded to a molar dissociation constant of 2097 μM and was within 10% of the value observed in the AUC experiments. If instead the association constant was held at the corresponding AUC value and N fit for, a value of 2.0 was obtained. Unfortunately, the confidence interval about N was 30% of the value. Sigma in this case corresponded to a z_{eff} of 1.98, which is, at best, 30% below that predicted by DHH theory.

When using experimental data collected in 200 mM KCl, NONLIN results for two species gave similar uncertainties. In the second set of experiments (see Tables 3.3.4.2 and 4.3.3.1), the parameter LnK was held at a value corresponding to the AUC findings (K_d = 16.27 μM) and the stoichiometry fit gave N = 2.0. However, the confidence interval for N was again about 30%. At a higher concentration, better results were obtained. In this case, the parameter Ln K was first fit and gave a molar dissociation constant of 20.0 μM, which is within 10% of the value reported by Horbett

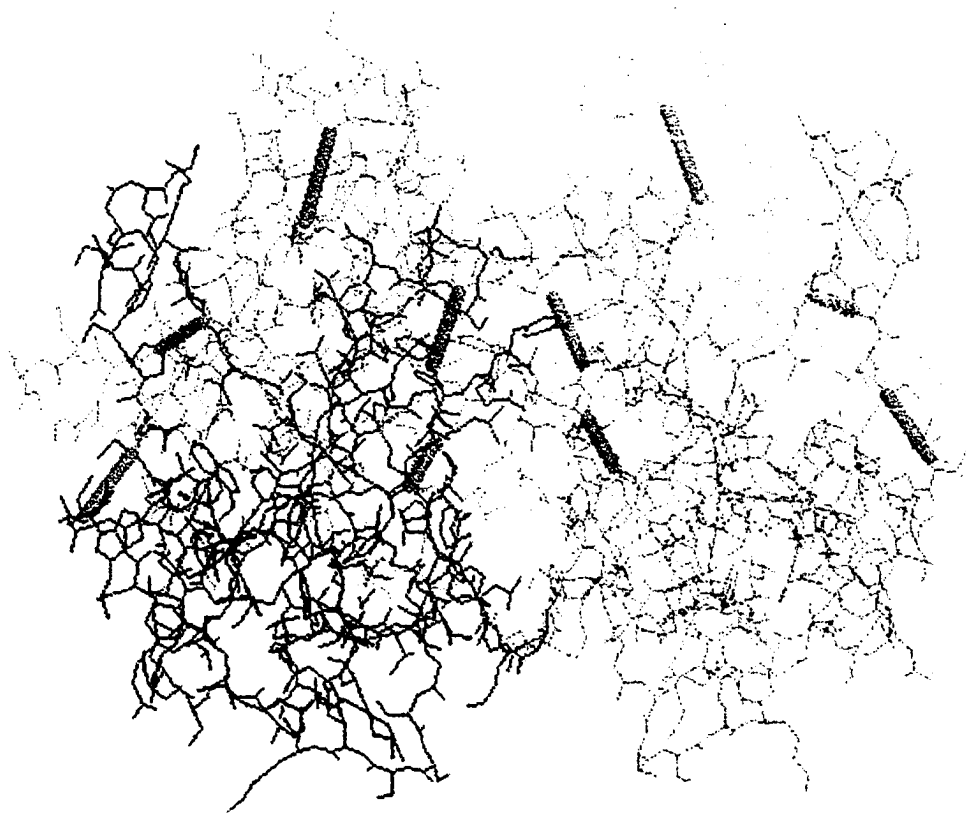

Figure 5.4.1: Structure of α-chymotrypsin dimer. Disulfide bonds are shown as thick yellow bars. Structure from the PDB site under the listing 5cha. The structure was originally reported by Belvins, R.A. (Belvins & Tulinsky, 1985)

and Teller (Horbett & Teller, 1974). Fitting for the stoichiometry gave N = 2.0 with a 1% confidence interval. The resulting sigma corresponded to an effective valence of 1.16 for the monomer.

One source of difficulty may be the formation of autolysis products. The lyophilized protein is reportedly free of autolysis products but once solubilized, autolysis products may form over the course of an MCE experiment, which can last a week or two. This would also lead to a population of truncated chymotrypsin molecules (Patel et al., 2002). Furthermore, trypsin (also cationic) is reportedly found in many preparations of α-chymotrypsin and could have contributed to the measured sigma. Another possible source of error may again be the membranes. Although derivatized membranes were used so as to eliminate small ion gradients, the nitrate test confirming this was done at only one field strength (E = 0.2 V/cm) and should be repeated at a range of fields. Work by Susan Chase (personal communication) has shown that in some cases small ion gradients are apparent only at higher field strengths. The highest field used in this work was 0.4 V/cm and future tests should therefore encompass this field. For comparison, the observed trend in the nitrate tests at pH 6.0 (10 mM BTP, 100 mM KCl) using underivatized membranes, was an accumulation of nitrate at the bottom of the cell. Therefore, by charge neutrality arguments, the effective ionic strength was increased at the bottom of the cell. Because this is where contributions from the dimer would be expected to be greatest, the increased salt would effectively mask the contribution of the dimer, especially at lower fields. If indeed there were small ion gradients in the α-chymotrypsin experiments, the result might be similar to what was observed in the fitting: a trend toward a single species fit.

It should be noted that N = 2 was expected based on previous results. Ford and Winzor investigated charge conservation of α-chymotrypsin in 1983 and found that the apparent charge was conserved (Ford & Winzor, 1983). They measured the net valence through a seemingly laborious method involving ultrafiltration and conductivity measurements using a calibration plot of their electrode.

5.5 MCE Instrument

Since its conception in the 1980's, several MCE prototypes have been constructed in this laboratory. This work has been done with the "silver box" prototype and is the same as that used in the thesis work of Wooll (Wooll, 1996) and nearly equivalent to "black box" prototype used by Kingsbury (Kingsbury, 2000). The major difference between the two prototypes is that the latter uses lenses for imaging the transmitted light onto the photodiode array. Earlier work on different prototype devices includes that done by Hayes (Hayes, 1993) and Hazard (Hazard, 1988).

In the course of this work, several existing concerns about the device itself have been readdressed. These include 1) the constancy of the electric field across the cell, 2) the limits and precision of the instrument, 3) the measurement of diffusion coefficients during electrophoresis and 4) the effect of membranes on the results. Some of the results presented are from collaborative efforts with Timothy Wilson, Susan Chase, and Thomas Moody. Though not the primary objective of this dissertation, it is useful to discuss the insights on these points briefly because we assert that the results obtained by MCE are *accurate*, and not merely precise.

Constancy of the Electric Field

Early in this work, an attempt was made to readdress whether or not the electric field across the cell remains constant. Typically, experiments were done with a constant applied current and it is possible that the local electric field dropped slightly as a result of increased concentration of macroion at the bottom of the cuvette (k is a monotonically increasing function of ion concentration). Godfrey has speculated that the perturbation in the solvent composition would be insignificant as long as the macroion/total diffusible ion concentration ratios were < 0.02 (Godfrey, 1989). Even under the lowest ionic strength conditions used in the T4 lysozyme work, this ratio was less than a quarter of that value. If however, the macroion concentration was to contribute to a drop in field, it was speculated (Timothy Wilson, personal communication) that this drop would be on the order of one mV/cm or less.

Previous work by Stephenson showed a slight macroion concentration dependence of conductivity (k) for DNA in 20 mM Tris, 1mM EDTA, pH 8.0 (Stephenson, 1995). However, more recent MCE work (Susan Chase, personal communication) has shown anomalous effects due to EDTA which may have contributed to this earlier finding. In an attempt to measure the drop in field (if any) due to the macroion, voltage difference measurements (V with current on - V with current off) were made with and without sample present. In theory $\Delta V_{sample} - \Delta V_{buffer} = \Delta\Delta V$, the drop in the potential difference due only to the macroion. In order for the $\Delta\Delta V$ to be meaningful, the drift in the measurement must be minimal. To determine this, voltage measurements (Keithely 197A multimeter) were collected every minute for 75 minutes with 20uA of current applied to a 20bp DNA sample in 20mM KCl, 10 mM Tris pH 8.0.

The systematic noise in the voltage data was fit to a polynomial and subtracted. The magnitude of the remaining random noise was still on the order of the expected measurement we were trying to make. Thus, we are still operating on the theoretically reasonable assumption that the field is constant but have not been able to verify this experimentally.

Limits and Precision

As shown in Figure 4.1.4.3, steady state σ values are expected to vary linearly with field. For the field domain, the limits of linearity have been estimated previously to be from 0.05 to 0.20 V/cm (Wooll, 1996). The experiments presented in this work indicate this can be extended to 1.10 V/cm with no noticeable deviation from linearity (see TM data in Figure 4.1.4.3 and Table 3.3.2.4). Additionally, the lower limit of the range of effective valence that can be measured in the present MCE apparatus is z_{eff}= 0.22, as found for QM at an ionic strength of 0.02 M (Table 4.6.1). The precision of z_{eff} for repeated measurements, previously reported as ±1, was found to be ±0.1 (N = 3, z = 2.28, TM T4 lysozyme at I = 0.16 M) in this work. A negligible decrease in precision from ±0.1 was found for WT lysozyme (N = 3, z = 8.28, I = 0.16 M) and thus it seems to be independent of z in the valence range of two to eight. Similarly, repeated experiments with RNase Sa gave an overall precision for z_{eff} of ±0.1 for both WT and 5K proteins (N = 2, I = 0.11 M, untreated membranes, "black box" prototype).

Measurement of Diffusion Coefficients

Previous attempts to measure diffusion coefficients in the MCE by boundary spreading during mobility experiments have met with little success. It was concluded by

Wooll that the diffusion coefficient "derived from boundary spreading increases with E field and can show significant variation from experiment to experiment" (Wooll, 1996). While the field dependence was not found in this work, significant variation was certainly observed. As Figure 5.5.1 shows, D could vary by as much as 33% under the same set of conditions.

This and other problems of this nature are likely to be rooted in polarization of the membranes used (see next section). Unfortunately, all diffusion coefficient determinations were made before a method for testing for membrane polarization was developed. It would be of value for future studies to reassess this using derivatized membranes which do not show polarization effects.

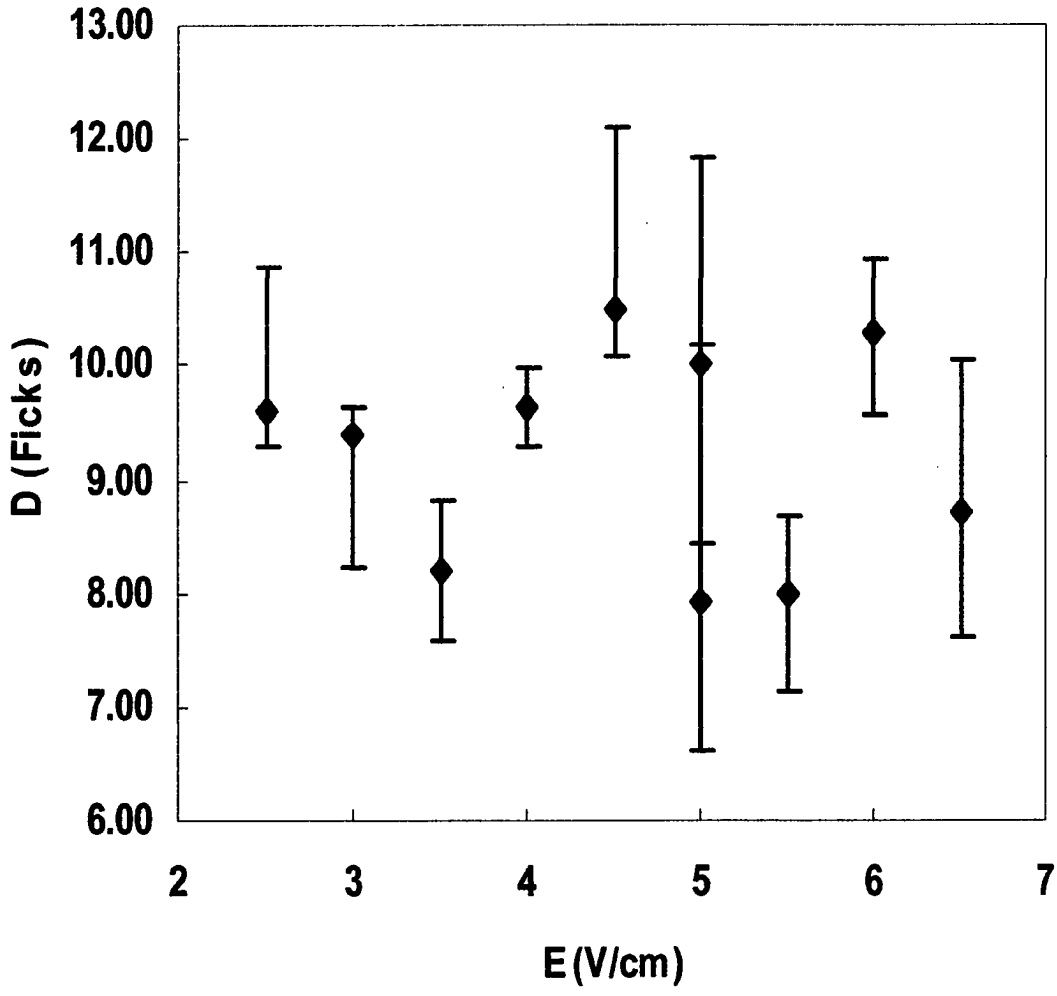

Figure 5.5.1: Diffusion coefficient as a function of field for SM T4 lysozyme. Measured by MCE velocity experiments. Even greater variation was observed for the other T4 lysozymes.

Effect of Membranes

Difficulties with previous MCE studies are likely attributable to the membranes used. For this reason, it was desirable to be able to determine the effect of different membranes not only on the macroion, but also on the background electrolyte (primarily KCl).

Recently, a method for assessing the behavior of the nitrate anion (NO_3^-) in the MCE has been developed in our laboratory. This method uses the optical absorbance of nitrate at 300 nm to monitor its concentration across the cuvette. Since the size, λ^∞, valence, and hydrodynamics of NO_3^- are very close to those of Cl^-, nitrate should be a good indicator for Cl^- behavior. In support of this, MCE experiments where KNO_3 is used in place of KCl, yield an effective valence that is identical, within experimental error. Furthermore, conditions under which KCl-containing-solvents yield aberrant electrophoretic behavior do so for KNO_3-containing-solvents as well. These measurements indicate that under certain conditions a significant gradient in the small ions can develop. Extensive testing has shown, however, that NO_3^- gradients do not form under the steady-state conditions used in the work reported here.

At other pHs (6, 6.5, and 8) and in the case of much higher fields (as used in mobility experiments), some gradient formation is seen and is a likely cause of inconsistent results when varying charge by varying solvent pH (results not given). Residual anion on the dialysis membranes due to oxidative generation of carboxyls seems to be the source of the problem. A method for chemically neutralizing this charge has been developed (see Figure 3.3.1.1). Tests with derivatized membranes show a significant improvement (decreased NO_3^- gradient) over the underivatized membranes.

Several T4 lysozyme experiments were repeated to verify that the pH 7.5 results were indeed not membrane dependent (as the nitrate studies had suggested). The repeated results indicate no membrane dependence at this pH.

Prototype Consistency

As a final note on the accuracy of MCE and its dependence on the "state of the device", instrument to instrument variation ("silver box" to "black box" prototypes) was investigated. Parallel experiments in the two instruments at E = 0.4 V/cm with RNase A in 100 mM KCl, 10 mM BTP at pH 7.5 gave sigmas (B*=0) of 10.98±0.21 and 9.38±0.25 corresponding to effective valences of 0.69±0.01 and 0.59±0.02, respectively. This is a 17% difference. The optics of both devices were subsequently realigned by Thomas P. Moody. More recent parallel experiments in the two realigned instruments with RNase Sa WT protein (100 mM KCl, 10 mM BTP at pH 7.5) gave a global z_{eff} (B*=0) value of -1.59±0.13 in the "silver box". In the "black box", repeated measurements gave global z_{eff} (B*=0) values of -1.75±0.02 and -1.81±0.11. This is a 12% difference between the "silver" and average "black" prototype result. Similarly, RNase Sa 5K protein under the same conditions gave a global z_{eff} (B*=0) value of 0.62±0.02 in the "silver box". In the "black box", repeated measurements gave global z_{eff} (B*=0) values of 0.72±0.01 and 0.67±0.01. This is a 13% difference between the "silver" and average "black" prototype result.

5.6 Summary

There have been significant improvements recently in predicting pK_a's and the influence of ionic strength on pKas. Antosiewicz has developed a model which in its fully implemented form, can theoretically take into account aa-aa as well as salt influences on pKas. While results for HEL and RNase A have been published, how available the model is for the study of other macroions is unknown. Furthermore, these types of models still cannot predict small ion binding.

Although crystallographic structures often show bound ions, the conditions under which crystallizations are done may not reflect solution conditions. Furthermore, ions which are less specifically bound will likely not appear in these structures even though they may make a significant contribution to the overall valence of the macroion. Proton titration studies may also fail to detect ion binding and require substantial amounts of material to conduct. The most direct way of obtaining true net valence is thus by electrophoretic means which, until recently, was limited to mobility measurements. With the development of the MCE, this can now also be accomplished with only 30-40 ug of sample by measuring the effective valence by the steady-state method. Simple DHH theory provides an adequate link between this measurement and net valence. DHH generally overestimates effective valence by 10-30%, but knowing this is in itself useful. Slightly better results are obtained using Booth's model. BE modeling provides a much more accurate correlation with experiment, but requires a detailed structural model.

In this work, the T4 lysozyme protein and four of its charge mutants have served as the primary model for MCE and CE experimental comparisons with DHH, Booth, and BE theoretical predictions. These variants of WT allowed us to change valence without

changing pH. The hydrodynamic radius of these proteins was found, by sedimentation velocity and light scattering experiments, to remain constant under all conditions used in the electrophoretic experiments. Therefore changes in the measured electrophoretic values could be attributed solely to changes in charge. While the MCE and CE experimental results at I = 0.11 M were in excellent agreement with each other and with theory, the theories overestimated the z_{eff} vs. z slopes at I = 0.02 M and I = 0.16 M (summarized in Figure 5.2.2 and Table 5.2.1). In all cases, BE modeling provided the closest estimates for T4 lysozyme. Shifts in the cysteine pKas have been investigated and eliminated as a possible source of discrepancy between experiment and theory. Other pKa shifts, perhaps from new salt bridge formations at low ionic strength, or ion binding, at the high ionic strengths, may be responsible for the experimental slopes being lower than predicted by the models. In other words, the formal valence rather than the effective valence is predicted to be inaccurate.

Similar in size and charge to T4 lysozyme, the protein RNase Sa and 2 of its charge mutants were also investigated at I = 0.11 M. The RNase Sa series of mutants allowed study of a complete charge reversal case. Both MCE and CE measurements were again in good agreement with each other and with theory. DHH and Booth theoretical predictions of the z_{eff} vs. z slope were 15% and 10% high, respectively. No BE model predictions are available for this protein. As was the case for T4 lysozyme, the hydrodynamic radius was found, by sedimentation velocity and light scattering experiments, to be the same for each variant under these conditions. Investigation with RNase Sa of prototype to prototype accuracy indicates at most a 12% variation in the measured slope.

Whether MCE effective valence measurements of a multi-species system (a population of both α-chymotrypsin monomer and dimer) can be made remains unproven. Neither the reported K_d nor the stoichiometry could be obtained with sufficient confidence. Experiments in both the AUC and MCE with α-chymotrypsin are inconclusive.

Suggestions for future investigations of this nature follow. Foremost, further development of the BE model in terms of generality and availability would be extremely useful. The establishment of a database of MCE results and relative parameters (sample, hydrodynamic radius, effective valence, ionic strength, pH, buffer type, various model predictions, etc.) would also be helpful in sorting through the immense amount of information and identifying inconsistencies. In this age of proteomics, structure alone will not suffice to explain all the complexities of human biology and a comprehensive characterization of the predicted 200,000-300,000 proteins must include experimentally verified valence information. With limited amounts of sample available, the MCE may be one of the best options. Improvements on the MCE throughput would be helpful in this respect. Lastly, the MCE offers a new way in which to study denatured proteins. As Yang and Honig point out, "evidence has accumulated in recent years that a significant component of the electrostatic free energy difference between native and denatured states is due to a small number of amino acids who pK_a's are shifted anomalously in the native protein" (Yang & Honig, 1993). Some very preliminary work in the MCE shows a stable gradient could be maintained up to 50° C (the highest temperature examined to date). As has been done with CE recently (Negin & Carbeck, 2001), it may be possible to extend this range and look at the electrostatic interaction in protein folding.

APPENDIX

Symbol Clarification

Although one often sees D used for the dielectric constant, this is also the symbol for the diffusion coefficient. Therefore ε has been used in the equations to avoid confusion.

CE Sample Quantity

For a hydrodynamic injection on a 37 cm capillary with a 50 um internal diameter, the quantity (Q) of sample injected can be calculated by

$$Q = \pi r^2 l[c_i] = \pi r^2 \left[\frac{\Delta P r^2 t_{inj}}{8\eta L}\right][c_i]$$

where r is the radius in meters, l is the length of the sample plug, c_i is the sample concentration, ΔP is the pressure difference in $N \cdot m^{-2}$ (0.5 psi = 3.435 x 10^3 $N \cdot m^{-2}$), t is the injection time in seconds, η is the viscosity in $N \cdot s \cdot m^{-2}$, and L is the length of the capillary in meters (Altria et al., 1997). The viscosity used was that of the buffer and not sample solution due to limited amounts of the latter. At the sample concentrations used, the difference should be negligible. All values used correspond to those at 20 °C.

Nitrate Tests

An estimation Cl^- behavior can be made using nitrate. The behavior of the nitrate anion (NO_3^-) in the MCE is assessed by monitoring the optical absorbance of nitrate at 300 nm. Since the size, λ^∞, valence, and hydrodynamics of NO_3^- are very close to those

of Cl^-, we believe nitrate is a good indicator for Cl^- behavior. By this method it has been concluded that under certain conditions a sometimes significant gradient in the small ions may develop. For example, a gradient in NO_3^- is observed for 100 mM KNO_3, 10 mM BTP at pH 6 (no protein) if underivatized SpectraPor membranes are used (see Section 3.3.1). We therefore believe a similar situation exists for 100 mM KCl, 10 mM BTP at pH 6. Extensive testing has shown, however, that these NO_3^- gradients do not form under the steady-state conditions used in this thesis work. It should be noted that there is some uncertainty at the lower ionic strengths (for example 10 mM KCl, 10 mM BTP pH 7.5) because the absorbance due to NO_3^- (when substituted for Cl^-) is low.

REFERENCES

CRC Handbook of Chemistry and Physics. Linde, D. R. **74th**. 1993. Boca Raton, Florida, CRC Press.

Allison, S. A. Modeling the electrophoresis of rigid polyions: inclusion of ion relaxation. *Macromolecules* **29**, 7391-7401 (2002).

Allison, S. A., Chen, C., and Stigter, D. The length dependence of translational diffusion, free solution electrophoretic mobility, and electrophoretic tether force of rigid rodlike model duplex DNA. *Biophyics Journal* **81**, 2558-2568 (2001).

Allison, S. A. and Mazur, S. Modeling the free solution electrophoretic mobility of short DNA fragments. *Biopolymers* **46**, 359-373 (1998).

Allison, S. A., Potter, M., and McCammon, J. A. Modeling the electrophoresis of lyzozyme. II. Inclusion of ion relaxation. *Biophyics Journal* **73**, 133-140 (1997).

Allison, S. A. and Tran V. Modeling the electrophoresis of rigid polyions: application to lysozyme. *Biophyics Journal* **68**, 2261-2270 (1995).

Altria, K. D. *et al.* Calculations for Practical Use *In* Handbook of Capillary Electrophoresis. Landers,J.P. (ed.), 865-872, CRC Press LLC, New York, (1997).

Anderson, D. E. (1992) Ph.D. Dissertation, University of Oregon.

Anderson, D. E., Becktel, W. J., and Dahlquist, F. W. pH-Induced Denaturation of Proteins: A Single Salt Bridge Contributes 3-5 kcal/mol to the Free Energy of Folding of T4 Lysozyme. *Journal of the American Chemical Society* **29**, 2403-2408 (1990).

Antosiewicz, J., Briggs, J., Elcock, A., Gilson, M., and McCammon, A. Computing Ionization States of Proteins with a Detailed Charge Model. *Journal of Computational Chemistry* **17**, 1633-1644 (1996a).

Antosiewicz, J., McCammon, A. & Gilson, M. The Determinants of pKas in Proteins. *Biochemistry* **35**, 7819-7833 (1996b).

Barnett, L. B. and Bull, H. B. Electrophoresis of ribonuclease and of beta-lactoglobulin: isoelectric points of proteins. *Arch.Biochem.Biophys.* **89**, 167-172 (1960).

Bashford, D. and Karplus, M. pKas of ionizable groups in proteins: atomic detail from a continuum electrostatic model. *Biochemistry* **29**, 10219-10225 (1990).

Bell, J. A. et al. Comparison of the crystal structure of bacteriophage T4 lysozyme at low, med, and high ionic strengths. *Proteins* **10**, 10-21 (1991).

Belvins, R. A. and Tulinsky, A. The refinement and the structure of the dimer of alpha-chymotrypsin at 1.67 A resolution. *Biological Chemistry* **260**, 4264 (1985).

Bergethon, P. R. & Simons, E. R. Introduction to Electrolytic Solutions *In* Biophysical Chemistry., 152-170, Springer-Verlag, NY, (1990).

Booth, F. The cataphoresis of spherical, solid non-coducting particles in a symmetrical electrolyte. *Proceedings of the Royal Society of London* **A203**, 514-533 (1950).

Bull, H. B. An Introduction to Physical Biochemistry. F. A. Davis Company, Philadelphia (1964).

Cann, J. R. Principles of Electrophoresis and Ultracentrifugation *In* Interacting Macromolecules. Horecker,B., Kaplan,N.O., Marmur,J. & Scheraga,H.A. (eds.), 1-44, Academic Press, New York, (1970).

Carbeck, J. D. and Negin, R. S. Measuring the Size and Charge of Proteins Using Protein Charge Ladders, Capillary Electrophoresis, and Electrokinetic Models of Colloids. *J.Am.Chem.Soc.* **123**, 1252-1253 (2001).

Castellan, G. W. Physical Chemistry. The Benjamin/Cummings Publishing Company, Inc., Menlo Park (1983).

Crocker, J. C. and Grier, D. G. Interactions and Dynamics in Charge-Stabilized Colloid. *MRS Bulletin* **23**, 24-31 (1998).

Dao-pin, S. et al. Cumulative Site-directed Charge-change Replacements in Bacteriophage T4 Lysozyme Suggest that Long-range Electrostatic Interactions Contribute Little to Protein Stability. *Journal of Molecular Biology* **221**, 873-887 (1991).

Debye, P. J. The Electric Field of Ions and Salting Out *In* Z.Physik.Chem., 56-64, Cohen Festband, (1927).

Debye, P. J. and Huckel, E. On the Theory of Electrolytes. I. Freezing Point Depression and Related Phenomena. *Physikalische Zeitschrift* **24**, 185-206 (1923a).

Debye, P. J. and Huckel, E. On the theory of electrolytes. II. Limiting law for electric conductivity. *Physikalische Zeitschrift* **24**, 305-325 (1923b).

Derjaguin, B. V. and Landau, L. *Acta Phys.* **16**, 633 (1941).

Durant, J. A., Chen, C., Laue, T. M., Moody, T. P., and Allison, S. A. Use of T4 Lysozyme Charge Mutants to Examine Electrophoretic Models. *Biophysical Chemistry* **101-102**, 593-609 (2002).

Edsall, J. T. & Wyman, J. Electrostatics *In* Biophysical Chemistry., 241-320, Academic Press Inc, NY, (1958).

Eisenberg, D. & Crothers, D. Physical Chemistry with Applications to the Life Sciences. The Benjamin/Cummings Publishing Company, Inc., Menlo Park (1979).

Elcock, A. Realistic modeling of the denatured states of proteins allows accurate calculations of the pH dependence of protein stability. *J.Molecular Biology* **294**, 1051-1062 (1999).

Elcock, A. and McCammon, J. A. Calculation of Weak Protein-Protein Interactions: The pH Dependence of the Second Virial Coefficient. *Biophysical Journal* **80**, 613-625 (2001).

Ford, C. L. and Winzor, D. J. Experimental tests of charge conservation in macromolecular interactions. *Biochmica et Biophysica Acta* **756**, 49-55 (1983).

Friedl, W., Reijenga, J. C., and Kenndler, E. Ionic strength and charge number correction for mobilities of multivalent organic molecules in capillary electrophoresis. *Journal of Chromatography A* **709**, 163-170 (1995).

Friend, S. H., Matthew, J. B., and Gurd, F. R. N. Protein-Protein Interactions: Nature of the Elelctrostatic Stabilization of Deoxyhemoglobin Tetramer Formation. *Biochemistry* **20**, 580-586 (1981).

Godfrey, J. E. Steady-state electrophoresis: A technique for measuring phyiscal properties of macro-ions. *Proc.Natl.Acad.Sci.USA* **86**, 4479-4483 (1989).

Gouy, G. *J.Phys.Theor.Appl.* **9**, 457 (1910).

Harvey, S. Treatment of Electrostatic Effects in Macromolecular Modeling. *Proteins: Structure, Function, and Genetics* **5**, 78-92 (1989).

Havranek, J. J. and Harbury, P. B. Tanford-Kirkwood Electrostatics for Protein Modeling. *Proc.Natl.Acad.Sci.USA* **96**, 11145-11150 (1999).

Hayes, D. B. (1993) Ph.D. Dissertation, University of New Hampshire.

Hazard, A. L. (1988) Undergraduate, University of New Hamphshire.

Henry, D. C. The Cataphoresis of Suspended Particles. Part I - The Equation of Cataphoresis. *Proceedings of the Royal Society of London* **133**, 107-141 (1931).

Hermans, J. and Scheraga, H. A. Structural Studies of Ribonuclease. V. Reversible Change of Configuration. *J.Am.Chem.Soc.* **83**, 3283-3292 (1961).

Honig, B. and Nicholls, A. Classical Electrostatics in Biology and Chemistry. *Science* **268**, 1144-1149 (1995).

Horbett, T. A. and Teller, D. C. Proton Binding Changes in a-Chymotrypsin Dimerization. *Biochemistry* **13**, 5490-5495 (1974).

Kalman, F., Ma, S., Fox, R. O., and Horvath, C. Capillary electrophoresis of S. nuclease mutants. *Journal of Chromatography* **705**, 135-154 (1995).

Kingsbury, J. S. (2000) Undergraduate, University of New Hampshire.

Klein, D. and Bates, R. *Journal of Solution Chemistry* **9**, 289 (1979).

Kohda, D., Sawada, T., and Inagaki, F. Characterization of pH Titration Shifts for all the Nonlibile Proton Resonances in Protein by Two-dimensional NMR: the Case of Mouse Epidermal Growth Factor. *Biochemistry* **30**, 4896-4900 (1991).

Ladokhin, A. S. and White, S. H. Protein chemistry at membrane interfaces: non-additivity of electrostatic and hydrophobic interactions. *J.Molecular Biology* **309**, 543-552 (2001).

Laue, T. M. Sedimentation equilibrium as a thermodynamic tool. *Methods in Enzymology* **259**, 427-452 (2002).

Laue, T. M., Hazard, A. L., Ridgeway, T. M., and Yphantis, D. A. Direct determination of macromolecular charge by equilibrium electrophoresis. *Anal.Biochemistry* **182**, 377-382 (1990).

Laue, T. M., Johnson, A. E., Esmon, C. T., and Yphantis, D. A. Structure of Bovine Blood Coagulation Factor Va. Determination of the Subunit Associations, Molecular Weights, and Asymmetries by Analytical Ultracentrifugation. *Biochemistry* **23**, 1339-1348 (1984).

Laue, T. M. *et al.* Insights from a New Analytical Electrphoresis Apparatus. *Journal of Pharmaceutical Sciences* **85**, 1331-1335 (1996).

Laue, T. M., Shepard, H. K., Ridgeway, T. M., Moody, T. P. & Wilson, T. J. Membrane-confined analytical electrophoresis In: *Methods in Enzymology* **295** Ackers,G.K. & Johnson,M.L. (eds.), 479-490, Academic Press, New York, (1998).

Laurents, D. V. *et al.* Charge-Charge Interactions are Key Determinants of the pKa Values of Ionizable Groups in Ribonuclease Sa (pI = 3.5) and a Basic Variant (pI = 10.2). *J. Molecular Biology* **325**, 1077-1092 (2003).

Li, D., Fu, S., and Lucy, C. A. Prediciton of Electrophoretic Mobilities.3. Effects of Ionic Strength in Capillary Zone Electrophoresis. *Anal.Chemistry* **71**, 687-699 (1999).

Linderstrom-Lang, K. U. On the ionization of proteins. *C.R.Trav.Lab.Carlsberg.* **15**, 1-29 (1924).

Marini, M. A. and Wunsch, C. *Biochemistry* **2**, 1454-1460 (1963).

Matsubara, N. and Terabe, S. Separation of closely related peptides by capillary electrophoresis with a nonionic surfactant. *Chromatographia* **34**, 493 (1992).

Matthew, J. B. and Gurd, F. R. N. Stabilization and destabilization of protein strucure by charge interactions. *Methods in Enzymology* **130**, 437-454 (1986).

Matthew, J. B. et al. pH-dependent processes in proteins. *CRC Critical Reviews in Biochemistry* **18**, 91-97 (1985).

Mazur, S., Chen, C., and Allison, S. A. Modeling the electrophoresis of short duplex DNA: Counterions K+ and Tris+. *J.Phys.Chem.* **B 105**, 1100-1108 (2001).

Moody, T. P. and Shepard, H. K. Nonequilibrium Thermodynamics of Membrane-Confined Electrophoresis. *Biophysical Chemistry* **in press**.

Negin, R. S. and Carbeck, J. D. Measurement of electrostatic interaction in protein folding with the use of protein charge ladders. *J.Am.Chem.Soc.* **124**, 2911-2916 (2001).

Nicholson, H., Becktel, W. J., and Matthews, B. W. Enhanced protein thermostability from designed mutations that interact with a-helix dipoles. *Nature* **336**, 651-656 (1991).

O'Brien, R. W. and White, L. R. Electrophoretic mobility of a spherical colloid particle. *J.Chem.Soc.Raraday Trans.* **2**, 1607-1626 (1978).

Oda, R. P. and Landers, J. P. Effect of cationic buffer additives on capillary electrophoretic separation of serum transferrin from different species. *Electrophoresis* **17**, 331 (1996).

Onsager, L. and Fuoss, R. M. Irreversible Processes in Electrolytes. Diffusion, Conductance, and Viscous Flow in Arbitrary Mixtures of Strong Electroyltes. *J.Phys.Chem.* **36**, 2689 (1932).

Overbeek, J. TH. G. Theorie der electrophorese. *Kolloidchem.Beih.* **54**, 287-364 (1943).

Overbeek, J. TH. G. *Advan.Colloid Sci.* **3**, 97 (1950).

Pace, C. N., Alston, R. W., and Shaw, K. L. Charge-Charge interaction influence the denatured state ensemble and contribute to protein stability. *Protein Science* **9**, 1395-1398 (2000).

Patel, C. N. et al. Effects of molecular crowding by saccharides on a-chymotrypsin dimerization. *Protein Science* **11**, 997-1003 (2002).

Perry, K. M., Onuffer, J. J., Gittelman, M. S., Barmat, L., and Matthews, C. R. Long-range electrostatic interactions can influence the folding, stability, and cooperativity of dihydrofolate reductase. *Biochemistry* **28**, 7961-7968 (1989).

Pietta, P. G. et al. Application of capillary electrophoresis at low pH to oligonucleotide quality control. *Journal Chromatography A* **853**, 355-358 (1999).

Pitts, E. *Proceedings of the Royal Society, A* **217**, 43-70 (1953).

Pitts, E. *Transactions of the Faraday Society* **66**, 693 (1970).

Ridgeway, T. M. et al. An apparatus for membrane-confined analytical electrophoresis. *Electrophoresis* **19**, 1611-1619 (1998).

Schellman, J. A. *J.Phys.Chem.* **57**, 472 (1953).

Segel, I. H. Biochemical Calculations. John Wiley & Sons, Inc., New York (1976).

Shaw, K. L., Grimsley, G. R., Yakovlev, G. I., Makarov, A. A., and Pace, C. N. The effect of net charge on the solubility, activity, and stability of ribonuclease Sa. *Protein Science* **10**, 1206-1215 (2001).

Shire, S. J., Hanania, G. I. H., and Gurd, F. R. N. Electrostatic effects in myoglobins. Hydrogen ion equlibria in sperm whale ferrimyoglobin. *Biochemistry* **13**, 2967-2975 (1974).

Smoluchowski, M. *Bull.Acad.Sci.Cracovie* 182 (1903).

Sokal, R. R. & Rohlf, F. J. Biometry. W.H. Freeman and Co., San Francisco (1981).

Stellwagon, N. C., Gelfi, C., and Righetti, P. G. The free solution mobility of DNA. *Biopolymers* 687-703 (1997).

Stephenson, D. A. (1995) Undergraduate, University of New Hampshire.

Stigter, D. & Dill, K. A. Charge Effects on Folded and Unfolded Proteins. *Biochemistry* **29**, 1262-1271 (1990).

Tanford, C. Physical Chemistry of Macromolecules. John Wiley & Sons, Inc., New York (1961).

Tanford, C. Protein Denaturation. *Adv.Protein Chem.* **24**, 1-95 (1970).

Tanford, C. and Kirkwood, J. G. Theory of protein titration curves. I. General equations for impenetrable spheres. *J.Am.Chem.Soc.* **79**, 5333-5339 (1957).

Tellam, R., de Jersey, J., and Winzor, D. J. Evaluation of equilibrium constants for the binding of N-acetyl-L-tryptophan to monomeric and dimeric forms of a-chymotrypsin. *Biochemistry* **18**, 5316-5321 (1979).

Tsugita, A. and Inouye, M. Purfication of Bacteriophage T4 Lysozyme. *Journal of Biological Chemistry* **243**, 391-397 (1968).

Urry, D. W. Physical chemistry of biological free energy transduction as demonstrated by elastic protein-based polymers. *J.Phys.Chem.* **101**, 11007-11028 (1997).

van Holde, K. E., Johnson, W. C. & Ho, P. S. Physical Biochemistry. Prentice Hall, Upper Saddle River (1998).

Verwey, E. J. & Overbeek, J. TH. G. Theory of the Stability of Lysophobic Colloids. Elsevier, Amsterdam (1948).

Whitten, S. T. and Garcia-Moreno, B. E. pH dependence of stability of staphylococcal nuclease: Evidence of substantial electrostatic interactions in the denatured state. *Biochemistry* **39**, 14292-14304 (2000).

Wiersema, P. H., Loeb, A. L., and Overbeek, J. TH. G. Calculation of the Electrophoretic Mobility of a Spherical Colloid Particle. *Journal of Colloid and Interface Science* **22**, 78-99 (1966).

Wiersema, P. H. & Overbeek, J. TH. G. The Interpretation of Electrophoretic Mobilities *In* Electrophoresis: Theory, Methods, Applications. Bier,M. (ed.), 1-52, Academic Press, NY, (1967).

Wills, P. R. and Winzor, D. J. Studies of solute self-association by sedimentation equilibrium: allowance for effects of thermodynamic non-ideality beyond the consiquences of nearest-neighbor interactions. *Biophysical Chemistry* **91**, 253-262 (2001).

Wooll, J. O. (1996) Ph.D. Dissertation, University of New Hampshire.

Xu, J. et al. Structural and thermodynmaic analysis of the binding of solvent at internal sites in T4 lysozyme. *Protein Science* **10**, 1067-1078 (2001).

Yang, A. and Honig, B. On the pH dependence of protein stability. *J.Molecular Biology* **231**, 459-474 (1993).